Assessing the Impact of Breakwater Spatial Design on Hydrodynamics for Mangrove Restoration

A Case Study in Bạc Liêu, Vietnam

Rosita Vos

Delft University of Technology

TU Delft

Assessing the Impact of Breakwater Spatial Design on Hydrodynamics for Mangrove Restoration

by

R.K. Vos

to obtain the degree of Master of Science
at the Delft University of Technology,
to be defended publicly on June 24th, 2025

Student Number:	4731417	
Project duration:	September, 2024 - June, 2025	
Faculty:	Faculty of Civil Engineering and Geosciences, Delft	
Chair committee:	Dr. D.S. Van Maren	TU Delft
Committee members:	Mr. Dr. Ir. C. Mai Van	TU Delft
	Dr. Ir. A.J.H.M. Reniers	TU Delft
	Dr. Ir. A.G.M. Gijón Mancheño	TU Delft
Additional supervisor:	Dr. S.H. Trương	Thuyloi University

TU Delft

Preface

This thesis is the final step in obtaining my Civil Engineering Master's degree. Over the last nine months, I've focused on assessing the impact of breakwater spatial design on hydrodynamics for mangrove restoration in Bạc Liêu. I developed an interest in sustainability and working abroad during my studies in Delft. I have the ambition to work in countries facing big challenges and less knowledge of hydraulic engineering, to help improve people's lives in these regions. The goal of the Living Lab programme aligns closely with my interests, so I am very grateful to have the opportunity to contribute to this project. I hope my research can make a valuable contribution to the Living Lab and be useful or inspiring to others.

I would like to share my gratitude towards everyone who guided and supported me during my thesis in various ways. Firstly, I want to thank my supervisor and chair, Bas, for guiding me through the whole process and always passionately thinking along with every challenge I faced. Alejandra really helped me start up the project and fieldwork, you always guided me in a motivated and kind way. Ad was the biggest support regarding the numerical model. You were very helpful, and your positive feedback kept me going in times when the model didn't. Cong joined the committee later, providing a lot of useful feedback and insight with his expertise not only in engineering but also about the whole study area. I would like to express a special thanks to Sơn (and his project DTDL.CN-51/23), Linh, Tùng, Hùng, Trung, and everyone who welcomed and guided me during my stay in beautiful Vietnam. Also to Lindsey and Marjan, for involving me in the Living Lab and making this Master's thesis topic possible for me. Thank you all so much for your time and assistance. Additionally, I would like to thank FAST University Fund TU Delft, Lamminga Fonds, and the Living Lab for their financial support, which made the project and fieldwork possible. Finally, I thank my friends and family for all their support throughout this thesis and all my study years in Delft. I am grateful for the amazing time I had in Delft during my studies, for everything I've learned on a personal and professional level, and for all the lifelong friendships I've formed.

Rosita Vos
Delft, June 2025

Summary

Mangrove ecosystems play an important role in (sub)tropical coastal zones by providing services such as carbon storage, biodiversity support, and natural protection against erosion and flooding. Their dense root systems trap sediment and reduce wave energy, contributing to shoreline stability. Despite these benefits, global mangrove areas have declined rapidly in recent decades, mainly due to deforestation and coastal retreat. In response, various restoration measures have been implemented, including the construction of permeable structures along eroding coastlines. These structures aim to reduce hydrodynamic energy and promote sediment deposition, creating conditions suitable for mangrove re-establishment. However, they do not always succeed in providing the required sediment accumulation.

This study focuses on a breakwater in the study area, located along the coast of Bạc Liêu, Vietnam. The area has a concave bed profile with limited wave energy dissipation and short inundation-free periods, which, together with net erosion, hinder both mature mangrove stability and seedling establishment. Hydrodynamic forces such as longshore currents, tidal flows, and waves generate bed shear stresses that resuspend sediment and limit sediment deposition near the shore. The existing permeable breakwater fails to provide the sheltered conditions needed for mangrove survival and recovery. As part of the Mangrove Living Lab project, this study investigates how the spatial design of the existing Pile-Rock Breakwater (PRBW) influences hydrodynamic processes relevant to sediment transport and deposition, focusing on minimising the maximum bed shear stress near the mangrove fringe. The considered spatial design parameters of the permeable breakwater are the gap width and the distance to shore. Field measurements and numerical modelling using Delft3D are combined to assess current conditions, evaluate the effectiveness of the existing design, and explore potential improvements.

Results show that narrower gaps reduce wave energy in the sheltered area but concentrate flow through the gaps, locally increasing velocities. Placing the breakwater further offshore allows more space for dissipation and reduces bed shear stress at more exposed areas behind the gaps, but also increases the incoming energy near the mangroves in more sheltered zones. The recommended spatial design requires a balance of these effects, with the breakwater placed approximately 70 metres further offshore and featuring narrower gaps to enhance shelter and reduce resuspension. Recommendations for future work include more detailed modelling including diffraction, long waves, and morphodynamics, as well as gathering more data from the area to improve understanding. Further research should also investigate simultaneous adjustments of the spatial design parameters and explore alternative breakwater types.

Overall, this research shows the complexity and importance of a site-specific breakwater design. Optimising the spatial layout offers potential to improve the breakwater's effectiveness, but further research is needed to improve the design and develop a more thorough understanding of the local conditions and ongoing coastal processes. These improvements are essential to support sedimentation and establish stable conditions for mangrove survival and long-term restoration along the coast of Bạc Liêu.

Contents

List of Figures

List of Tables

Nomenclature

Abbreviations

Abbreviation	Definition
MHW	Mean High Water
MLW	Mean Low Water
MSL	Mean Sea Level
MKD	Mekong Delta
PRBW	Pile-Rock Breakwater
RTK	Real Time Kinematic
SSC	Suspended Sediment Concentration
RMSE	Root Mean Squared Error
Spatial Dimensions	
D	Distance to Shore
G	Gap Width
L	Structure Length
Cardinal Directions	
N	North
W	West
S	South
E	East
Symbols	
τ_{max}	Maximum Bed Shear Stress
H_s	Significant Wave Height

1

Introduction

1.1. Research Context

Coastal regions worldwide face increasing threats, including rising sea levels, intensified storms, and erosion [37]. Traditional hard defences like seawalls and dikes are costly, can harm ecosystems, and lack resilience. They limit the ability of coastal systems to adapt to sea-level rise or recover from erosive events [31]. Mangrove forests can offer an effective and sustainable solution for coastal defence, particularly in (sub)tropical muddy coastal areas [85]. Mangroves stabilise sediments, reduce wave energy, and prevent shoreline retreat. Their dense root systems trap fine sediments, supporting sediment accretion and the natural resilience of the coast [3, 50]. Mangroves and sediment dynamics create a positive feedback loop that stabilises and grows mangrove ecosystems. Mangroves decrease flow velocities with their complex root systems, which reduces wave energy and facilitates the deposition of fine sediments [97]. This sediment trapping raises the soil level, improving conditions for mangrove root development and enabling mangroves to further expand seaward [39]. In turn, increased mangrove cover provides more friction against tidal flows and waves, enhancing sediment deposition and further stabilising the coastline [49]. These processes are schematised below in figure 1.1.

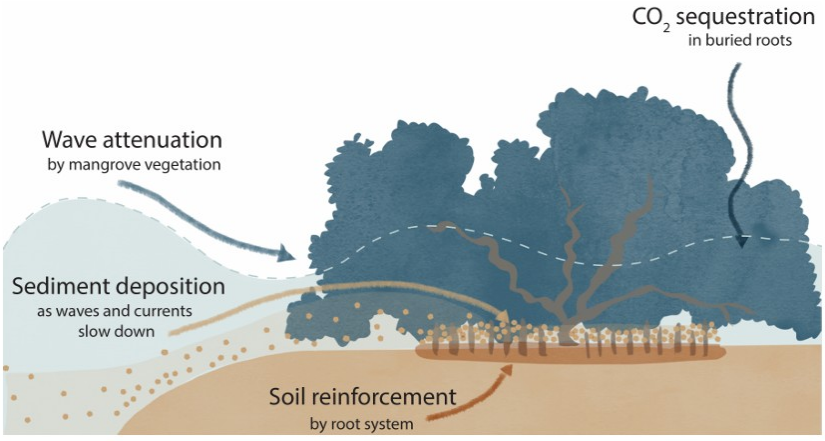

Figure 1.1: Illustrated how mangroves help mitigate climate change by storing carbon, stabilising soil, reducing erosion, and stimulate sediment trapping [44].

This natural capacity to reduce wave energy provides coastal communities with increased protection, as illustrated in figure 1.2, often resulting in reduced storm damage when sheltered by mangrove forests [78]. In addition to coastal protection, mangrove ecosystems offer several other benefits. They are among the most efficient carbon-capturing ecosystems on Earth. Mangroves also support high biodiversity and improve water quality by acting as natural filters [84]. Their complex root structures create

habitats for various marine species, which improves fisheries and supports local livelihoods.

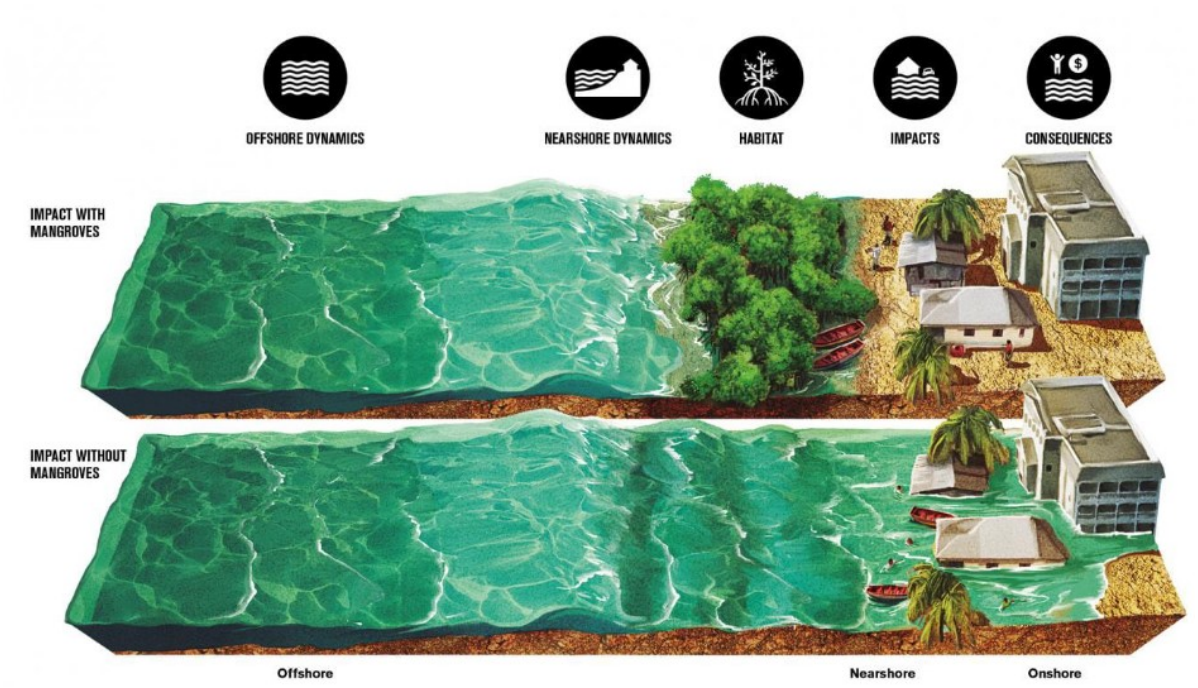

Figure 1.2: The impact of mangroves on coastal protection [63]

In 2020, the global mangrove area spanned 147,358.99 km², accounting for 14.93% of the world's 2,139,308.93 km coastline. However, mangroves face significant threats, with approximately 20% already lost to coastal development, aquaculture, and infrastructure projects [84, 19]. Between 1996 and 2020 alone, the world lost 5,245.24 km² of mangroves, primarily due to aquaculture expansion and coastal erosion [68, 91]. The most significant losses occurred in Asia between 1980 and 2005, with an estimated 1,900 million hectares of mangroves destroyed [4]. In coastal areas affected by deforestation, aquaculture, farming, or reduced sediment supply from river damming and hard structures, erosion can limit mangrove presence and hinder restoration efforts [98, 2]. When erosion accelerates, mangrove roots lose their stabilising effect, leading to increased sediment loss and weakened soil structure. As mangroves disappear, wave energy and erosion intensify further, preventing sediment accumulation and causing continued habitat degradation. The loss of mangroves not only disrupts their ability to protect coastlines and reduce storm impacts, but also affects marine ecosystems such as seagrass beds and coral reefs. This destruction leads to decreased biodiversity and adversely impacts local communities that depend on mangroves for food, livelihoods, and protection [84, 19].

To address mangrove loss due to coastal erosion, various interventions such as brushwood structures and breakwaters have been implemented globally. This research focuses on a permeable breakwater at the coast of Bạc Liêu, located in the Mekong Delta in Vietnam. The total area of mangrove forests in the Mekong Delta has decreased drastically due to various causes, such as coastal erosion and land subsidence [12, 80]. Several interventions have been implemented to restore these mangrove forests. The current coastal intervention in the study area is Pile-Rock Breakwaters (PRBW), shown below in figure 1.3.

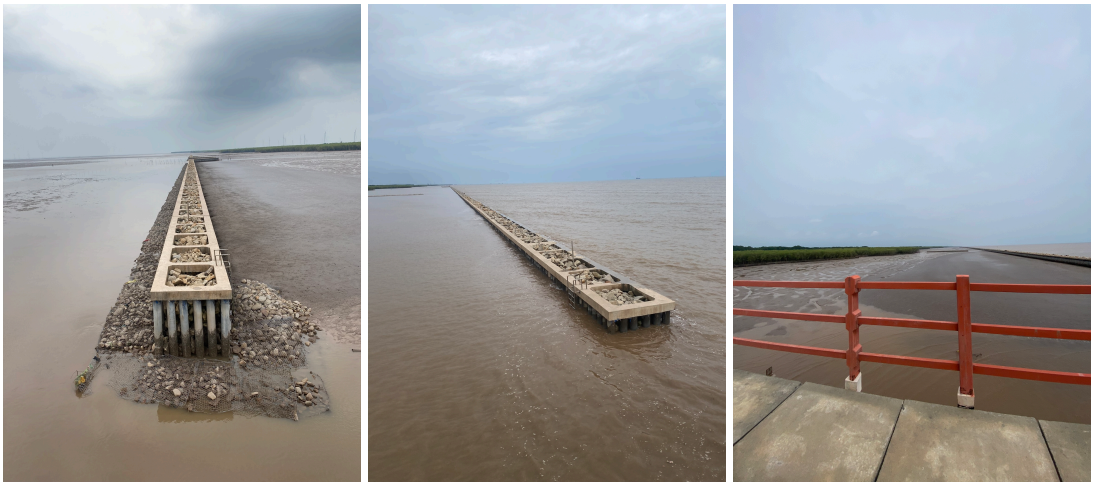

(a) Breakwater during low tide **(b)** Breakwater during high tide **(c)** Difference in bed elevation

Figure 1.3: The current permeable breakwater, Pile-Rock Breakwater (PRBW), located in the study area at the coast of Bạc Liêu.

These permeable breakwaters are placed to restore mangrove habitats by rearranging the sediment balance [64][24]. Permeable dams reduce wave-induced erosion and can support sedimentation [44]. These structures may be temporary and can become unnecessary once mangroves are rehabilitated [98]. The permeable structures are placed parallel to the coast, with gaps between the components. These gaps are built to enable a continuous exchange of water between the sheltered area and the open sea [69]. Even though these structures are known to support sedimentation and shoreline stabilisation, there is no clear guideline for their spatial design [52]. This is largely due to the strong site-specific dependence of their effectiveness, which varies with factors like local hydrodynamics, sediment supply, and environmental conditions. This knowledge gap is relevant in the study area in Bạc Liêu, where the current breakwater shows insufficient sedimentation near the mangrove fringe and its spatial dimensions have not yet been assessed [69].

1.2. Problem Statement

Large parts of the fine-grained, mangrove-fringed east coast of the Mekong Delta are eroding, driven by factors such as wave exposure, relative sea-level rise, reduced sediment supply, and land subsidence. An example of an eroding section with degraded mangroves is the Bạc Liêu coast. To mitigate this, Pile-Rock Breakwaters (PRBW) have been built to reduce wave energy and promote sediment accumulation near the mangrove fringe. However, the current breakwater in the Bạc Liêu area insufficiently traps sediments to regenerate mangroves. This suggests that the design of the breakwaters is suboptimal for coastal protection. While it is known that the spatial dimensions of the structures, specifically structure length, gap width, and distance to the mangrove fringe, influence the hydrodynamics that control sediment dynamics, their effectiveness along mangrove–mud coasts is not well understood [52, 58]. This study assesses how these spatial design factors affect hydrodynamic conditions that influence fine sediment transport and deposition in the study area in Bạc Liêu.

1.3. Research Objectives

This study aims to quantify how the spatial dimensions of a Pile-Rock Breakwater (PRBW) affect the hydrodynamics controlling sediment dynamics in the study area at the coast of Bạc Liêu. These design parameters are schematised below in figure 1.4.

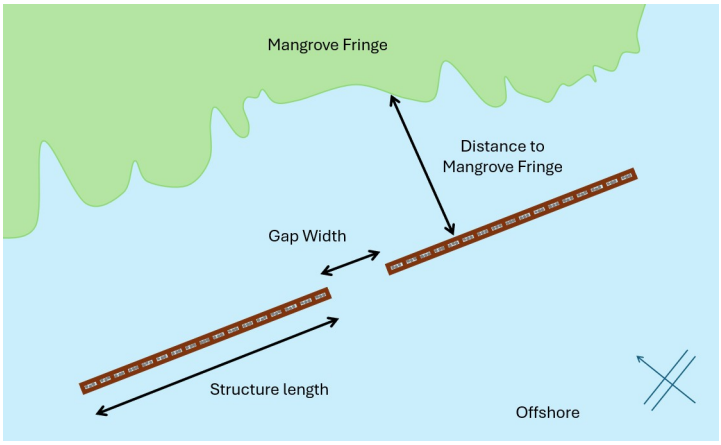

Figure 1.4: Schematisation of the design parameters considered in this study

The focus of this study is on understanding how the spatial design influences hydrodynamic conditions relevant to sediment transport and deposition. The assumption is that the current spatial layout of the breakwater is not optimal and may insufficiently promote sedimentation near the mangroves. It is expected that modifying its design could enhance flow and bed shear stress patterns in ways that strengthen sediment accumulation (compared to the current design), creating conditions favourable for mangrove restoration. The research questions are formulated below to address the research objectives.

Main Research Question
How do the spatial dimensions of the permeable breakwater affect the hydrodynamics controlling sediment dynamics relevant for mangrove restoration?

Sub-Questions

- Which hydro- and morphodynamic conditions favour mangrove restoration, and how do the area's characteristics fail to provide these conditions?
- How do the hydrodynamic processes potentially drive sediment transport and morphologic changes in the study area?
- Which design guidelines exist for breakwaters, and how does the current breakwater design compare to these guidelines?
- How does the current breakwater affect the maximum bed shear stress and flow pattern in the study area?
- How are the maximum bed shear stress and flow pattern influenced by the spatial dimensions of the breakwater?
- How do the modified hydrodynamics influence sediment transport and coastal erosion?

1.4. Research Methodology

The research methodology to answer the research questions consists of three main components: literature review, data collection, and numerical modelling.

Literature Review

A literature study was conducted to understand the problem context, identify knowledge gaps, and determine the required input data for modelling. Vietnamese partners contributed local insights to better define the problem and refine the modelling approach.

Data Collection

Data was obtained from various sources, including scientific publications, open datasets, and fieldwork conducted during a site visit to Bạc Liêu. During this visit, local knowledge was exchanged with stake-

holders, and additional bathymetric and hydrodynamic measurements were gathered as addition to existing data.

Data Analysis and Modelling

Field observations and measurements are analysed, and the current spatial design is compared to existing guidelines. The gathered data is used as input to create a Delft3D model of the study area. The model is first validated by comparing known states to determine whether it accurately represents reality, ensuring it is suitable for reliable research. Once validated, the processes in the current state of the area can be observed and analysed. Additionally, an assessment is carried out to evaluate the effects of modifications to the current design. These outputs are then analysed and combined with the data analysis to draw conclusions for the research.

1.5. Living Lab

This research is conducted as part of the Living Lab. The Living Lab for Mangroves is a partnership between TU Delft, Thuy Loi University (TLU), and Hanoi University of Natural Resources and Environment (HUNRE). The living lab in the Mekong Delta is a centre for gathering and sharing valuable knowledge and insights gained from diverse scientific field measurement campaigns conducted within the region. It also serves as a permanent physical site for showcasing a range of innovative solutions to relevant stakeholders. The Living Lab is both a research platform and a real-world demonstration site. It has two main goals: (1) improving knowledge about coastal processes through field experiments and monitoring, and (2) showing different coastal protection solutions to local communities and decision-makers in Vietnam [82]. This research supports the goals of the Living Lab by doing research to help restore mangroves. The focus is on reducing bed shear stresses, which will support sedimentation and create stable conditions for mangroves to grow. The data and findings of the research will be shared for possible further research.

1.6. Report Outline

This chapter introduced the research context, problem statement, objectives, research questions, methodology, and the Living Lab supporting this study. Chapter 2 reviews relevant literature on mangrove ecology, restoration conditions, and the functioning and design of detached permeable breakwaters. Chapter 3 describes the study area in Bạc Liêu, Vietnam, including its geographical characteristics, mangrove ecology, hydrodynamic conditions, and coastal interventions. Chapter 4 outlines the numerical modelling approach using Delft3D, elaborating on the model set-up, simulation scenarios, and the analysis of model outputs. Chapter 5 presents the results of fieldwork and modelling, focusing on the hydrodynamic responses to variations in breakwater design. Chapter 6 analyses all findings by answering the sub-questions and develops a conceptual framework. Finally, Chapter 7 draws conclusions by answering the research question and provides recommendations for future research.

2

Literature

The chapter provides a short summary of existing research on the study to understand what is already known and highlight the research gaps.

2.1. Mangroves

This section provides an overview of the available literature on mangrove ecology. The characteristics and requirements for mangrove restoration, and the conditions needed for their long-term survival are described.

2.1.1. Mangrove Ecology

Mangrove forests are found in muddy coastal intertidal zones of (sub)tropical regions. The intertidal zone lies between where the mean high water (MHW) and mean low water (MLW) levels intersect with the coastline [55]. A healthy mangrove habitat relies on a stable coastline that is in dynamic equilibrium between erosion and accretion [96]. Mangroves are characterised by their unique ability to thrive in tidal areas, which expose them to both salt and brackish water, as well as in soil with low oxygen levels [72][70]. Figure 2.1 provides an overview of the essential conditions for a mangrove habitat.

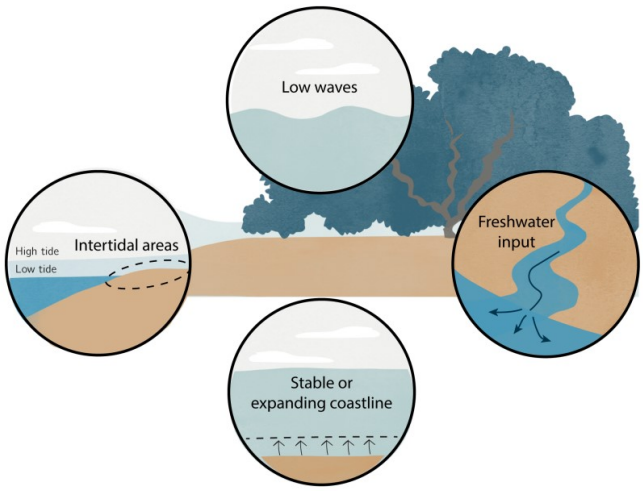

Figure 2.1: Schematic illustration of the conditions required for a mangrove habitat [44]

2.1.2. Mangrove Restoration

Mangroves are ecosystem engineers, they adapt their environments to facilitate their own persistence. For instance, their branches reduce wave energy and their roots strengthen the sediment bed. When mangrove forests are destroyed or removed, the environments change (weaker soil and/or stronger waves) and as a result, restoration can be very difficult. When natural or human causes altered the mangrove habitat, it is necessary to create favourable conditions for the mangrove seedlings to successfully establish and mature.

The ”Windows of Opportunity” (WoO) provides a systematic approach for understanding vegetation establishment under variable hydrodynamic conditions. WoO consists of two critical phases: WoO1, an initial inundation-free period that allows seedlings to settle their roots, and WoO2, a following period where bed shear stresses must remain below a critical threshold to support further root growth and resist hydrodynamic forces [4]. The critical bed shear stress threshold increases as seedlings grow, due to their root development and therefore their growing ability to withstand hydrodynamic disturbances [35]. Balke et al. [4] identifies three main thresholds for successful establishment of *Avicennia alba* on tidal flats: (1) The seedlings must develop roots during an inundation-free period, (2) root growth sufficient to resist hydrodynamic forces, and (3) protection from erosion during later development. These stages are illustrated in figure 2.2, with an expansion by Bijsterveldt, Griffin, Friess, et al. [7]. The original concept is extended by including two additional stages: (0) propagule limitations and (4) growth limitations, due to factors like predation, disease, or nutrient shortage.

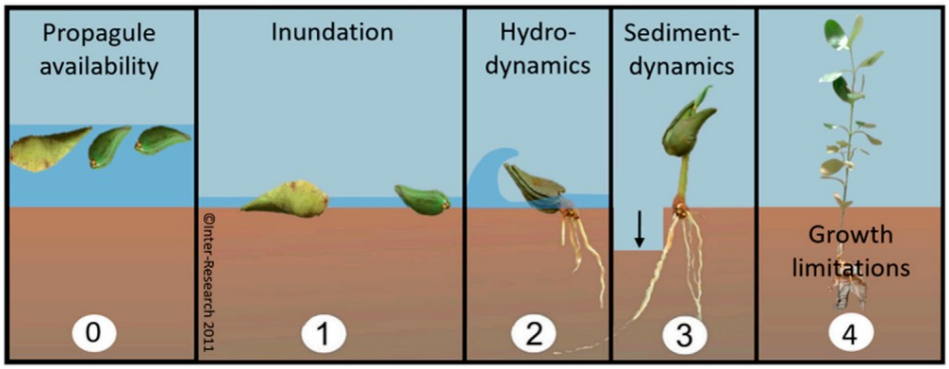

Figure 2.2: Stages in mangrove seedling establishment and growth, based on the Windows of Opportunity framework. Panels 0–3 reflect key physical thresholds to be overcome for establishment; panel 4 indicates potential growth limitations [4, 7].

These phases together highlight the importance of creating stable conditions that support the early survival. Hydrodynamic forces, primarily driven by tidal currents and waves, are a significant challenge to seedling survival, as bed shear stresses can uproot seedlings or destabilise sediment if root anchorage is insufficient. Tidal flat morphology plays an important role, regarding the bed shear stresses. Convex profiles, characterised by gentle slopes, dissipate wave energy more effectively, reducing bed shear stresses and creating more favourable conditions for seedling survival compared to steeper or concave profiles. The convex profiles also have a broader horizontal area at higher elevations, resulting in longer inundation-free periods that are crucial for seedling root establishment [35, 7]. The shape of these profiles is shown in figure 2.3.

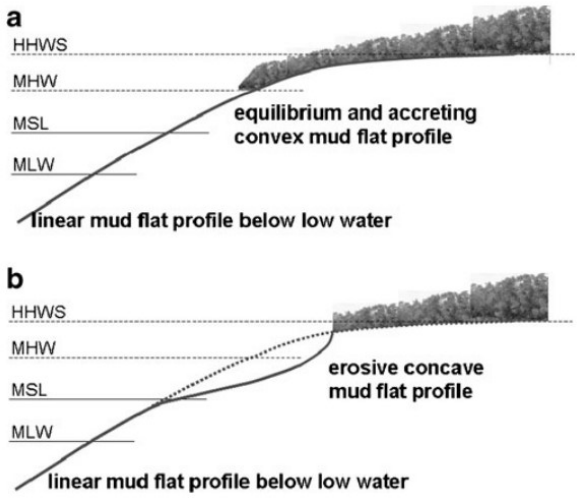

Figure 2.3: Comparison of convex (accreting) and concave (erosive) mudflat profiles in front of vegetation [97].

Providing stable conditions and having a suitable tidal flat for mangrove restoration also requires sediment stability, like the bed shear strength and grain size. Muddy areas with finer sediments have a lower critical shear stress, these areas are therefore easily eroded by bed shear stresses. Sandy areas have higher values, providing a more stable bed for mangrove seedlings. For mangroves restoration, the Windows of Opportunity with low bed shear stresses is important so seedlings can develop the roots without being washed away [22].

2.2. Detached Permeable Breakwater

This section provides an overview of the functioning and key design aspects of detached permeable breakwaters, including their impact on coastal hydrodynamics and sediment transport, with a focus on their role in mangrove restoration.

2.2.1. Coastal Processes and Breakwater Functioning

A coastline is stable when there is a dynamic equilibrium between sedimentation and erosion, as schematised in figure 2.4.

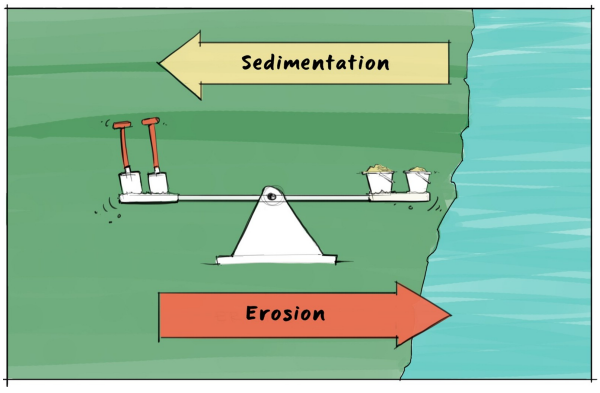

Figure 2.4: Schematisation of sediment balance under undisturbed conditions [95]

Sedimentation and erosion are driven by a combination of wave action, tidal currents, and sediment transport [96]. Variations in the global climate, such as increased storm activity, can affect the spatial distribution of sediment along the coast by these waves and currents. Additionally, the sediment balance can be disrupted by activities such as sand mining and upstream dams in a river, which removes

sediment from the system and reduces the sediment supply [44]. When the sediment supply is higher than the erosive processes, the coastline is accreting. But when the sediment supply can not keep up, the coast is eroding. A breakwater can be placed to mitigate the erosive processes, restore the sediment balance and create a stable coastline [95]. When mangrove areas have become sub-tidal, detached permeable structures can be used to reduce erosion. These structures attenuate waves and can support sedimentation, creating better conditions for mangroves restoration, as illustrated in figure 2.5 [44].

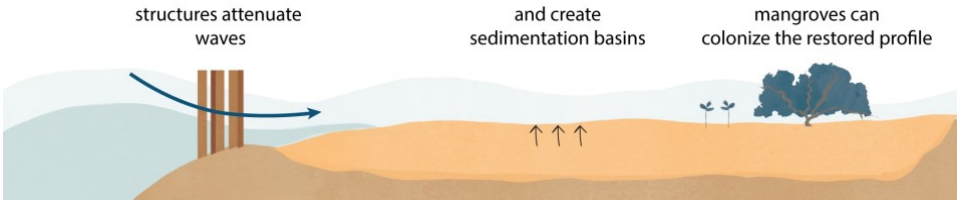

Figure 2.5: Schematic illustration of the functioning of a permeable breakwater [44]

By reducing the wave energy, a shadow zone is created where sediment accumulates. However, this interruption in sediment transport can cause erosion further along the coast due to sediment starvation. These effects depends on the breakwater design and local conditions [8].

Permeability

A permeable breakwater is designed to dissipate wave energy while allowing some water to pass through it [100]. The permeability of a breakwater affects currents, waves and sediment transport [44]. Permeable breakwaters let some waves pass, gradually reducing their height, and maintaining water flow and sediment transport. Higher permeability improves sediment transport but weakens the wave attenuation, creating a higher-energy area where sediments may not be able to settle down. Impermeable breakwaters significantly reduce wave energy but can disturb the natural sediment transport [95].

Diffraction

Wave diffraction is important in determining how wave energy propagates around and through gaps in breakwater structures. Diffraction occurs in the lee of the breakwaters on both sides of the gap [8]. When a wave propagates through a breakwater gap, it bends into the shadow zone behind the structure, influencing wave attenuation and sediment transport patterns [88]. This process is illustrated in the figure 2.6.

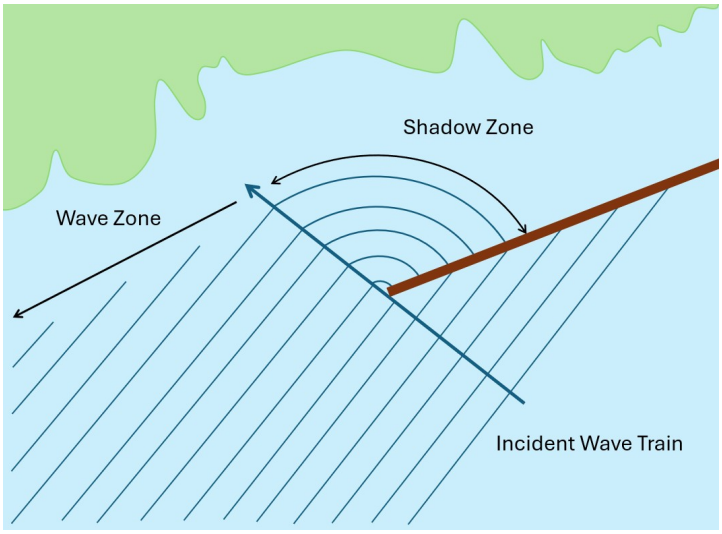

Figure 2.6: Schematisation of wave diffraction caused by a detached breakwater.

The amount of diffraction depends on the gap width relative to the incoming wavelength. A smaller gap causes more diffraction, spreading out the wave energy more evenly, while larger gaps allow more direct wave penetration into the protected area [42]. The wave ray at the boundary between the shadow zone and the wave zone experiences a reduction in wave height due to the lateral transfer of wave energy. According to the linear wave theory, for a constant depth, the reduction of the wave height is approximately 50% for regular waves and 30% for irregular directional waves. As waves move further into the shadow zone, their height decreases. The amount of wave energy that reaches the area behind an obstacle depends on the ratio of the structure length to the wavelength. If the breakwater is small compared to the wavelength (wave length / structure length « 1), the wave energy reaches the entire shadow zone. But for a long breakwater, diffraction occurs mainly around its ends, which limits the energy behind it. When waves pass through a gap between two breakwaters, diffraction happens on both sides. If the gap is large, the diffraction patterns remain separate, but for smaller gaps widths, they may interact [8]. The balance between wave diffraction, wave dissipation and wave reflection determines the amount of wave attenuation [73].

Flow Pattern

Detached permeable breakwaters influence nearshore hydrodynamics by modifying the wave energy and current patterns. Permeable structures allows flow through gaps and porous elements. These openings create spatial variations in pressure and velocity, especially when combined with gradients in water surface elevation and bathymetry [8]. An important hydrodynamic effect of narrowing is the acceleration of flow, which can occur either due to structural narrowing or a local reduction in the seabed. This can be described by Bernoulli's principle for inviscid, steady, and incompressible flow [11]. Assuming negligible height differences, Bernoulli's equation simplifies to:

$$\frac{1}{2}\rho v^2 + p = \text{constant} \tag{2.1}$$

where ρ is the fluid density, v is the flow velocity, and p is the pressure. As the flow enters a narrower or shallower region, the pressure must decrease or the velocity must increase to conserve energy. The velocity through a breakwater gap can also be estimated from the difference in water surface elevation between the offshore and onshore sides:

$$v = \sqrt{2g\,\Delta\eta} \tag{2.2}$$

with g the gravitational acceleration and $\Delta\eta = \eta_{\text{offshore}} - \eta_{\text{onshore}}$ the surface elevation gradient driving the flow [11]. This locally accelerated flow forms a jet that propagates into the sheltered area behind the breakwater. Due to momentum exchange with the surrounding slower moving water, this jet induces a horizontal recirculation pattern. Flow exiting the gap spreads sidewards and curls back toward the structure, creating two eddies on either side of the jet axis. These vortices contribute to sediment redistribution and mixing in the area behind the breakwater. The strength and extent of this circulation depend on the width of the gap, the water depth, and the incident wave or pressure conditions [8, 103]. This happens at a smaller scale for flow passing through the porous elements of the breakwater, where small jets and local eddies are formed. However, the flow passing through the larger gaps between the segments leads to larger scale circulation patterns and is important for the sediment transport [103]. These larger scale acceleration and circulation patterns, caused by the breakwater gap, is schematised below in figure 2.7.

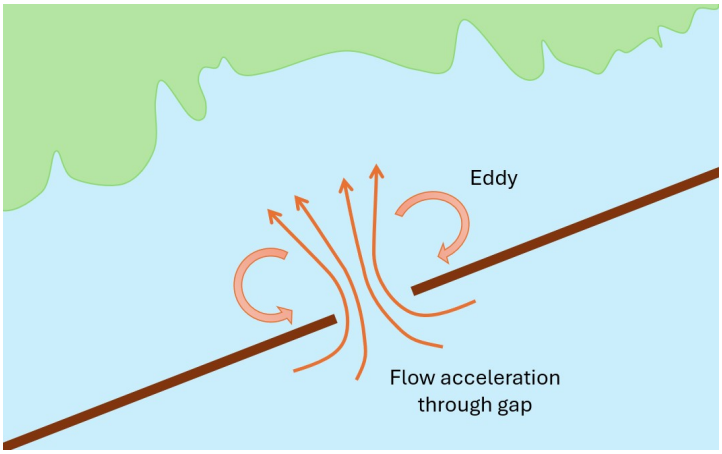

Figure 2.7: Schematisation of current patterns caused by narrowing at a breakwater gap.

These sediment redistribution can create local bathymetry features such as bars or channels which affect where waves break and where wave set-up occurs, which in turn changes the horizontal pressure gradients. These gradients interact with the breakwater and can either increase or reduce the flow through the gaps. In areas behind the breakwater where flow velocities are lower, sediment is more likely to settle and build up. On the other hand, areas with higher flow velocities near the structure can lead to scouring [29].

2.2.2. Spatial Dimensions

The gap width, structure length, and distance of the breakwater from the shore are very important design parameters that influence the hydrodynamics and morphodynamics.

Gap Width

Smaller gap widths between breakwaters limit wave energy penetration, creating calmer conditions behind the structures and promoting sediment deposition [14]. However, very small gaps may increase flow velocities and limit tidal flow, leading to reduced sediment resuspension, which can lead to less sediment transport [104]. Larger gap widths allow greater tidal exchange and sediment transport between the breakwaters and open water [88]. However, if the gaps are too wide, wave energy may enter the sheltered area with minimal dissipation, reducing the effectiveness of the breakwater system in reducing bed shear stresses [42].

Structure Length

The structure length determines the size of the sheltered zone and the amount of wave attenuation. Longer breakwaters provide more protection by dissipating wave energy over a larger area and creating larger shadow zones [71]. However, very long breakwaters can disrupt natural sediment transport, leading to erosion or deposition patterns further along the coast. Shorter breakwaters allow for more localised wave attenuation while maintaining a stronger connection with the hydrodynamics, which supports natural sediment transport processes [88]. Studies indicate that an optimal balance between breakwater length and gap width is necessary to prevent excessive sediment trapping while ensuring sufficient sediment supply to adjacent areas [42].

Distance to Shore

The distance of the breakwater from the shore influences how wave energy interacts with the coastline. Nearshore breakwaters provide direct shoreline stabilisation by reducing wave impact in critical erosion zones but may require more frequent maintenance due to sediment accumulation [73]. These structures often create more immediate and stronger sedimentation, which can be beneficial for coastal restoration projects. Offshore breakwaters, positioned further from the coast, allow for a more gradual reduction of wave energy, facilitating natural sediment transport and the formation of stable sandbanks and mudflats [9].

2.2.3. Sediment Resuspension

The spatial design of permeable breakwaters strongly affects hydrodynamics, influencing sediment resuspension and deposition patterns behind the structure. The flow velocities combined with the near bed orbital wave velocities, stir up sediments once critical the bed shear stress is exceeded, which depend on sediment characteristics such as grain size and cohesion [4, 88]. The wave orbital velocities are oscillatory water particle motions beneath the surface, created by waves [8]. Additionally, waves breaking near the mangrove edge generate turbulence and wave-driven currents, creating sediment resuspension [96]. These processes are schematised below in figure 2.8. The resuspended sediments are transported by the flow toward zones with a lower bed shear stress where they can settle down [44, 7].

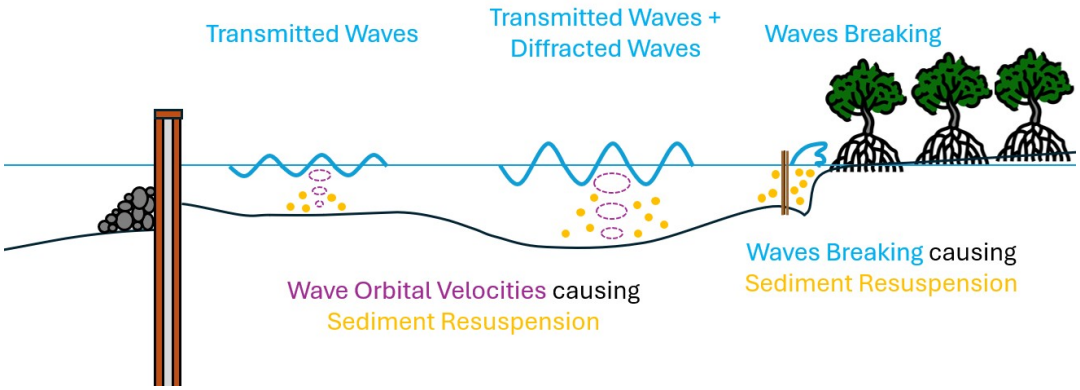

Figure 2.8: Schematisation of sedimentation resuspension caused by wave energy

The response to hydrodynamic forcing differs between sandy and muddy environments. In sandy settings, sediment transport is mainly initiated when the bed shear stress exceeds a relatively critical threshold, with transport dominated by bedload and more short-term events. In contrast, muddy sediments have cohesive properties, meaning resuspension depends not only on the magnitude of bed shear stress but also more on the duration. Even moderate bed shear stress, if sustained, can gradually resuspend and erode fine particles, which remain in suspension longer due to their lower settling velocities [8].

For sediment to accumulate behind the breakwater, there must be a net inflow of suspended sediment. This occurs mainly through the gaps and permeable parts of the structure. The design of gaps and porosity controls the sediment inflow by influencing flow speeds and pressure differences across the structure [95]. Gaps allow tidal inflow of water with suspended sediments, while the permeable sections reduce wave energy and enable gradual flow through the structure.

2.2.4. Design Guidelines for Breakwaters

Several studies have been carried out to establish criteria for the optimal arrangement and use of permeable structures in relation to waves, currents, and morphodynamics. However, these structures often fail to accumulate sediments effectively, likely due to unclear design guidelines and limited understanding of how design parameters, such as the length of the structure and the size of gaps between them, influence their performance [44]. The study of Mussert [52] aimed to create an integrated design guideline for brushwood fences, which is a permeable structure, to support mangrove habitat rehabilitation along eroding coastlines. Additionally, the study aimed to create an understanding of how design parameters impact the effectiveness of these structures by simulating various configurations in a numerical, process-based model and evaluating their performance in reducing bed shear stress in the protected areas behind them.

It is important to distinguish between breakwater design guidelines for sandy and muddy coasts. Most traditional guidelines, including those for tombolo or salient formation (based on length-to-distance

ratios), were originally developed for sandy coastlines where longshore sediment transport is wave-dominated [10]. A tombolo is a sandbar that fully connects the breakwater to the shore, while a salient is a sediment accumulation behind the breakwater that does not fully connect the breakwater and shore [8]. These guidelines typically aim to interrupt and trap sand transported along the coast. For instance, Bricio, Negro, and Diez [10] and Khuong [38] studied detached impermeable breakwaters and the shoreline responses to the spatial dimension parameters on predominantly sandy coasts. In contrast, muddy coasts are characterised by fine, cohesive sediments with limited longshore transport, often dominated by suspended sediment transport during tidal flows or wave resuspension [29]. Therefore, applying design criteria developed for sandy coasts directly to muddy environments is not always appropriate. Guidelines specifically tailored for muddy environments remain limited, but some important insights have emerged. For example, muddy coasts require lower bed shear stress for sediment to settle and breakwaters must create sufficiently calm conditions over a broad area behind the structures to allow deposition of fine sediments [95]. Additionally, Winterwerp et al. [98] emphasises that in muddy environments, stakeholder involvement and system understanding are crucial, as the sediment dynamics and ecological conditions are more complex and slower to respond [98].

The evolution of coastal morphodynamics depends not only on the spatial dimensions of the structure but also on other characteristics, such as structural properties and environmental factors like hydrodynamics and sediment properties [8]. Winterwerp et al. [98] highlighted three important factors for the successful functioning of permeable breakwaters. First, it is important to understand how the physical and biological systems work. Second, patience and regular maintenance are needed because mangrove recovery takes many years. Lastly, involving stakeholders throughout the project is essential for success.

Table 2.1 summarises some existing design guidelines for permeable breakwaters based on the reviewed studies, highlighting typical ranges and their influence on hydrodynamic and sedimentation processes.

Table 2.1: Design Guidelines for Permeable Breakwaters (Mainly derived from Mussert [52] and Wilms, Wesenbeeck, and Tonneijck [95])

Parameter	Permeable Structures
Distance to Shore (D)	
Typical Range	80-230 m
Effective Range	$D < 198$ enhances bed shear stress reduction
Additional Insights	+33 m reduces bed shear stress by 3%
Structure Length (L)	
Typical Range	60-240 m
Ratio	$L/D > 1.3$ (Tombolo), $0.5 < L/D < 1.3$ (Salient)
Additional Insights	+66 m reduces bed shear stress by 5%
Gap Width (G)	
Typical Range	10-100 m
Ratio	$L_{\text{gap}}/L > 1 - 1.5$
Additional Insights	+66 m reduces bed shear stress by 2%

Similarly, table 2.2 presents some existing design parameters for impermeable breakwaters.

Table 2.2: Design Guidelines for Impermeable Breakwaters (mainly derived from Khuong [38], Bricio, Negro, and Diez [10], and Bosboom and Stive [8])

Parameter	Impermeable Structures
Distance to Shore (D)	
Typical Range	20-610 m
Effective Range	$XB/LB < 1$ (Tombolo), $XB/LB > 1$ (Salient)
Additional Insights	Most common: 60, 100, 160 m offshore [10, 38]
Structure Length (L)	
Typical Range	15-1000 m
Additional Insights	Common lengths: 40–120 m
Gap Width (G)	
Typical Range	10–100 m
Ratio	$GB/XB < 0.8$ (No erosion), $GB/XB > 1.3$ (Erosion)
Additional Insights	5-10 % of front structure length

3

Study Area

This chapter describes the mangrove ecology, hydrodynamic conditions, and coastal interventions in the Mekong Delta, with a focus on the study area at the coast of Bạc Liêu province.

3.1. Mekong Delta

This section outlines the ongoing environmental challenges in the Mekong Delta and how they contribute to mangrove loss and coastal vulnerability.

3.1.1. Challenges in the Mekong Delta

The Mekong Delta, situated in the southern region of Vietnam, spans an area of approximately 41,000 square kilometers. Over 17 million people are living in this area [92]. The Mekong Delta is the largest wetland in Vietnam and is formed between 6,000 and 8,000 years ago through alluvial deposition from the Mekong River. These large sediment fluxes expanded the delta seaward for the last 3,500 years. The Lower Mekong Delta (LMD) is shaped by these sediment fluxes, land-holding mangrove forests, and the hydrodynamics of the sea [83]. Partly due to its fertile land, this region plays a critical role in Vietnam's agriculture, aquaculture, and overall economic development. However, it is also facing significant environmental challenges, like land subsidence and coastal erosion [77].

Erosion in the Mekong Delta coast is driven by natural and human factors, like sediment dynamics, reduced river sediment supply, mangrove loss, blocked sediment flow, and land subsidence [2]. The main causes of reduced sediment supply coming from the Mekong are the shortage of fine sediment caused by upstream dams, the shortage of coarse sediment due to extensive sand mining downstream, and historic channelisation of the delta [21, 40]. The coastal erosion is leading to the shrinking of the Mekong Delta by approximately 500 hectares annually [21]. A natural contributor to ongoing subsidence is the rapid compaction of soil. In addition, extensive groundwater extraction plays a major role in subsidence. This effect can be observed in Ho Chi Minh City, where extensive groundwater extraction has led to noticeable subsidence rates [86, 56]. The current subsidence rate in the Mekong Delta due to groundwater extraction is approximately 1.1 to 1.6 centimeters per year, which could result in up to 1 meter of inundation by 2050. This is concerning taking into account the sea-level rise and that the delta lies 1 to 2 meters above sea level [25]. As a result, the Mekong Delta is becoming increasingly vulnerable to flooding, while also salinisation of both surface water and groundwater is intensifying [18]. Saltwater intrusion now extends up to 90 km inland, threatening agriculture and freshwater availability. This is mainly driven by upstream dams, subsidence, and sea-level rise. Typhoons further increase these risks, bringing storm surges and heavy rains, with past events causing surges of 1 to 2 meters along the coast. [25]

3.1.2. Mangroves Losses

The largest total loss of mangroves occurred in Asia [4]. In Vietnam, the mangrove area decreased by 92.72 km² between 1996 and 2020. As of 2020, Vietnam had 1,871.47 km² of mangroves, covering

25.25% of its 18,010.98 km coastline [91]. In the Mekong Delta, the mangrove area decreased from 185,800 ha in 1973 to 102,160 ha in 2020. This loss is mainly due to aquaculture expansion, which caused a reduction of 2,150 ha per year, and coastal erosion, which resulted in an annual loss of 430 ha [68]. Mangrove forests in the Mekong Delta play an important role in protecting the coastline by preventing soil erosion and dissipating strong waves. They also provide essential resources such as seafood and help store carbon. However, they are under increasing pressure from various factors, including the expansion of aquaculture, weak enforcement of policies, lack of financial support, urbanisation, and poor site selection for restoration [12, 80]. Factors like pollution, land use change, sediment shortage, coastal erosion, and mangrove squeeze hinder the coasts to provide the favourable conditions for the mangroves. Since 2010, several projects are implemented in the Mekong Delta by organisations and the Vietnamese government as an attempt of mitigating the coastal erosion and therefore restoring the mangroves. These projects have led to a small increase in mangrove area, but the success rate is relatively low [68].

3.2. Bạc Liêu

This section describes relevant aspects of the study area in Bạc Liêu, located in the Mekong Delta.

3.2.1. Location

Bạc Liêu is one of the twelve provinces of the Mekong Delta. The coastline is at the South China Sea and is affected by coastal erosion. The research area is located on the part of Bạc Liêu's coast that is currently eroding, as shown in figure 3.1. This ongoing erosion is contributing to the degradation of the mangroves in the area.

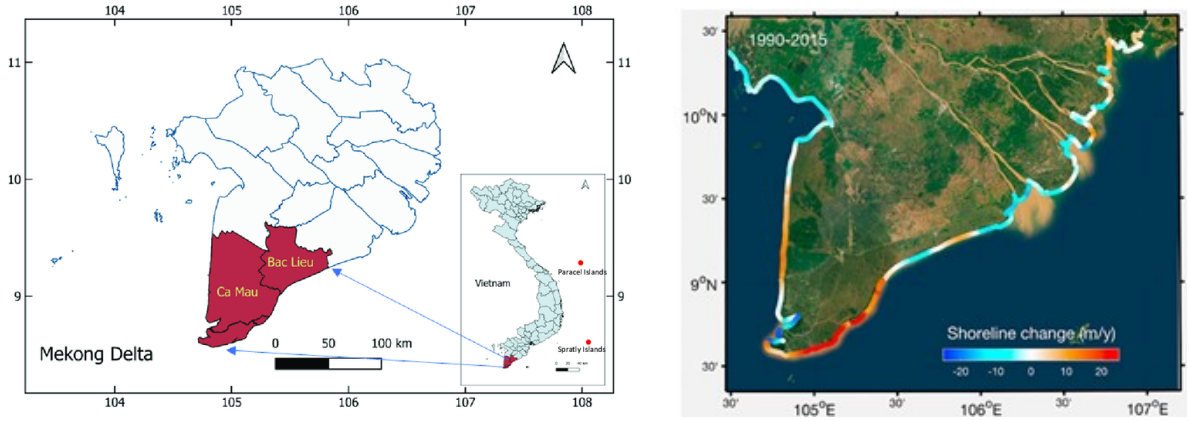

(a) Location of the province Bạc Liêu in Vietnam[53]

(b) Shoreline change rate between 1990 and 2015[46]

Figure 3.1: The location of the province Bạc Liêu and the corresponding shoreline erosion rates, indicating coastal retreat.

The retreat of the mangrove fringe over time in the study area is shown in figure 3.2, illustrating the ongoing degradation at the coast. Between 2006 and 2024, the mangrove fringe has retreated by approximately 140 meters, which corresponds to an average retreat rate of around 8 meters per year, based on the satellite images from these three years. The main reasons for the degradation of mangrove forests in the area is human-induced coastal and estuarine squeeze due to aquaculture and/or agricultural over-exploitation [67, 34], and coastal erosion due to natural causes [65]. Another important reason is the probable decrease in sediment supply coming from the Mekong (branches) [69].

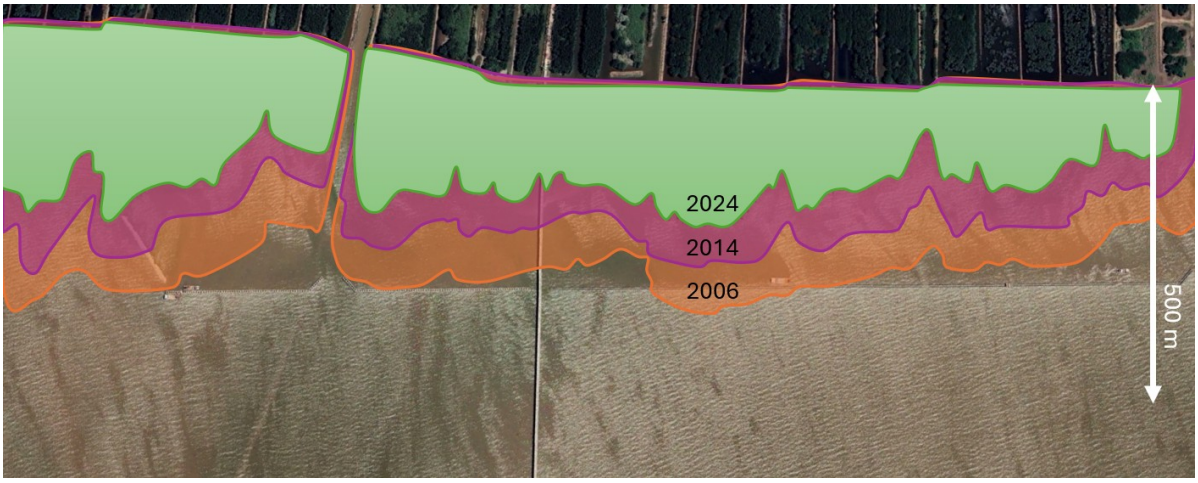

Figure 3.2: Shoreline retreat of the mangrove fringe at the Bạc Liêu coast between 2006 and 2024. The coloured outlines indicate the position of the vegetation edge in different years, showing landward migration and loss of mangrove area over time. The scale bar represents 500 metres.

3.2.2. Mangroves Ecology in Bạc Liêu

Vietnam has 33 mangrove species, which are distributed along the coastline and play an important role in supporting diverse coastal ecosystems [91]. In Bạc Liêu, the dominant species are *Avicennia alba (A. alba)* and *Rhizophora apiculata (R. apiculata)*. *A. alba* is well-adapted to saline environments and has the ability to a rapid growth, making it effective in stabilising coastal sediments. *R. apiculata* has robust stilt roots that improve shoreline protection by dissipating wave energy [30]. Due to these properties, *A. alba* species dominate the seaward zones due to their high tolerance for salinity and frequent inundation, whereas *R. apiculata* species are more common landward, succeeding in more stable conditions [47].

Seedlings typically establish on gently sloping mudflats in the intertidal zone, specifically between mean sea level (MSL) and mean high water (MHW), where inundation-free periods occur naturally during tidal cycles [4, 28]. The specific elevation for further growth after seedlings accomplishment depends on the species. Loon et al. [41] created a hydrological classification of common Southeast Asian mangrove species, which is shown in figure 3.3.

class -	*elevation* *[cm + MSL]*	duration of inundation [min per day]	duration of inundation [min per inundation]	species -
1	*<0*	>800	>600	none
2	*0–50*	400–800	450–600	*A. alba* Blume, *Sonneratia sp.*
2*	*50–100*	250–400	200–450	*Avicennia sp.*, *Rhizophora sp.*, *Bruguiera sp.*
3	*100–150*	150–250	100–200	*Rhizophora sp.*, *Ceriops sp.*, *Bruguiera sp.*
4	*150–210*	10–150	50–100	*Lumnitzera sp.*, *Bruguiera sp.*, *Acrosticum aureum* L.
5	*>210*	<10	<50	*Ceriops sp.*, *Phoenix paludosa* Roxb.

Figure 3.3: Hydrological classification of common Southeast Asian mangrove species [41]

3.2.3. Interventions in Bạc Liêu

Over the past decades, several coastal interventions have been implemented in Bạc Liêu province to support mangrove restoration. This section describes these interventions and the current intervention in the study area, namely the pile-rock breakwater.

Past Interventions

Because the coast of the Mekong Delta was seen as a economic potential area, regarding the agriculture and aquaculture, the area needed to be protected from the sea. Dike systems were built behind the mangroves, but not all turned out to be effective. This was, among others, the case for the system at Bạc Liêu. The coastal processes vary a lot between different parts of the coast in the Mekong Delta, so there is not one type of design of an intervention showing effectiveness always [69].

Due to the complexity of addressing and solving the main causes of the erosion, it is important to explore solutions that mitigate its effects and enables to restore. Nature-based interventions such as dredging have not yet been considered politically, primarily because Vietnam currently lacks a dredging-nourishment industry, so different interventions are considered [69]. Multiple interventions have been implemented over time along the Mekong Delta coast. The most efficient intervention so far is the Pile-Rock Breakwater (PRBW), which is also the current intervention in the specific study area, illustrated in figure 3.4. However, the structure in the study area shows inefficient sediment trapping close to the mangrove fringe. It is also a suitable research area, as it provides optimal conditions for field measurements. The location is at the Hòa Bình wind farm, where equipment can be installed offshore using the pier and is secured under the supervision of the wind farm's management (appendix A.3).

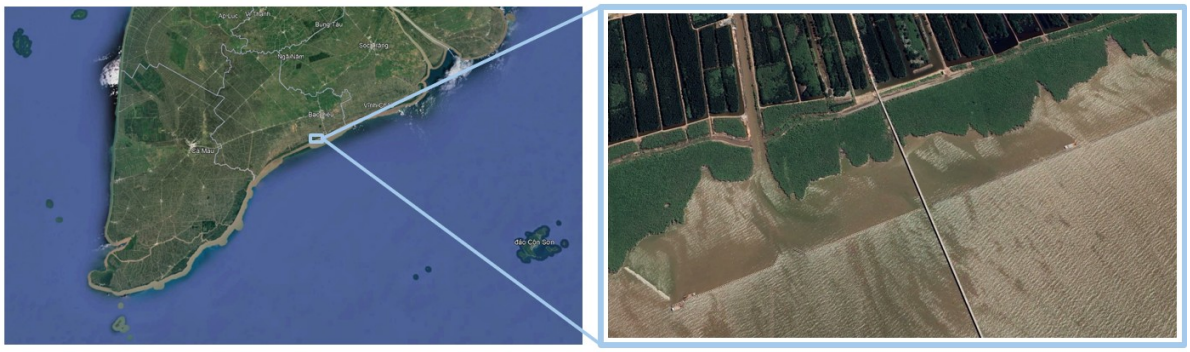

Figure 3.4: Location of the study area in Bạc Liêu province, Mekong Delta (left), and a close-up image showing the mangrove fringe and the current breakwater along the coast (right) [23].

Pile-Rock Breakwater

The current intervention in the study area is the Pile-Rock Breakwater (PRBW), shown in figure 1.3, a permeable coastal structure designed to reduce wave energy and promote sediment deposition. It consists of two parallel rows of pre-stressed concrete piles and is filled with crushed rocks. The rows are spaced about 2 meters apart. Melaleuca poles are placed at the base to prevent the rocks from sinking into the soft, muddy bed. Initially, reinforced concrete beams were used at the ends, but were eventually replaced by steel beams to reduce costs and allow easier relocation as the mudflat expands [69]. A typical cross section of the structure is shown in figure 3.5, which includes melaleuca mattresses, a geo-textile layer, and concrete beams. In the study by Xuan et al. [101], which focused on this specific PRBW design, the structure was given a porosity of 44%, representing its permeability. PRBWs are particularly effective in deltaic muddy environments [101].

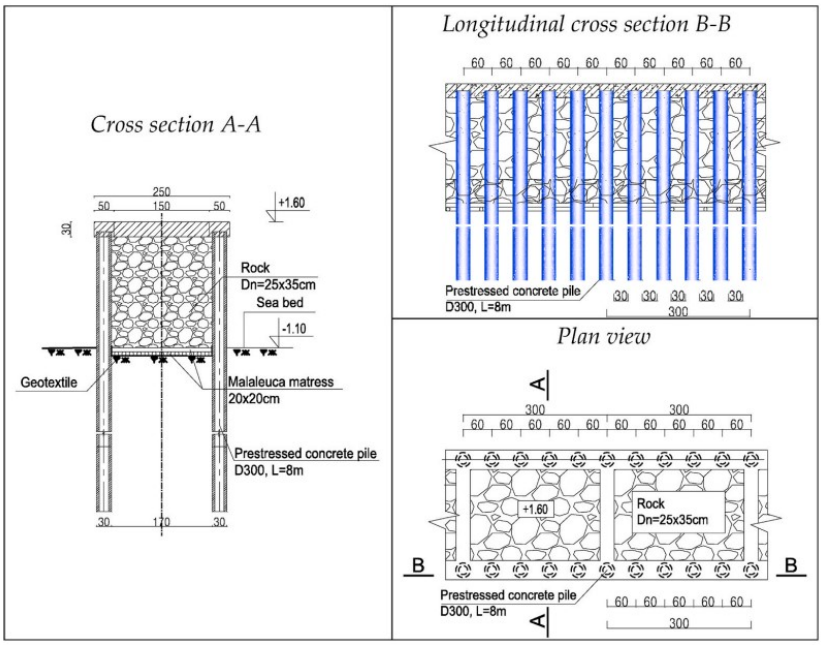

Figure 3.5: Cross sections of a PRBW structure [101]

The breakwaters are placed parallel to the coast and include gaps between sections to allow water exchange between the sheltered area and the open sea. However, the effectiveness of these gaps in supporting sediment dynamics and reducing erosion has not been fully evaluated [69]. Research by Nguyen et al. [58] on a PRBW using experimental and numerical models shows that gap placement strongly influences velocity fields, sediment transport, and shoreline morphology. Gaps can modify flow velocities and wave energy behind the structure, potentially impacting erosion in some cases. However, under low-energy conditions, they can enhance sediment supply and support accretion. PRBWs are particularly effective at dissipating short-period waves [101].

3.2.4. Hydrodynamics

The dominant wave, tidal, and current conditions in the study area are described below.

Wind and Waves

The climate in the Mekong Delta is formed by the monsoons, which is a seasonal shift in the dominant wind direction [54]. This climate has two main seasons, namely the winter and summer. The winter is the dry season during from December to April. During winter, there are high energy waves generated by the Northeast monsoon, having a wave height of around 0.5 to 1.5 meters and periods between approximately 4 and 5 seconds [25]. The average wind speed during winter is around 4.6 m/s [57]. The summer, also known as the rainy season, lasts from May to November. The Southwest monsoon during this period generates low energy waves with a wave height of 0.2 to 0.8 meters. The corresponding wave periods are between 3.5 and 5 seconds [25]. The mean wind speed during summer is around 3.6 m/s[57]. The waves approaching the shore experience a lot of depth-induced energy loss, it namely has an average slope of approximately 1/500 [87].

Tide

The tidal regime along the Bạc Liêu coast is mixed but predominantly semi-diurnal, while in most of the South China Sea there is a diurnal regime [66]. A diurnal tide has one high and one low water per day due to dominant diurnal tidal constituents, while a semi-diurnal tide has two high and two low waters per day driven by dominant semi-diurnal tidal constituents [8]. This variation may result from shoaling and resonance of the M_2 semi-diurnal component [65]. So the study area experiences a mixed macro-tidal regime, combining both diurnal and semi-diurnal patterns, leading to irregular water level fluctuations over 24 hours. Tidal amplitudes can reach up to 3.8 meters, with a mean amplitude of 2.5 meters, approaching macro-tidal conditions. This mix results in complex tidal patterns, with diurnal inequality

where sequent high and low tides differ in height [99]. Phan et al. [66] and Phan [65] computed the tidal velocities during the falling and the rising period, showing the a nodal point near Bạc Liêu province. This point is causing tidal flow velocity patterns perpendicular to the coast as shown in figure 3.6.

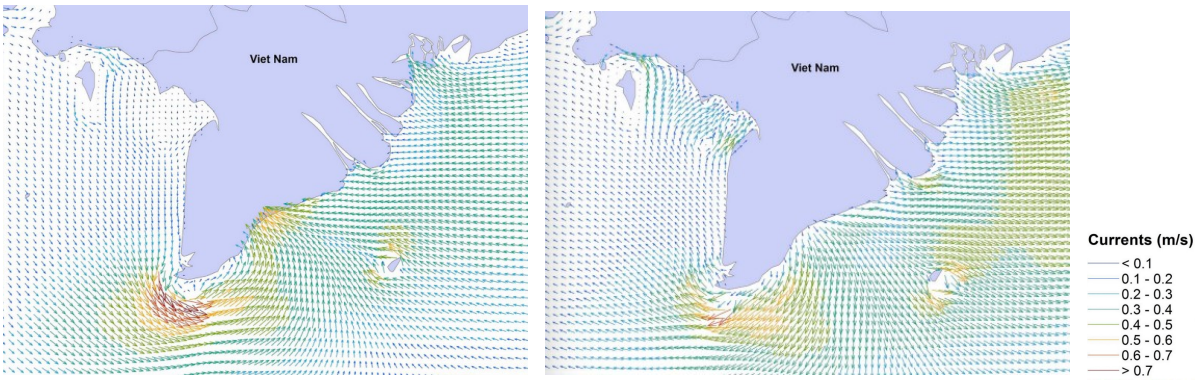

(a) Tidal flow velocities during the rising period

(b) Tidal flow velocities during the falling period

Figure 3.6: Tidal flow velocities at the coast of Bạc Liêu during the rising and falling tide, based on model results by Phan et al. [66]. The velocities show a nodal point near the study area, resulting in predominantly shore-perpendicular tidal currents. Flood flows are stronger than ebb flows, indicating a flood-dominant system.

Currents

The computed tide-induced residual currents by Phan et al. [66] and Phan [65] are relatively weak, reaching only a few centimeters per second southward. However, these currents are strongly influenced by monsoon winds, generating a southward flow of 2–4 cm/s during winter, while reversing to a weaker northward flow of 0–1 cm/s in summer [25]. A different study by Marchesiello et al. [46] reported a stronger southward current with higher velocities. While the exact velocities remain uncertain, the general direction of the annually averaged longshore current aligns between both studies. Longshore transport is generally considered the dominant mechanism for sediment redistribution along the Bạc Liêu coast, with cross-shore processes playing a secondary role [69, 25]. Fine-grained sediments from the Mekong River mouths are transported into the sea and therefore subsequently transported Southwest by the dominant longshore currents [106]. The coastal zone at Bạc Liêu consists mainly of cohesive, fine-grained sediments such as silt and clay, which is typical for the muddy coasts of the Mekong Delta [25, 69].

4

Modelling

This chapter describes the numerical modelling approach used to assess the effect of the existing breakwater and variations in its spatial design on the nearshore hydrodynamics.

4.1. Delft3D

To assess the impact of different spatial designs of the Pile-Rock Breakwater (PRBW) on local hydrodynamics, a numerical model is built using Delft3D. Delft3D is a numerical model developed by Deltares, designed to simulate flow, waves, sediment transport, and other coastal and riverine processes [1]. It supports both depth-averaged (2DH) and fully three-dimensional (3D) simulations. This study uses Delft3D-4, which applies a structured grid system. A nested grid approach is used, where a high-resolution grid is placed around the PRBW to resolve local hydrodynamic conditions, while a coarser grid is used farther offshore to reduce computational time [20]. This setup allows for a detailed analysis of flow and wave behaviour near the structure while keeping the model efficient. The model couples the FLOW module for tidal currents and water level variation with the WAVE module, which is based on the SWAN model, for short-wave propagation [16, 17]. This coupling makes it possible to evaluate how changes in the spatial layout of the PRBW affect wave energy reduction and current patterns.

Relevant Processes and Model Assumptions

The numerical model is developed for this research to simulate the changes in dominant physical processes when varying the spatial design parameters influencing the hydrodynamics relevant for sediment dynamics. The model is developed to represent only the most relevant physics, and therefore simplifications have been made. The most important simplification is that only hydrodynamics are computed, and not sediment transport or morphological changes. Instead, the hydrodynamics are interpreted in terms of potential erosion (and changes therein). This is motivated by the high degree of complexity in modelling sediment transport in a mud-dominated area, such as the Bạc Liêu coast, in combination with the available time.

Processes that are less influential or require detailed data that is not available are excluded. The model includes short-wave propagation using the WAVE module (SWAN), and tidal currents and water level variations through the FLOW module. A morphostatic approach is applied, meaning the bed level remains fixed during simulations, and sediment transport and morphodynamic feedbacks are not included. Baroclinic processes caused by salinity and temperature gradients are probably much less important than tidal flows, and are therefore not included. Wind is not used to drive currents (in the FLOW module), but is used to compute wave generation (in the WAVE module). River inflow and local structures, such as the bridge columns above the main breakwater gap, are excluded. These may locally affect the flow but fall outside the model resolution and scope. Waves are modelled using SWAN, accounting for wave growth by wind, depth-induced breaking, and energy losses by bottom friction. The wave model is primarily used to evaluate wave-driven bed shear stress (representing sediment resuspension). Wave–current interaction is switched off because wave-induced breaking is probably limited (relatively small waves) and because waves largely refract normal to the coast due to

the wide delta front. Both the wave direction and height will likely result in relatively weak wave-driven currents. Wave diffraction is not included. Long-period and infragravity waves, which were observed in the field, are also excluded, as SWAN does not resolve these processes in combination with a permeable breakwater. Lastly, ecological processes, such as vegetation growth and root resistance, are not represented in the model.

4.2. Modelling Steps

These modelling steps ensure that the model accurately simulates the relevant physical processes in the study area, so it is capable of identifying the impact of design changes on the area.

Step 1: Validation and Calibration

To ensure the model is accurate and reliable, tidal levels and wave propagation are validated using field data, including pressure sensor measurements from the study site. The selected offshore data for the validation matches the time and interval of the reliable wave pressure gauge dataset. These conditions are stored in a wavecon file to allow time-varying conditions in Delft3D. The model output at the gauge location, obtained using an observation point, is compared with the wave pressure gauge data. Validation will start with FLOW only, to check tidal water levels. Then, FLOW and WAVES will be run together to validate wave conditions. The model's bathymetry and PRBW structure properties will be based on field measurements.

Step 2: Reference Scenario Analysis

The reference case focuses on analysing the effect of the existing PRBW structure on bed shear stresses and current patterns under different forcing conditions. To assess the impact of the PRBW, simulations will be performed for both the current situation (with the structure) and a scenario without the structure, providing a direct comparison of hydrodynamic changes. By comparing the results from the simulations with and without the PRBW structure, the specific effects on flow patterns and bed shear stresses can be identified.

Step 3: Sensitivity Analysis

A sensitivity analysis will be conducted to assess the impact of varying key parameters on hydrodynamic conditions behind the PRBW. The parameters will be adjusted separately in order to clearly identify the cause of the system's response and understand the individual impact of each design factor.

The key parameters considered in this analysis include:

- **Structure length and gap width**: These parameters are interdependent, meaning that changes to one will also affect the other.
- **Distance to shore**

All design alternatives will be tested under different forcing conditions, including summer, winter, and storm scenarios. Each simulation will run for four days during a spring tide, which has the highest tidal range in a tidal cycle and therefore causes the strongest hydrodynamic forces.

4.3. Model Set-Up

This section describes how the Delft3D model was set up, including the used grids, bathymetry, and the input for the WAVE and FLOW modules.

Grids

The model domain is divided into an $M \times N$ grid, where M represents the number of grid cells in the east–west direction and N represents the number of grid cells in the north–south direction. Each grid cell has a fixed resolution (ΔXY), which defines the level of detail in the simulation [20]. To improve accuracy, the model uses two grids: a large-scale grid and a finer nested grid, shown in figure 4.1. The large-scale grid, used only in the Delft3D-WAVE module, is dimensioned based on the location of the offshore wave boundary conditions, allowing waves to propagate correctly towards the study area. The nested grid, used for both wave and flow modelling, focuses on the study area with higher resolution to capture the important hydrodynamic processes. All output assessments focus on the study area within the nested grid.

Figure 4.1: Large-scale and nested grid used in the Delft3D model [23].

The details of both grids are shown in table 4.1.

Table 4.1: Grid specifications for the large-scale and nested grids

Parameter	Large-scale Grid (Coarse)	Nested Grid (Fine)
Number of grid cells ($M \times N$)	400 $\times$ 328	650 $\times$ 350
Grid resolution ΔXY [m]	100 $\times$ 100	5 $\times$ 10
Origin XY [m]	(573134, 978870)	(573134, 978870)
Grid rotation [°]	22.5	22.5

Bathymetry

The bathymetry was collected using a Lowrance fish radar, and the cross-sections with an RTK GPS. Both devices are described in appendix A.2. In Vietnam, the reference point for the national levelling system (MSL = 0) is located in Hai Phong, in the north, and is known as the Vietnamese Reference Datum (VRD). The MSL in southern Vietnam is higher than in the north. To account for this, tidal data for 2024 is analysed to determine tidal levels at the coast of Bạc Liêu, relative to the VRD [81]. The determined tidal levels for 2024, referenced to VRD = 0, are:

- Mean High Water (MHW): +1.75 m VRD
- Mean Sea Level (MSL): +0.66 m VRD
- Mean Low Water (MLW): –0.31 m VRD

The model uses the EPSG:32648 coordinate system, corresponding to WGS 84 / UTM Zone 48N, which is a Cartesian system [20]. The local time zone for all simulations is UTC+7 (GMT+7) [36]. In Delft3D, depth values are positive below mean sea level (MSL). This applies to the bathymetry, which is developed using QUICKIN, a Delft3D module for interpolating and processing bathymetric data [15]. As Delft3D operates with the national reference system, all bathymetry and water level data in the model are referenced to VRD.

To create a more realistic and complete bathymetry in the Delft3D model, additional depth samples were incorporated into the depth file. For the large coarse grid, the available depth samples, shown in figure B.3, have relatively low resolution. In contrast, the nested grid contains higher-precision depth values obtained from fieldwork (appendix A.3). To ensure a smooth transition between the two grids, depth values around the nested grid were adjusted and interpolated to appropriate values based on fieldwork measurements. Additional depth samples were also incorporated into the nested grid (fieldwork

area) to make the bathymetry more complete and realistic. To accurately represent the bathymetry, the shapes of mangroves and cliffs were derived from Google Earth [23]. Furthermore, to capture the bed level difference in front of and behind the breakwater, specific depth values were manually added based on field measurements and observations. The depth samples used to create the bathymetry, including manually added values, are shown in appendix B.1.1. These samples were interpolated in QUICKIN to generate the bathymetry for the area. The offshore section of the nested grid was smoothed to prevent excessive acceleration of flow velocities, which could introduce errors in simulations. For the simulations with the design alternatives without the structure, with the structure closer to the mangroves, and with the structure further offshore, the bathymetry around the structure is smoothed. This is done to reduce the impact of the existing bed level jump most likely caused by the existing structure and to create more consistent conditions for all design scenarios. The bathymetry of the nested grid, including the current structures, is shown in figure 4.2.

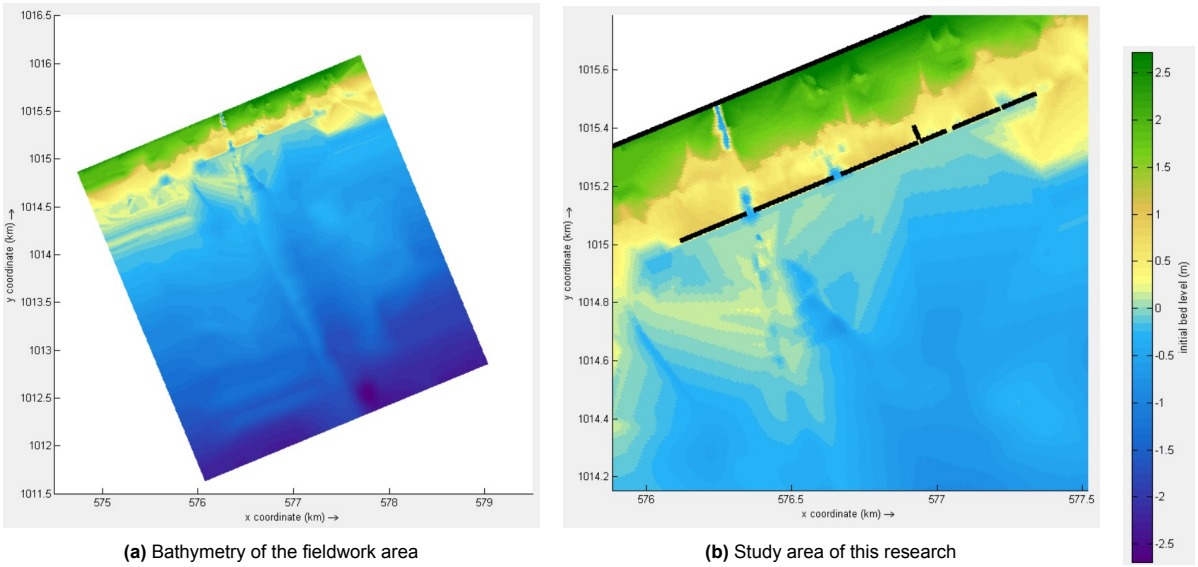

(a) Bathymetry of the fieldwork area

(b) Study area of this research

Figure 4.2: Bathymetry of the fieldwork area and the study area with existing breakwaters as porous plates, illustrated in QUICKPLOT (Delft3D)

Delft3D-FLOW

Delft3D-FLOW uses an implicit numerical scheme to solve the shallow water equations [16]. A computational time step of 0.2 minutes is used to resolve the hydrodynamics with sufficient accuracy. The offshore boundary in the nested grid is set as a water level boundary, with flow conditions represented by tidal constituents. Based on Phan et al. [66] and Marchesiello et al. [46], eight primary tidal constituents affect the tidal behaviour at the coast of Bạc Liêu. Additionally, constituent A_0 is included to account for storm surge water levels [76]. The details of the tidal constituents are shown in table B.1. The boundary is positioned along the southern edge of the nested grid, located from grid point M = 2 to M = 641 at N = 1. The breakwaters are applied in both modules, only within the study area. In Delft3D-FLOW, they are represented using porous plates, which are permeable barriers defined at velocity points to allow partial flow exchange between adjacent computational cells. A quadratic friction coefficient of 50 is applied, representing a permeability of 0.44 based on Thillaigovindarasu [79]. This approach is appropriate for this study since it allows for a realistic representation of the breakwater's influence on large-scale flow dynamics.

Delft3D-WAVE

In the Delft3D-WAVE module, bottom friction is set to 0.038 m²/m³, following the formulation by Vledder, Zijlema, and Holthuijsen [90]. The breaker index (γ) is applied to account for different seasonal and storm conditions, based on the method of Battjes and Stive [5], as detailed in appendix B.1.4. Specifically, the values used are $\gamma_{\text{Summer}} = 0.73$, $\gamma_{\text{Winter}} = 0.72$, and $\gamma_{\text{Storm}} = 0.85$. Breakwaters within this module are implemented as sheet obstacles, with their locations defined by specific coordinates. The breakwaters have a porosity of 0.44, as described in section 3.2.3, and no wave reflection is applied

in the simulations to simplify the interaction dynamics. ERA5 data [13] is used to obtain the mean offshore conditions. A distinction is made between summer (May–October) and winter (November–April) seasons. The offshore data is extracted at a location approximately 32 kilometres offshore, with coordinates 9.0°N, 106.0°E in the WGS 84 coordinate system (EPSG:4326) [26]. The dataset spans from 2014 to 2024 with a frequency of 60 minutes. The average summer and winter conditions over these 11 years are used as time-constant inputs for the boundary conditions in the Delft3D model, representing the seasonal mean forcing conditions. Storm conditions are defined separately and are based on the event data provided by Thanh et al. [76]. The wave boundary is located along the south-east, south-west, and north-east boundaries of the large-scale grid. Further details on the offshore conditions are provided in appendix B.1.3. An overview of the values used in the model is presented below in table 4.2.

Table 4.2: Offshore wave and wind conditions for the different modelling conditions

Parameter	Summer (May-Oct)	Winter (Nov-Apr)	Storm conditions
Wave conditions			
Mean Significant Wave Height [m]	0.57	0.87	5.29
Mean Peak Period [s]	4.25	5.42	8.96
Mean Wave Direction [°]	197.63 (SSW)	85.74 (E)	90
Directional Spreading [-]	4	4	4
Wind Conditions			
Mean Wind Speed [m/s]	3.82	5.67	22
Mean Wind Direction [°]	241.87 (WSW)	77.95 (E)	90

4.4. Simulation Scenarios

The simulation periods are selected during spring tides, when bed shear stresses are highest and hydrodynamic forcing is strongest. The exact dates were identified using available water level data. Field measurements were used to define the winter and storm periods, shown in figure B.9, while tidal data [81] was used to define the summer period, shown in figure B.8. An overview of the simulation periods is provided below.

- **Summer:** 21/08/2024 00:00 – 25/08/2024 00:00
- **Winter:** 15/12/2024 00:00 – 19/12/2024 00:00
- **Storm:** 15/12/2024 00:00 – 19/12/2024 00:00

Gap width and distance to shore are varied independently in this study to assess their individual influence on hydrodynamics. Because structure length and gap width are typically interdependent, only the gap width is explicitly varied in this analysis for clarity. The gap width is varied in steps of 5 metres per design variation, while the distance to shore is varied in steps of 20 metres. These variations depend on the grid cell size, which is 5 × 10 metres. Since distance to shore is a larger-scale parameter, its variation is set to two grid cells instead of one, so that the relative changes in both parameters are more comparable. An overview of all breakwater design scenarios used in the sensitivity analysis is provided in table 4.3, and exact dimensions can be found in appendix B.2.

Table 4.3: Overview of the 9 breakwater design variations tested in Delft3D. Distance to shore (D) and gap width (G) are varied independently. The current structure (D3-G3) serves as reference.

Design	Distance to Shore (= D)	Gap Width (= G)
Baseline		
$Without\ Structure$	-	-
$Current$	D3	G3
Gap Width Variation		
$Closed_2$	D3	G1
$Closed_1$	D3	G2
$Open_1$	D3	G4
$Open_2$	D3	G5
Distance to Shore Variation		
$Near_2$	D1	G3
$Near_1$	D2	G3
Far_1	D4	G3
Far_2	D5	G3
	G1 < G2 < G3 < G4 < G5 D1 < D2 < D3 < D4 < D5	

The variations in gap width and distance to shore are schematic illustrated below in figure 4.3.

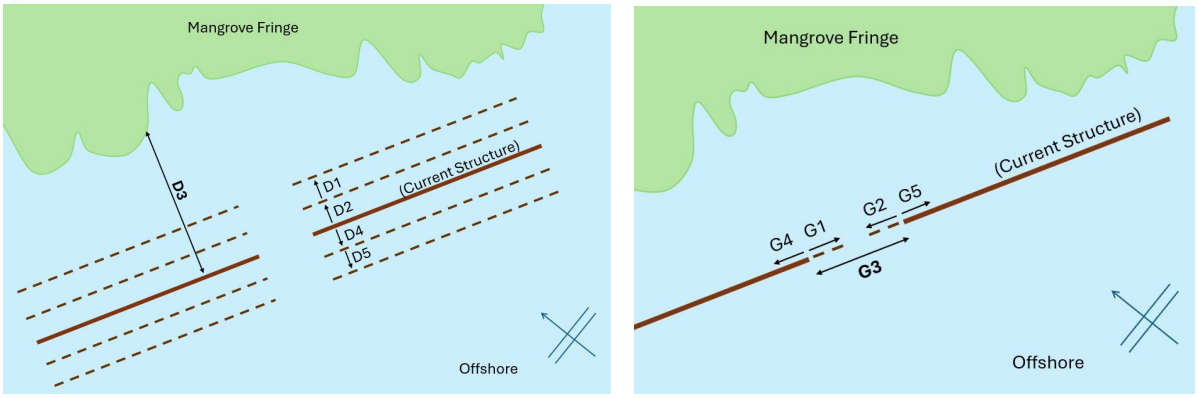

(a) Overview of the five different distance from the mangrove fringe alternatives used in the simulations (D1–D5), compared to the current structure (D3). Each variation step changes the distance by 20 meters.

(b) Overview of the five gap width alternatives used in the simulations (G1–G5), compared to the current structure (G3). Each variation step changes the gap width by 5 meters.

Figure 4.3: Schematic overview of the spatial design parameters tested in the study: distance to shore (D) and gap width (G).

4.5. Output Analysis

The output analysis focuses on three variables: the maximum bed shear stress (τ_{max}), the significant wave height (H_s), and depth-averaged flow velocities during rising tide. These outputs are evaluated under storm, winter, and summer conditions to assess the hydrodynamic impact of the current and alternative breakwater layouts. Since the primary aim is to assess erosion risk, the analysis is based on peak values rather than averages. The maximum bed shear stress (τ_{max}) is the bed shear stress due to waves and currents combined during maximum wave-induced orbital velocities. Since this bed shear stress represents the maximum hydrodynamic stress exerted on the seabed, it determines when sediment is mobilised. The interaction between waves and currents results in a non-linear increase in bed shear stress, with the highest values occurring during the maximum wave velocity [75]. Assessing τ_{max} behind the breakwater helps to predict when sediments are mobilised or deposited [74]. Combining this information with depth-averaged velocity vectors provides insight into where the mobilised sediment may be transported. The flow velocity analysis is limited to the rising tide period under storm conditions,

as this phase typically generates the strongest onshore-directed currents. Depth-averaged velocity patterns are observed in the area of the transects to evaluate whether flows are deflected, concentrated, or dissipated near the mangrove fringe depending on the breakwater design.

The analysis is carried out at two transects: Transect 1 passes through the breakwater gap, and Transect 2 is located at the centre of a breakwater segment, as shown in figure 4.4. Along each transect, five observation points are defined for the analysis: (1) in the mangroves, (2) at the cliff at the mangrove fringe, (3) near the mangrove fringe, (4) behind the breakwater or the gap, and (5) offshore.

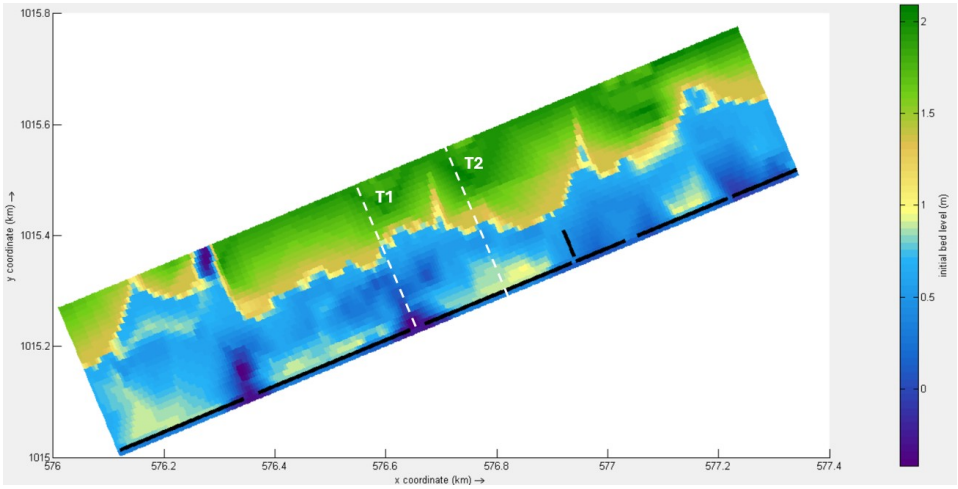

(a) Model bathymetry of the study area showing bed elevation relative to VRD. Transects 1 (T1) and 2 (T2) are indicated with dashed lines perpendicular to the coast.

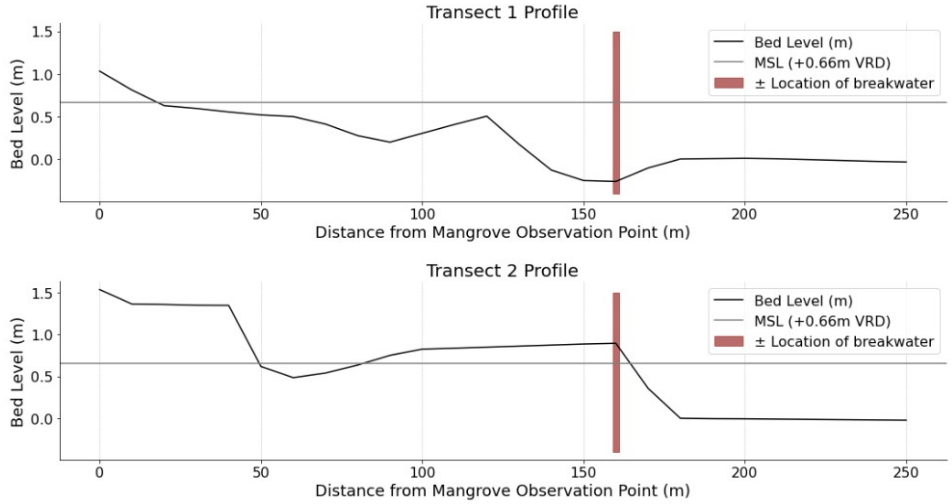

(b) Measured bed level profiles along transect 1 and transect 2, both starting from the mangrove observation point and extending offshore.

Figure 4.4: Overview of the transects used for analysis. Transect 1 is positioned at a gap between breakwater segments, while transect 2 crosses the centre of a breakwater segment.

For each simulation, the average of the top 10% highest values of τ_{max} per time series is extracted at each observation point and in the area near the mangrove fringe along the transects. The analysis primarily focuses on the area near the mangrove fringe, where inefficient sediment deposition negatively impacts mangrove survival and growth. To compare designs, a spatially averaged τ_{max} is computed for two fixed nearshore regions of 25 m $\times$ 30 m, located in front of the mangrove fringe along the transects. An overview of the observation points and the nearshore regions used in the analysis is shown in figure 4.5.

In the study area around the PRBW structures, sediment samples show median grain sizes (D_{50}) of

approximately 0.007 mm [22], typical of light sandy mud (appendix B.3). A critical bed shear stress of 0.25 N/m^2, based on Mitchener and Torfs [51], is used as a reference to evaluate the potential for sediment erosion or deposition. Significant deviations from this threshold may indicate model inaccuracies or uncertainty in the critical value.

The significant wave height is included in the analysis because it directly influences bed shear stress through orbital velocities. The average of the top 10% highest H_s values per condition is extracted from both the nearshore regions and the observation points along the transects to assess spatial gradients and the wave attenuation effect of the breakwater. The goal is to minimise τ_{max} in the area near the mangrove fringe while enhancing current patterns that transport sediments towards this region, thereby creating favourable conditions for sedimentation and mangrove survival.

(a) Image showing the observation points along each transect, classified by location type. Details of the different observation locations can be found in table B.4

(b) Satellite image of the study area showing the near shore region locations of Transect 1 and Transect 2. These regions are used to compare the output of different scenarios.

Figure 4.5: Overview of the transects and near shore regions used for analysis. Transect 1 is positioned at a gap between breakwater segments, while transect 2 crosses the centre of a breakwater segment. The near shore regions are spatially averaged

5

Results

This chapter presents the main findings from fieldwork, spatial analysis of the breakwater compared to guidelines, and numerical modelling. The fieldwork section describes observed hydrodynamics, sedimentation patterns, and measured bathymetry. The spatial analysis assesses how the spatial dimensions of the existing breakwater align with existing design guidelines for breakwaters. The modelling results then quantify how variations in gap width and distance to shore influence the maximum bed shear stress, significant wave height, and flow patterns.

5.1. Fieldwork

This section presents the findings from the fieldwork in Bạc Liêu. The detailed diary of the planning and observations can be found in appendix A.3. Field observations are summarised to describe important hydrodynamic and morphological features relevant to sediment transport. The collected bathymetry data is used to analyse the bed profile and assess sedimentation and erosion patterns around the breakwater. Finally, the measured water levels, wave conditions, and wind data are presented to characterise the local hydrodynamics and provide a basis for model validation.

5.1.1. Fieldwork Observations

During the fieldwork in Bạc Liêu, several relevant observations were made regarding hydrodynamics and sediment transport. The measurements were carried out during winter, with temperatures around 27°C. Wind conditions were generally calm, with low wind speeds (approximately 3 m/s), except on the final day when wind speeds increased (approximately 5 m/s). This led to the generation of more short waves nearshore, which were visibly more active compared to earlier days. It was observed that long waves seem to largely penetrate through the breakwater and reach the mangroves, where they seem to break just before or inside the vegetation. These long waves, which occur on the low-sloping muddy coast of Bạc Liêu, are likely infragravity waves with periods ranging from 25 to 100 seconds. They are generated offshore in wave groups and become more dominant in shallow water, where they can contribute to erosion, particularly near reflective structures and mangrove fringes [67]. Additionally, a strong cross-shore current was observed at the wave buoy deployment location during rising tide, which likely influences sediment transport patterns. It was also observed that the bed elevation behind the breakwater is higher compared to near the mangrove fringe, suggesting that the sediment shadow zone does not fully extend to the mangrove edge. This can be seen in the pictures taken during fieldwork, shown in figure 1.3. The difference in bed level between the front and back of the breakwater is estimated to be around 0.5 metres. The sediment composition varies in the area, with sandier material in front of the breakwater transitioning to muddier deposits closer to the mangroves. Erosion persists between the bamboo fences and the mangroves, possibly due to reflective wave action. An erosion cliff is observed in front of the mangroves, and no new root growth has developed, indicating potential stress on the mangrove system.

5.1.2. Bathymetry

Two cross-sections, shown in figure C.1, were obtained during fieldwork. The elevation measurements from these cross-sections were combined with tidal data to establish a reference level and for further analysis. Cross-section 2 provides the most reliable elevation profile, capturing the transition from the mangrove area to the mudflat and the breakwater. This cross-section is shown in figure 5.1 and is used for the analysis.

Figure 5.1: Cross-section 2 was collected during fieldwork and illustrates the measured profiles in the study area.

The mangrove area is elevated above mean sea level (MSL), remaining dry at MSL and experiencing inundation ranging from 0.2 to 1.4 metres during mean high water (MHW). Approximately 100 metres from the beginning of the natural mangrove forest, the bed elevation drops sharply, indicating a cliff at the transition to the mudflat. These cliffs are shown in the picture in figure A.3, taken during fieldwork. The mudflat gradually slopes downward, with water depths near the shore of approximately 0.66 metres at MSL and 1.75 metres at MHW. This indicates a deeper, more submerged area compared to the mangrove region. The elevation pattern remains similar from the mangrove fringe to the gap in the breakwater. This is because Cross-section 2 is located behind a gap, where higher flow velocities and turbulence prevent sediment from settling as easily as in the more sheltered region directly behind the breakwater [8]. In the region behind the breakwater, the bed elevation is therefore slightly higher, resulting in water depths of approximately 0.3 metres at MSL and about 1.4 metres during MHW. These findings are based on the bathymetry measurements and field observations, as shown in the images in figure 1.3. In front of the breakwater, the bed level is lower, resulting in water depths of approximately 0.9 metres at MSL and 2 metres at MHW. Breakwaters alter wave energy and current patterns, which can cause localised erosion, known as scour holes, due to increased turbulence and wave reflection [8]. During fieldwork, rocks were observed in front of the breakwater, placed as scour protection. The slope from in front of the breakwater to the furthest offshore bathymetry measurement is approximately 1:1185, indicating a very mild slope. This differs from the slope indicated in section 3.2.4, which is 1:500. The discrepancy could be due to the starting point of the measurements. In this case, the slope calculation begins in front of the breakwater, where the bed level is significantly lower than at the mangroves. Additionally, the literature data may extend further offshore, assessing a different bathymetric profile.

The bed level variations show the sedimentation and erosion patterns influenced by the breakwater. The cliff at the transition from the mangroves to the mudflat suggests significant erosion at this boundary. Field observations indicate that sedimentation is highest directly behind the breakwater. The bed level gradually decreases towards the shore, with a noticeable change around the midpoint, as shown in figure 1.3c, suggesting reduced sedimentation further away from the structure. The lower bed level in front of the breakwater, combined with observed scour protection, indicates localised erosion caused by wave reflection and turbulence. The *Avicennia alba* habitat zone (MSL to +50 cm) aligns with the seaward edge of the mangroves, where mangroves are observed (section 3.2.2). However, the steep cliff at the transition from the mangroves to the mudflat is not favourable for further mangrove expansion, as it creates an abrupt elevation drop that limits the gradual sediment accretion needed for seedling

establishment and root stabilisation.

5.1.3. Hydrodynamics

The locations of the measurement devices deployed during fieldwork are shown in figure 5.2. The water level gauge, weather gauge, and wave pressure gauge were installed on the 1st, 2nd, and 3rd of December 2024, respectively. All remained in place until the 9th of January 2025, covering a deployment period of approximately one month.

Figure 5.2: Locations of the deployed measurement devices for the hydrodynamic data [23].

However, only the water level gauge provided reliable data for the entire duration. These water level measurements are shown below in figure 5.3. The pattern displays two high waters and two low waters per day, each reaching different elevations [48]. This indicates a mixed, but predominantly semi-diurnal, tidal regime, as described in section 3.2.4, with a tidal range of approximately 4 metres during spring tide. The periodic variability also shows the spring–neap cycle, which occurs twice per month [8].

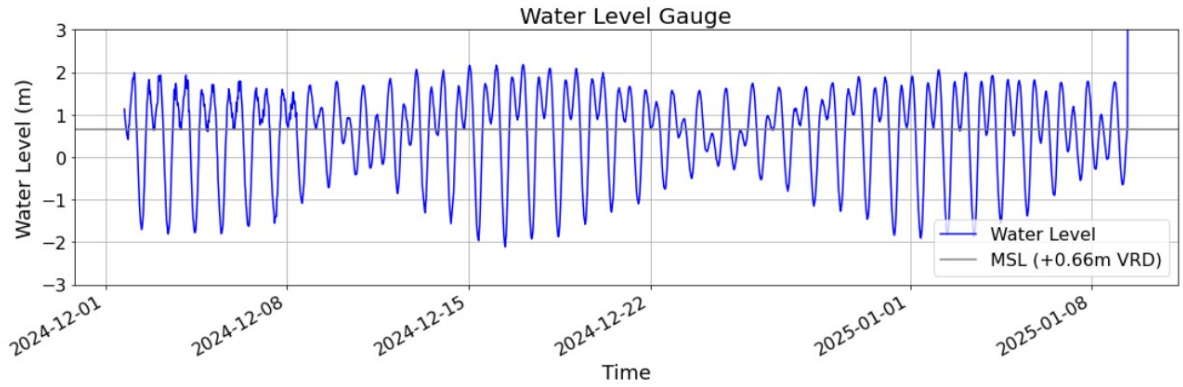

Figure 5.3: Water level measurements recorded by the water level gauge positioned approximately 3.4 km offshore. The data is plotted over the period from December 2, 2024, to January 10, 2025.

Only three days of data are used for comparison and analysis due to unreliable behaviour observed outside this period, caused by the wave pressure and weather gauges operating at too low a frequency.

These low sampling frequencies resulted in jumps in the dataset, making it unsuitable for analysis. The analysed data is from 4 December 2024 to 6 December 2024. First, the water level measurements at the two different locations are compared in figure 5.4. The measurement sites are separated by a distance of 3.3 kilometres, as shown in figure 5.2. One gauge is located near the shore, just behind the gap in the breakwater, while the other is positioned further offshore. This comparison is illustrated in figure 5.4. The results show that the datasets align well, indicating consistency in the recorded water levels. The analysed period corresponds to, or is close to, spring tide, resulting in a relatively large tidal range.

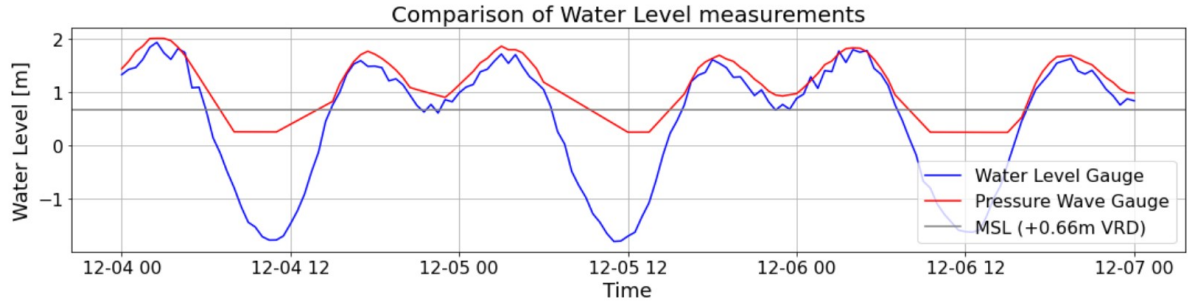

Figure 5.4: Measured water levels at the locations of the wave pressure gauge and the water level gauge, which are separated by a distance of 3.3 kilometres. One gauge is positioned near the shore, just behind the gap in the breakwater, while the other is located further offshore.

Time series of various parameters recorded by two devices are plotted below in figure 5.5: the wave pressure gauge near the shore and the weather gauge further offshore. The parameters in the top three plots, namely water level, significant wave height, and peak wave period, are measured by the wave pressure gauge. The bottom two, which are wind speed and wind direction, are recorded by the weather gauge. The method used to extract these datasets from the devices is explained in appendix A.2. The first observation is related to the peak wave period measured by the wave pressure gauge. To ensure that only realistic values are included, all peak period values above 10 seconds were filtered out. It appears that when the water level drops below 1 metre, the device struggles and provides unrealistic measurements. The large tidal range causes the area near the shore to have no water depth at higher elevations during low tide, and at lower elevations, there is only a very small water depth. The sensor of the wave pressure device is located in this area and may therefore not always be submerged. This could make it challenging for the device to perform reliable measurements. As a result, the dataset of the peak wave period only provides realistic values during higher water levels, when the sensor is fully submerged and able to capture wave characteristics more accurately. Another observation is that the water level and wave height have a very similar pattern. This could be explained by the influence of water depth on wave dynamics. In shallow nearshore areas, the wave height is strongly influenced by the water depth due to processes such as bottom friction and wave shoaling. During high tide, the increased water depth reduces bottom friction, allowing waves to retain more energy and larger wave heights. During low tides, the reduced water depth causes increased energy dissipation due to turbulence from bottom friction, leading to smaller wave heights [33]. Wave breaking seems to have a minimal effect when considering the shallow-water breaker index based on linear wave theory (H/d = 0.78) [33]. When comparing the water level and wave height of the dataset, the values do not reach this threshold, suggesting that wave breaking processes are likely not a dominant factor in the observed wave dynamics.

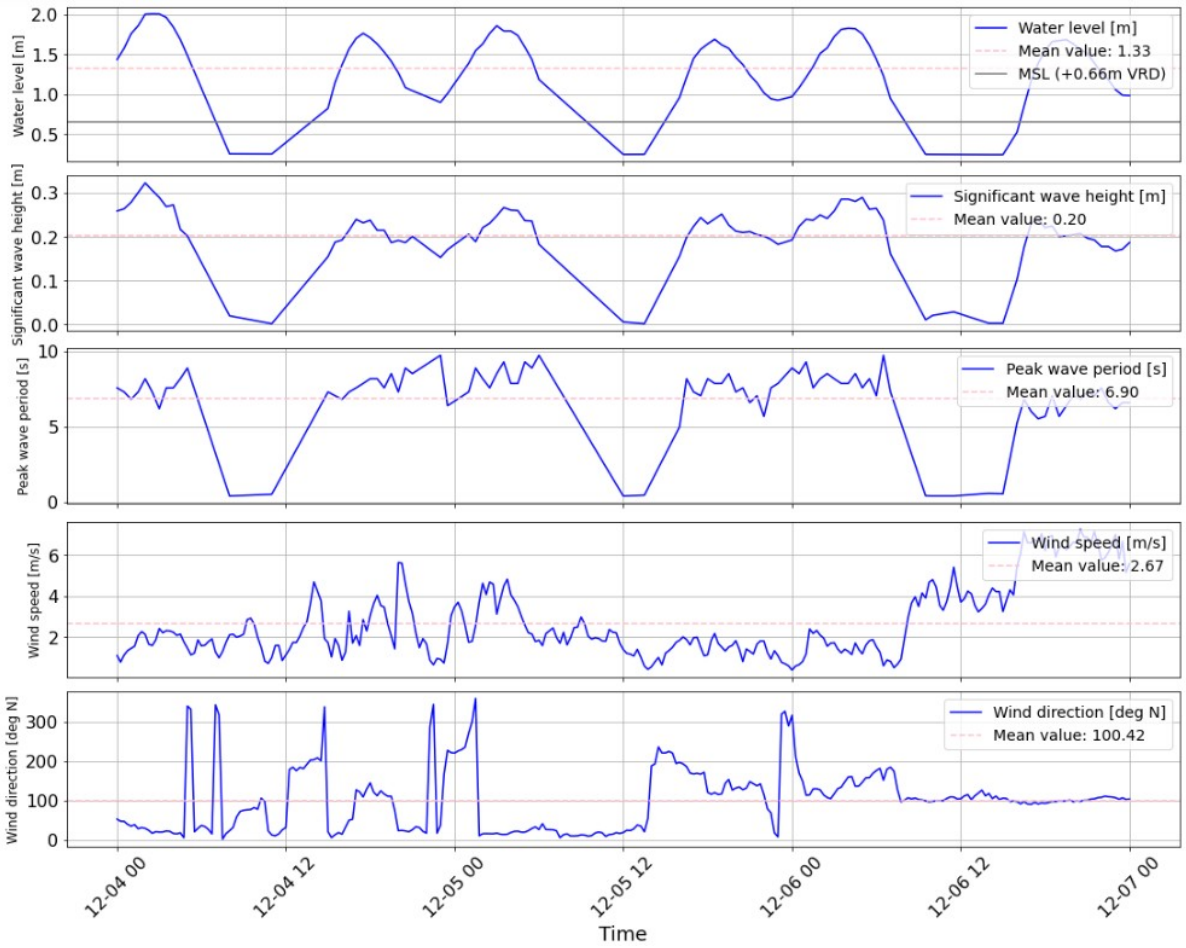

Figure 5.5: Time series of various parameters recorded by two devices: the wave pressure gauge near the shore and the weather gauge further offshore. The top three parameters, namely water level, significant wave height, and peak wave period, are measured by the wave pressure gauge. The bottom two, which are wind speed and wind direction, are recorded by the weather gauge.

The datasets were collected during the winter season. Comparing the observed values with the average winter conditions for the area, as provided in section 3.2.4, gives insight into deviations and their possible causes. The average wave height for the winter season in this area typically ranges between 0.5 and 1.5 metres, while the observed wave heights are slightly smaller, reaching up to 0.3 metres. This could be explained by energy dissipation caused by the breakwater structure and the shallow water depths near the shore, where the measurements were taken. The corresponding average peak period during winter ranges between 4 and 5 seconds. However, the observed peak wave periods were initially much larger, reaching values up to 200 seconds. To ensure more reliable results, all peak period values above 10 seconds were filtered out. This filtering improves data quality but also removes some potentially valid measurements, making the dataset less complete and possibly less representative of actual wave conditions. This could explain why the mean peak period after filtering deviates from the average winter range, as it is 6.9 seconds, which is higher than the typical 4 to 5 seconds. Nevertheless, during periods of increased wave heights, the observed wave periods (ranging between 5 and 10 seconds) align more closely with average seasonal values, indicating consistency under specific conditions. The average winter wind speed in the area is 4.6 m/s. The measured wind speeds are mostly slightly lower, though later in the time series they rise and align more closely with the seasonal average. The prevailing wind direction is typically around 45°, coming from the north-east. In the dataset, wind direction shows significant variability but is generally from the east, around 90°, which is a minor deviation and still relatively consistent with expected seasonal patterns.

In summary, while the wave properties show some deviations, these can be related to local effects such

as energy dissipation and limitations in data reliability. The wind conditions follow expected seasonal patterns, with some temporary variations. These field observations suggest that although local conditions and measurement limitations influence data quality, the recorded hydrodynamics broadly align with seasonal expectations and provide a suitable basis for validating model simulations and assessing breakwater performance in the following chapters.

5.2. Analysis of the Spatial Dimensions

The spatial dimensions of the existing breakwater in the study area, as shown in figure 5.6, are compared with the design guidelines for (permeable) breakwaters, as described in section 2.2.4. This distinction is important, as the breakwaters used in the study area are Pile-Rock Breakwaters (PRBW), which are permeable by design. Therefore, their hydrodynamic functioning, particularly in terms of wave attenuation and sediment trapping, differs from that of impermeable structures. Since the study area is located on a muddy coast, characterised by fine cohesive sediments, traditional guidelines developed for sandy coasts may not be directly applicable. However, the comparison is still carried out to provide a reference framework and gain insight into the spatial design's potential effectiveness. The analysis aims to improve understanding of the existing breakwater design and identify any deviations from the guidelines that could help explain the observed hydro- and morphodynamic behaviour.

Figure 5.6: The spatial layout of the existing breakwater in the study area [23]

Breakwater Length

The breakwaters in the study area vary in length, with segments ranging from 94 to 282 metres. These lengths broadly fall within the recommended range for permeable structures (60–240 m) and are generally sufficient for wave attenuation. The length-to-distance-from-shore ratio (L/D) in the study area ranges from 1.1 to 2.8, which, according to the design guidelines, suggests a favourable potential for sediment deposition—especially when L/D > 1.3. Combining both long and short segments could help maintain a balance between sediment retention and the facilitation of tidal and sediment exchange.

Gap Width

The gaps between the breakwaters range from 9 to 31 metres, resulting in varying degrees of tidal exchange and sediment transport. For permeable structures, maintaining gaps in the range of 10–100 metres supports both sediment retention and ecological connectivity. In the study area, the gap-width-to-distance-from-shore ratio remains below 0.8 in all cases, which, based on literature, suggests that significant erosion within the gap areas is unlikely to occur. The narrower gaps may further enhance sediment retention behind the structures.

Distance from Mangrove Fringe

The distance between the breakwaters and the mangrove fringe varies from 96 to 289 metres. According to the design guidelines for permeable structures, the effective range is 80–230 metres, with distances less than 198 metres being most effective in reducing bed shear stress. Segments located beyond 230 metres may fall outside the optimal zone, allowing more wave energy and lateral currents to affect the area behind the structures. In contrast, breakwaters located closer to the shore are more likely to reduce wave impact and promote sedimentation near the mangrove fringe.

To sum up, the spatial analysis of the breakwaters in the study area shows that the design parameters mostly fall within the recommended ranges for permeable breakwaters. However, certain segments exceed the suggested distance to the mangrove fringe, which may reduce their effectiveness in attenuating wave energy and promoting sediment deposition in critical areas. It is also important to interpret these values specifically in the context of permeable structure dynamics, as their function depends on partial energy dissipation and controlled water and sediment exchange.

5.3. Model

This section uses the Delft3D model to assess how the breakwater's spatial design affects hydrodynamics relevant to sediment transport. After validation with field data, the model compares the existing breakwater to a scenario without a structure and tests variations in gap width and distance to shore. The impact on maximum bed shear stress and flow patterns is analysed.

5.3.1. Validation and Calibration

Water level and significant wave height measurements from the wave pressure gauge are compared with Delft3D model outputs at the same observation point. Data from 4 December 06:00 to 6 December 18:00, 2024, are selected for comparison, as the gauge provided the most reliable readings during this period. The Root Mean Squared Error (RMSE) is used to evaluate the model's accuracy. RMSE is a standard metric for assessing model performance by measuring the average error between observed and simulated values [93]. The second validation assesses the setup used for the design change simulations. This validation focuses on understanding how the model performs under the conditions applied in the modelling assessment of this research. These deviations are considered when interpreting the results.

The first validation, shown in figure 5.7, compares the model with time-varying wave conditions from ERA5 and wind conditions recorded by the weather gauge during fieldwork, both provided through a wavecon file. The water level time series from the fieldwork's water level gauge is included via a bct file. This validation ensures the model's accuracy across all parameters and is critical for assessing model performance under realistic, time-varying conditions. The RMSE values for this validation are 0.21 m for water levels and 0.11 m for significant wave height. These values indicate that the modelled water level can deviate by up to 12% from the peak field value, and the significant wave height by up to 39% during peak conditions. The method and calculation details are provided in appendix C.3. The Delft3D model accurately simulates the water level variations, with the only noticeable deviation occurring at the first peak on 4 December. This is likely due to a spin-up effect in the model, where the initial conditions take time to stabilise. For significant wave height, the model consistently underestimates the observed values, particularly during periods of higher wave activity. This could be due to inaccuracies in the wave forcing inputs—such as wind and wave data from ERA5—or potential limitations within the model itself.

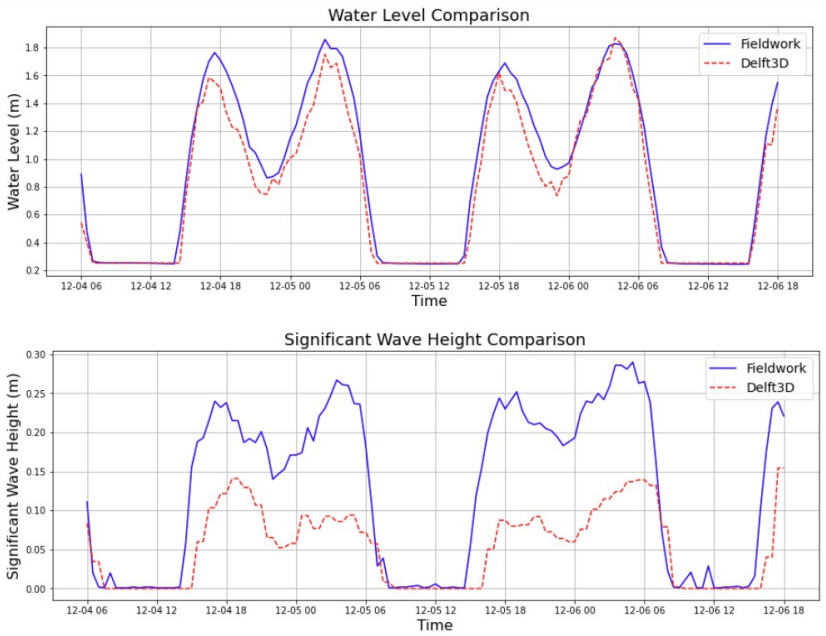

Figure 5.7: This figure shows a comparison of real-time fieldwork wave pressure measurements with Delft3D model outputs. The model uses time-series data for wave conditions from ERA5, wind conditions from fieldwork using a weather gauge, and water level data from fieldwork using a water level gauge, all collected between the 4th till the 6th of December, 2024.

The second validation, shown in figure 5.8, uses constant wave and wind conditions derived from average winter data from ERA5, along with tidal constituents for the water level. The RMSE for water levels in this case is 0.67 m, and the RMSE for the significant wave height is 0.14 m. The RMSE indicates that the modelled water level can deviate by up to 37% from the peak field value, and the significant wave height can deviate by up to 50% during peak conditions. The Delft3D model generally simulates the water level well, but there is an offset in the timing of the water level peaks and troughs. This deviation could be due to the model's tidal constituent input not fully aligning with reality. The lower and mistimed water levels in the model could be a primary cause of the deviations in the significant wave heights. Water level fluctuations directly impact wave amplitude and energy propagation. When water levels are lower and out of phase with observed data, the significant wave height is likely to behave similarly. This error in timing and amplitude could lead to an underestimation of the significant wave height, and therefore in the modelled maximum bed shear stress. This will be taken into account when analysing the output of the model, as inaccuracies in wave height predictions may affect the reliability of bed shear stress estimates. Despite these limitations, the Delft3D model remains a useful tool for assessing how design modifications affect bed shear stress and current patterns. For this study, the model accuracy is considered sufficient, as the focus lies on comparing relative effects of spatial design choices rather than producing absolute values.

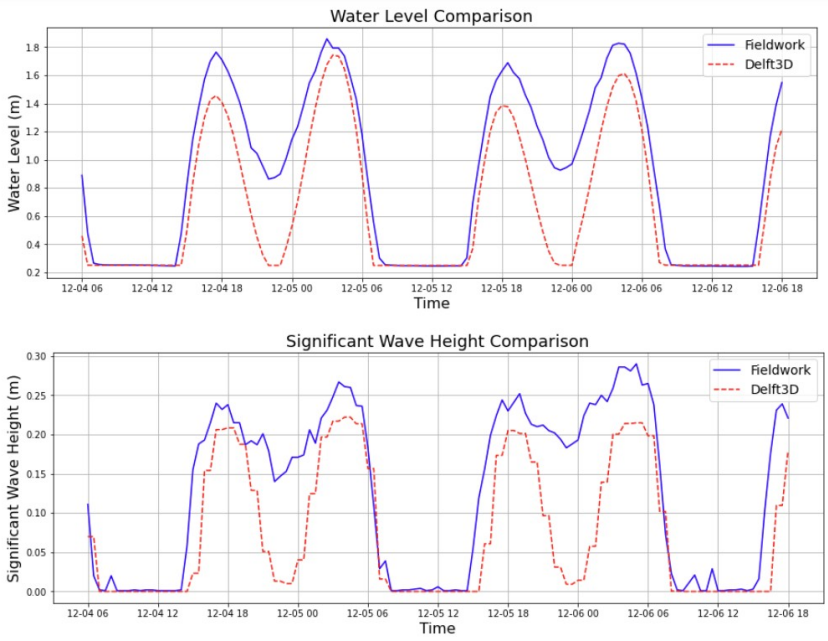

Figure 5.8: Comparison of real-time fieldwork wave pressure measurements with Delft3D model outputs under constant wave and wind conditions from ERA5, and tidal constituents from December 4 to December 6, 2024. The model output was manually shifted 2 hours earlier to better align with the field data. Additionally, the first and last 6 hours of the time series were excluded from the comparison due to model spin-up effects and missing data resulting from the time adjustment.

5.3.2. Model Results

This section presents the impact of variations in gap width and distance to shore on the maximum bed shear stress and current patterns. Two sets of modifications were tested, as shown in the overview in table 5.1. When varying the distance to shore (D), the gap width (G) is kept constant at G3. Similarly, when varying the gap width (G), the distance to shore (D) is fixed at D3.

Table 5.1: Spatial design variations for gap width (Set 1) and distance to shore (Set 2)

Gap Width	**± Value [m]**	**Distance to Shore**	**± Value [m]**
G1	20	D1	130
G2	25	D2	150
G3 (existing)	30	D3 (existing)	170
G4	35	D4	190
G5	40	D5	210

For clarification, these variations are schematised again in figure 5.9.

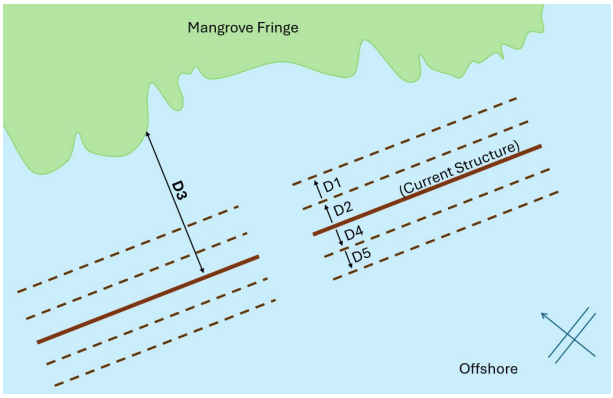

(a) Overview of the five different distance from the mangrove fringe alternatives used in the simulations (D1–D5), compared to the existing structure (D3). Each variation step changes the distance by 20 meters.

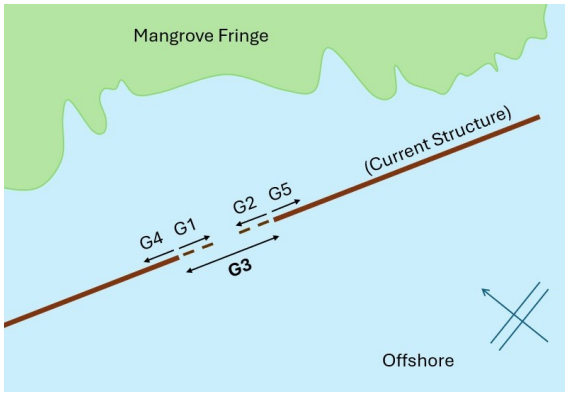

(b) Overview of the five gap width alternatives used in the simulations (G1–G5), compared to the existing structure (G3). Each variation step changes the gap width by 5 meters.

Figure 5.9: Schematic overview of the spatial design parameters tested in the study: distance to shore (D) and gap width (G).

All variations are compared with the existing breakwater design (D3 and G3). When adjusting the gap width, the distance to shore is kept constant (D3). When adjusting the distance to shore, the gap width remains the same (G3).

The results compare:

- Different conditions for the existing breakwater design
- The existing breakwater and a scenario without a breakwater
- Spatial design changes in both gap width and distance to shore

The first six hours of each simulation are not used for the analysis to avoid the influence of the spin-up phase, during which the model stabilises towards realistic conditions [105]. The analysis focuses on the nearshore region and selected transects with observation points, as referenced in figure 5.10. The focus is specifically on the area near the mangrove fringe, where inefficient sediment deposition negatively impacts mangrove survival and growth. To reduce sensitivity to local grid deviations, a spatial average is calculated over multiple grid cells for the nearshore region.

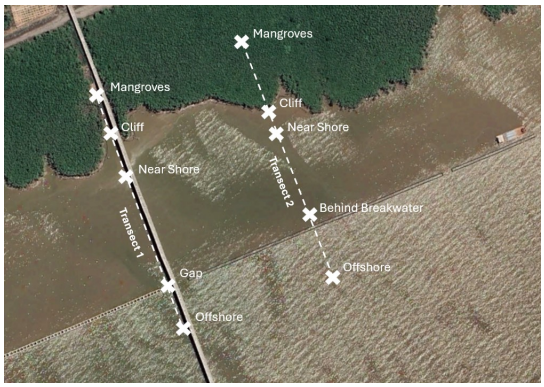

(a) Image showing the observation points along each transect, classified by location type. Details of the different observation locations can be found in table B.4

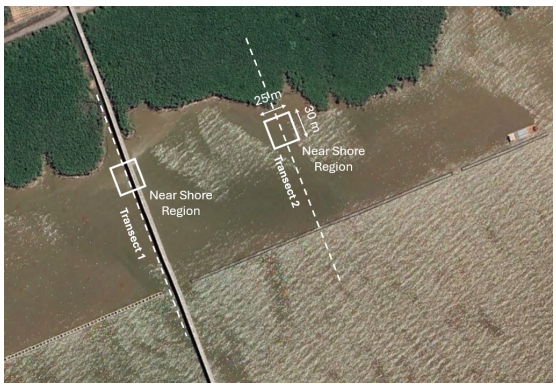

(b) Satellite image of the study area showing the near shore region locations of Transect 1 and Transect 2. These regions are used to compare the output of different scenarios.

Figure 5.10: Overview of the transects and near shore regions used for analysis. Transect 1 is positioned at a gap between breakwater segments, while transect 2 crosses the centre of a breakwater segment. The near shore regions are spatially averaged.

Different Conditions

In figure 5.11, the average of the top 10% highest values of the maximum bed shear stress (τ_{max}) is shown at the different locations along both transects under different conditions, plotted together

with the bed profile. The values show how the different conditions affect the maximum bed shear stress across the transects. The transects illustrate a clear increase in τ_{max} during storm conditions compared to the winter and summer conditions. For the storm conditions, τ_{max} exceeds 1 N/m² offshore for both transects, with a steady decrease towards the shore. Both transects show a similar effect, except for the increase in τ_{max} at the cliff location in transect 2. In both transects, summer and winter conditions show similar spatial patterns, in which the summer consistently results in lower bed shear stress values compared to the winter. In contrast, storm conditions consistently give significantly higher τ_{max} values, especially in the offshore sections. The cliff, which indicates the beginning of the mangrove area, and the breakwater align with changes in the τ_{max} gradient. The bed shear stress decreases behind the breakwater and continues to decrease towards the mangrove fringe. The results show a dampening effect of both the breakwater structure and the mangroves on τ_{max}, indicating a reduction in hydrodynamic energy closer to shore.

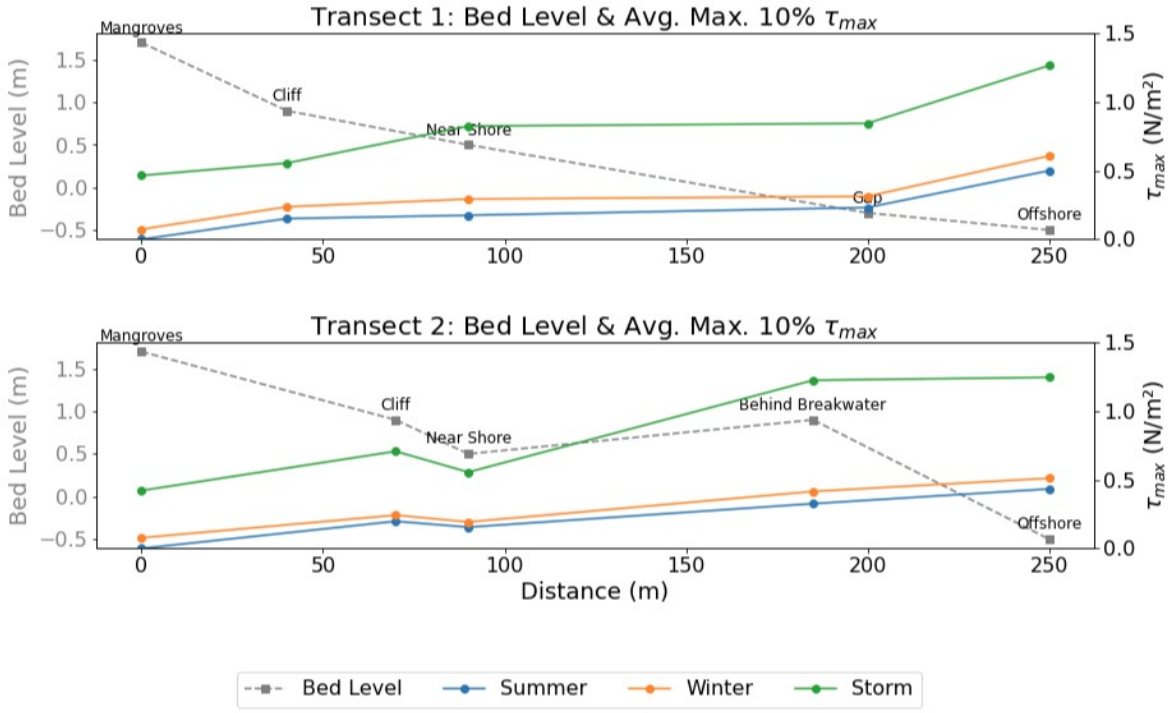

Figure 5.11: Modelled average of the top 10% highest values of the maximum bed shear stress (τ_{max}) along the transects for different conditions with the existing breakwater.

Figure 5.12 shows the temporal variation of τ_{max} in the nearshore area. Storm conditions cause the highest and most variable τ_{max}, with peaks up to 0.78 N/m^2 in transect 1 and 0.59 N/m^2 in transect 2. The average τ_{max} during storms is 0.27 N/m^2 in transect 1 and 0.28 N/m^2 in transect 2. In comparison, the average τ_{max} stays below 0.1 N/m^2 during summer and winter. The general pattern is similar for both transects, although small tidal variations are present due to different simulation periods. It can also be observed that τ_{max} never drops to zero during storm conditions in transect 2.

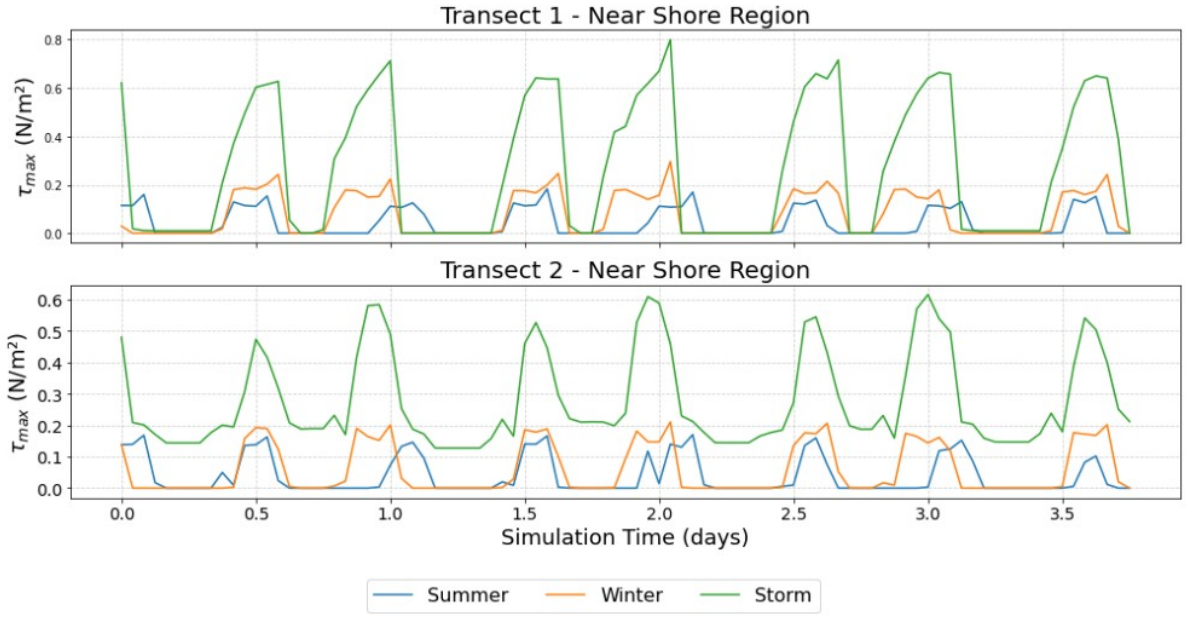

Figure 5.12: Time serie of the spatial averaged maximum bed shear stress in the near shore area along both transects for different conditions.

Based on these findings, the analysis of different design variations will focus on the winter and storm conditions, as these produce the highest bed shear stresses and therefore have the most potential impact.

Effect of Existing Breakwater

The effect of the breakwater is determined by comparing scenarios with and without the existing breakwater under winter conditions. The average of the top 10% highest values of the maximum bed shear stress (τ_{max}) at the different locations along both transects is shown in figure 5.13, together with the bed level of the transect locations. For both scenarios and along both transects, τ_{max} decreases in the landward direction. Also, in both transects, a breakwater results in a clear reduction in τ_{max} behind the structure. Offshore values are similar between the scenarios, indicating that the breakwater does not appear to have a significant impact at that location. This could partially be explained by the model setup, which excludes wave reflections and wave–current interaction, potentially underestimating the offshore influence of the structure.

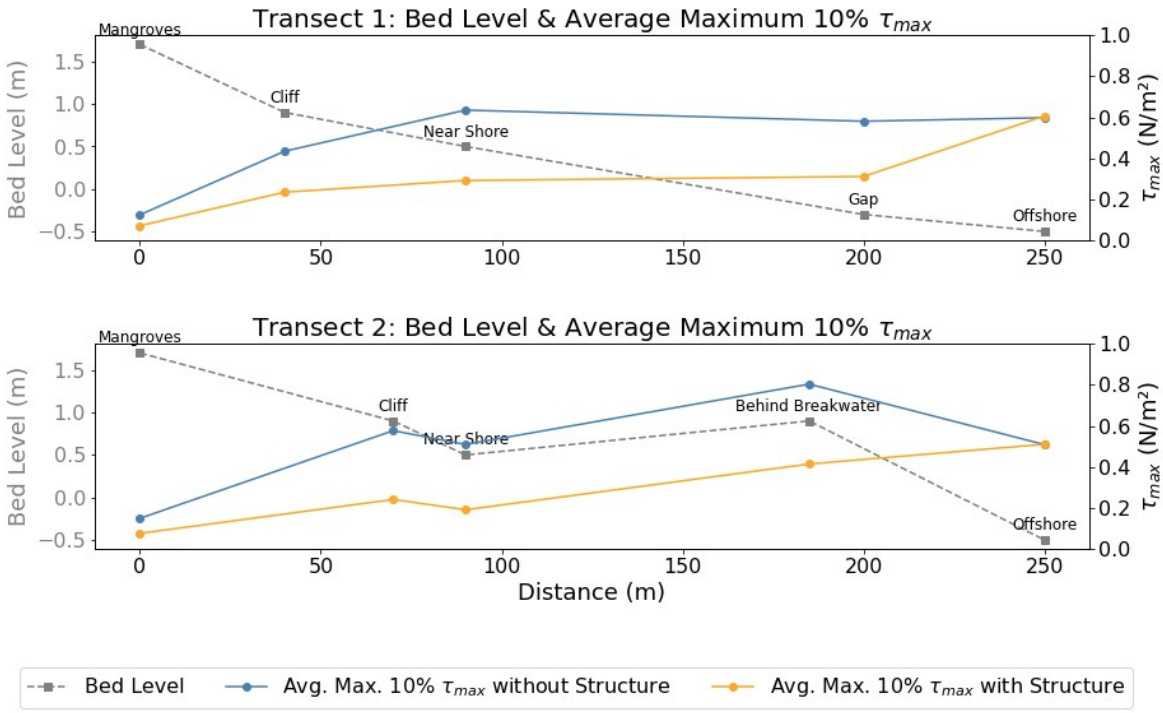

Figure 5.13: Reference scenario of the modelled average of the top 10% highest values of the maximum bed shear stress (τ_{max}) along the transects for the existing breakwater under winter conditions.

The time series of the spatially averaged maximum bed shear stress (τ_{max}) in the nearshore region, shown in figure 5.14, support this dampening effect caused by the breakwater in both transects. The greatest reduction occurs during peak values, which correspond to high tide.

Figure 5.14: Reference scenario of the spatial averaged maximum bed shear stress in the near shore area along both transects for the existing breakwater under winter conditions.

So, the results clearly show that the breakwater causes a reduction in maximum bed shear stress landwards of the structure. Offshore values for both transects are similar, but upon entering the breakwater zone, a noticeable decrease is observed. A similar trend is shown in figure 5.15, which presents the significant wave height H_s instead of τ_{max} for winter conditions. This figure, along with the significant wave heights for other conditions with the existing breakwater shown in figure C.3, indicates that significant wave height decreases by 50% after propagating through the breakwater at transect 2. This demonstrates the effectiveness of the breakwater in attenuating wave energy.

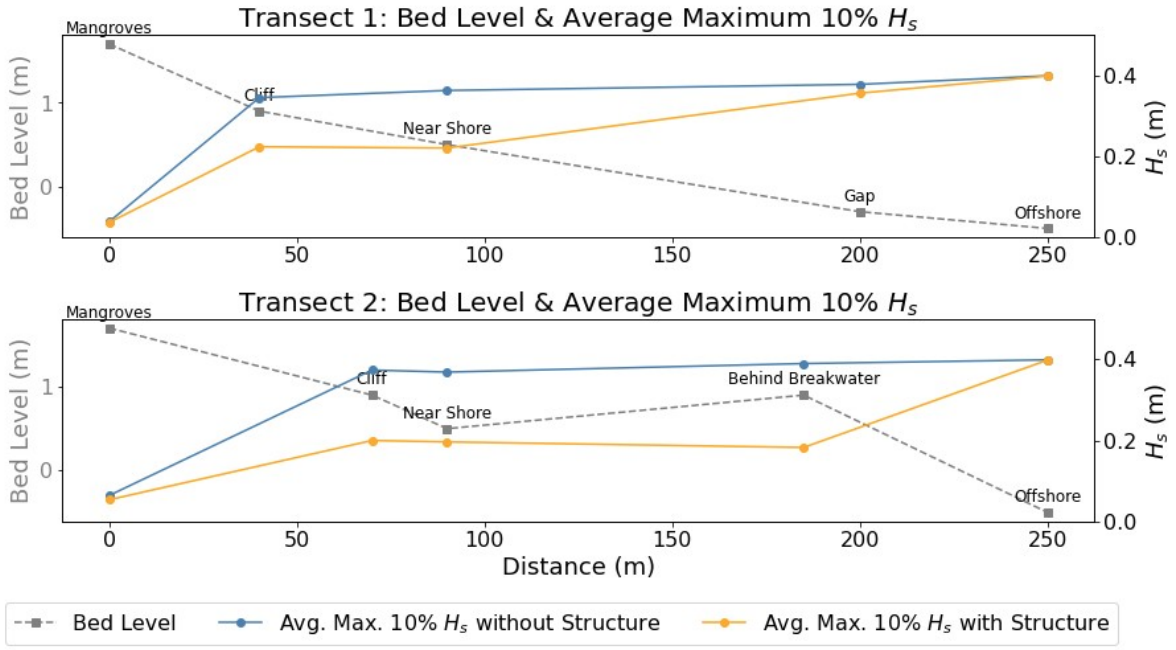

Figure 5.15: Reference scenario of the modelled average of the top 10% highest values of the significant wave height (H_s) along the transects for the existing breakwater under winter conditions.

Below in figure 5.16, the depth-averaged flow velocities are shown during the rising tide under storm conditions. These conditions were selected as they induce the highest velocities, making the differences between the scenarios more pronounced. In the presence of the breakwater (dark blue), flow is directed towards and accelerated through the gap, followed by a velocity reduction and lateral spreading in the sheltered zone behind the structure. The results show the expected circulation patterns. In contrast, the baseline scenario without a structure (light blue) mostly reflects the influence of the bathymetry, with flow acceleration where the bed level increases (and water depth decreases) and deceleration closer to the shore. A general westward flow direction is observed in this scenario.

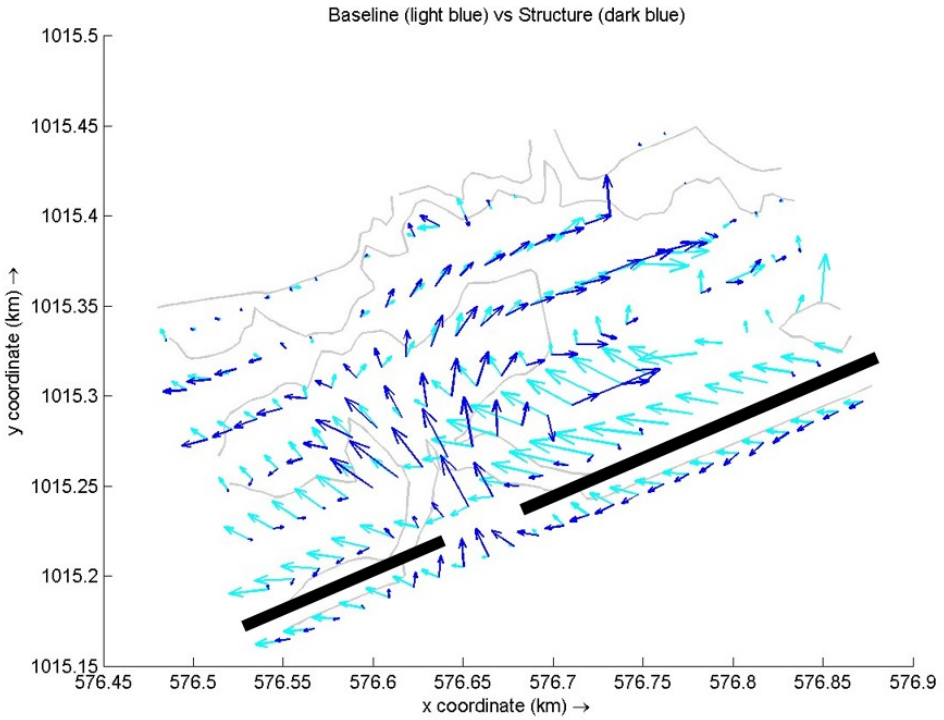

Figure 5.16: Flow velocity patterns in area of the transects for the existing breakwater and baseline (no structure) during rising tide under storm conditions.

Winter Conditions: Impact of Spatial Design Variations

The figures below show the average of the top 10% highest values of the maximum bed shear stress (τ_{max}) in the spatially averaged nearshore region for different design variations under winter conditions.

For transect 1 (location of gap), the bed shear stress (τ_{max}), taken as the average of the top 10% of values, decreases with increasing distance to shore and with a decreasing gap width (figure 5.17). The highest values are observed when the breakwater is positioned close to the shoreline (D1).

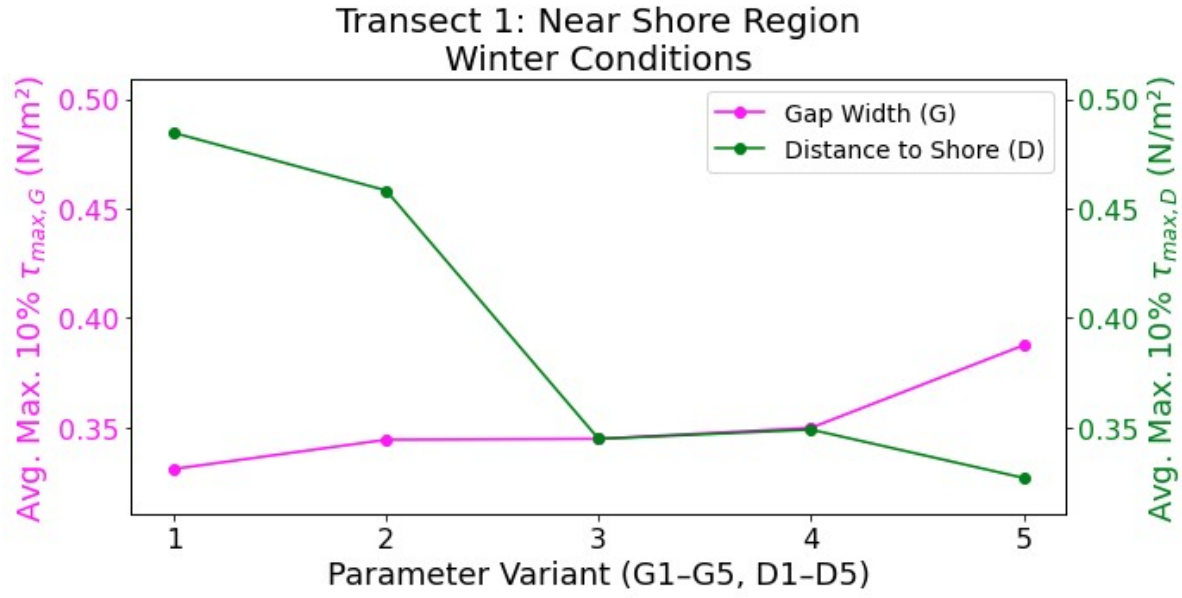

Figure 5.17: Spatial design variations: impact on the average of the top 10% highest values of τ_{max} along transect 1 during winter conditions. (G1:narrow gap - G5:wide gap - D1:close to shore - D5: further offshore)

In contrast, for transect 2 (in the middle of a segment), the average of the top 10% of τ_{max} increases with increasing distance to shore, while the influence of gap width is relatively small (figure 5.18).

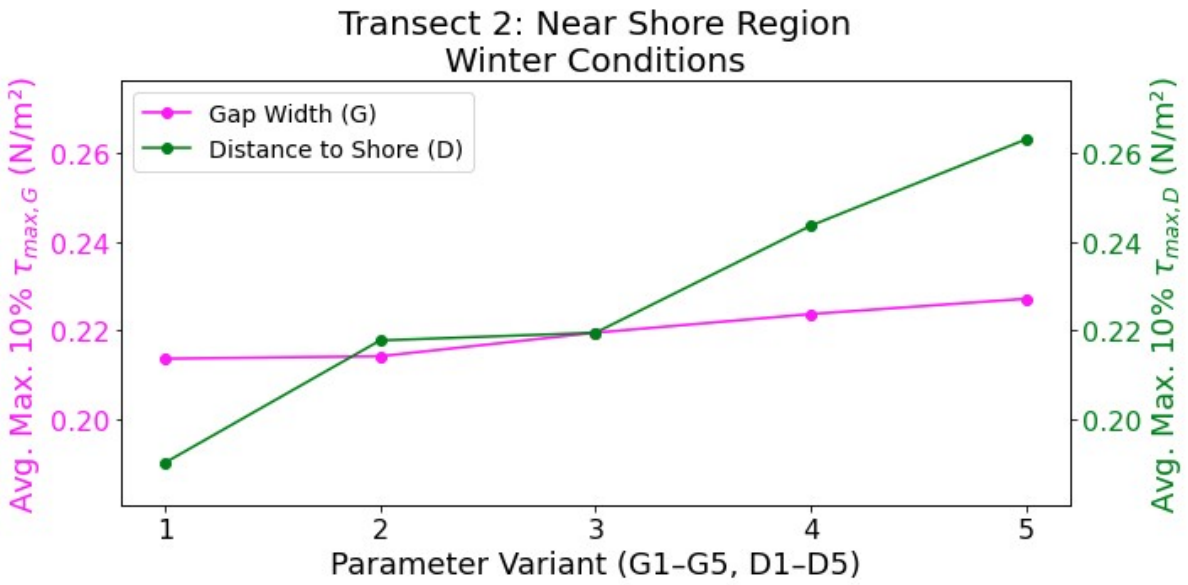

Figure 5.18: Spatial design variations: impact on the average of the top 10% highest values of τ_{max} along transect 2 during winter conditions. (G1:narrow gap - G5:wide gap - D1:close to shore - D5: further offshore)

The results show that the spatial parameters have a different impact on τ_{max} in transect 1 compared to transect 2. Transect 1 shows higher values and a more pronounced response to design variations. Transect 2 has overall lower τ_{max} values and a more gradual trend. The two design parameters affect τ_{max} in opposite ways. For transect 1, moving the structure offshore or narrowing the gap reduces τ_{max}, whereas for transect 2, offshore placement results in slightly increased shear stress.

Storm Conditions: Impact of Spatial Design Variations

The figures below show the average of the top 10% highest values of the maximum bed shear stress (τ_{max}) in the spatially averaged nearshore region for different design variations under storm conditions.

Figure 5.19 shows the results for transect 1. Wider gaps (G5) result in a significantly higher τ_{max}, exceeding 1.4 N/m^2, indicating a strong sensitivity to gap width under storm conditions. In contrast, the effect of increasing the distance to shore is relatively small, with only minor variations observed across the different offshore placements.

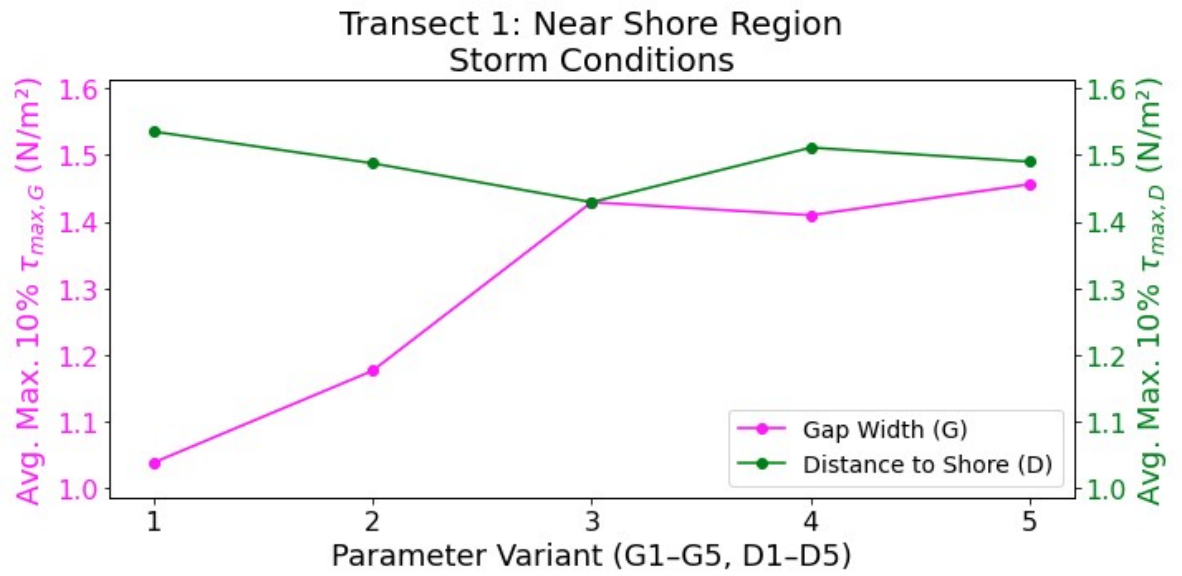

Figure 5.19: Spatial design variations: impact on the average of the top 10% highest values of τ_{max} along transect 1 during storm conditions. (G1:narrow gap - G5:wide gap - D1:close to shore - D5: further offshore)

Figure 5.20 shows both increasing the gap width and placing the breakwater further offshore lead to a continuous increase in the averaged τ_{max}, from approximately 0.5 N/m^2 to over 0.8 N/m^2.

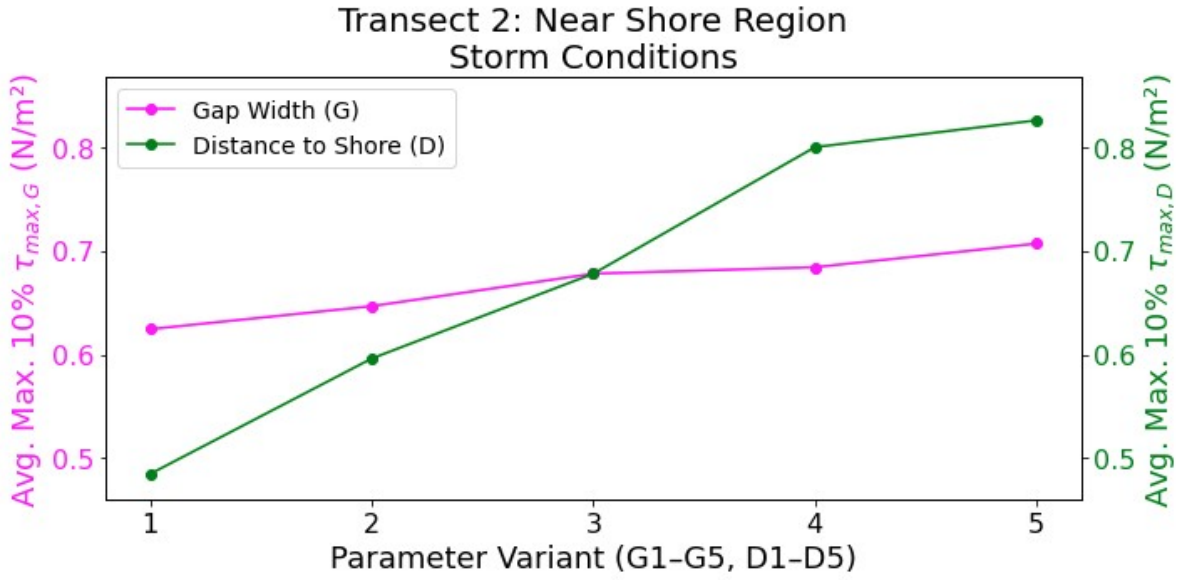

Figure 5.20: Spatial design variations: impact on the average of the top 10% highest values of τ_{max} along transect 2 during storm conditions. (G1:narrow gap - G5:wide gap - D1:close to shore - D5: further offshore)

The results show that the spatial design variations under storm conditions result in higher τ_{max} values in transect 1 compared to transect 2, consistent with the winter condition results. In transect 1, τ_{max} is reduced by narrowing the gap and by placing the structure further offshore. In transect 2, both an decreased gap width and smaller offshore distance lead to lower maximum bed shear stress values, although the overall values remain considerably lower than in transect 1.

An additional set of plots was created showing the average of the top 10% highest significant wave heights (H_s) for each spatial design variation and condition (see appendix C.4.1). These results show

similar trends with the maximum bed shear stress (τ_{max}), showing a strong relation between these parameters.

5.3.3. Optimal Spatial Dimensions

The aim of optimising spatial dimensions is to minimise the maximum bed shear stress (τ_{max}) in the nearshore area, close to the mangrove fringe. In this analysis, τ_{max} is represented by the average of the top 10% of values in the time series, to reflect the peak conditions. The two design parameters, gap width and distance to shore, are evaluated separately due to their differing effects between the two transects.

Gap Width

Across all conditions and both transects, narrower gaps consistently reduced τ_{max} in the model results. By limiting wave energy entering the nearshore zone, they reduce local velocities and promote conditions favourable for sediment deposition. However, very narrow gaps can also increase current velocities near the gap, which may transport energy into the nearshore area. This means there is likely a limit to how much narrowing improves conditions, because too small gaps could become counterproductive.

Distance to Shore

The effect of distance to shore (D) differs between the two transects. In transect 1, located at the gap, τ_{max} decreases as the structure is placed further offshore. In transect 2, behind the breakwater segment, the trend shows an opposite trend, namely increasing offshore placement leads to higher τ_{max}. To identify a design that balances both behaviours, linear extrapolation is applied outside of the modelled range (D1–D5), using the trend from D4 to D5. The intersection of the two extrapolated lines indicates a distance where the averaged τ_{max} is equal in both transects, suggesting an optimal breakwater placement that spreads the bed shear stresses more evenly across the nearshore region.

For the winter conditions (figure 5.21), the extrapolated lines intersect between variant D6 and D7, where both transects converge at $\tau_{max} \approx 0.30$ N/m^2. D6 represents a breakwater positioned 60 metres further offshore compared to the existing design at D3, and D7 corresponds to 80 metres further offshore.

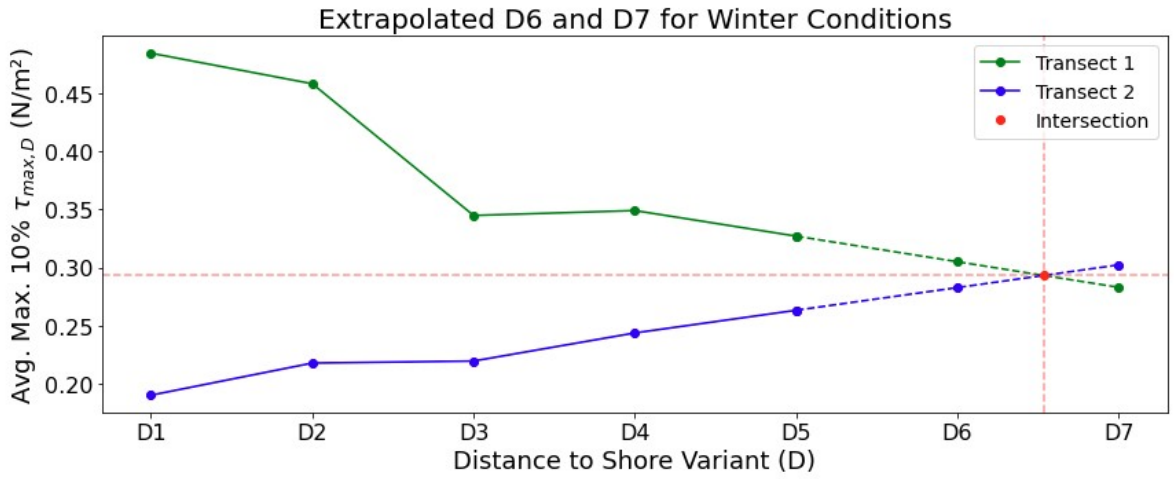

Figure 5.21: Optimisation of the distance to shore under winter conditions. D1–D5 represent modelled the average of the top 10% highest values of τ_{max}, D6 and D7 are extrapolated using the slope between D4 and D5. The red marker shows the intersection of Transect 1 and 2.

Under storm conditions (figure 5.22), no intersection is observed within the modelled range. Transect 1 consistently shows higher τ_{max} values than transect 2, and both exhibit relatively stable trends with relatively limited variation. In this case, there is no clear optimal offshore distance that simultaneously minimises τ_{max} for both transects.

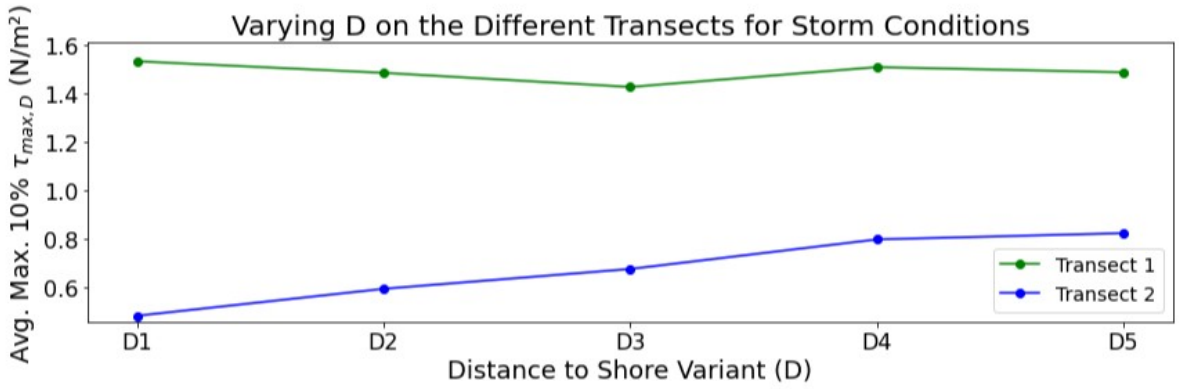

Figure 5.22: Comparison of the modelled average of the top 10% highest τ_{max} values across different transects for various distances to shore under storm conditions.

Based on these findings, the recommended breakwater location is between D6 and D7, corresponding to a position 70 metres further offshore than the existing breakwater placement. This placement provides a balanced reduction in peak bed shear stress across both transects under winter conditions. The storm scenario does not yield a converging point, but the results remain consistent with the trend that further offshore placement reduces τ_{max} in transect 1, which generally exhibits the highest values. These results are based on model simulations where the gap width was kept constant (G3, existing design).

Storm Conditions: Flow Pattern

The figures below show the depth-averaged flow velocities near the mangrove fringe under storm conditions during rising tide. Only the nearshore region is shown due to unreliable flow patterns near the breakwater, as the bathymetry is not adjusted for the modified breakwater positions as it would normally do. To clearly visualise the impact of spatial design, only the most extreme scenarios are compared.

In the gap width comparison, shown in figure 5.23, the narrower gap (G1, red) accelerates the flow slightly more through the opening, resulting in higher velocities directly behind the breakwater. This more concentrated jet results in higher flow velocities reaching the mangrove fringe. In contrast, the wider gap (G5, green) allows broader, less concentrated flow through the gap, reducing peak velocities behind the structure.

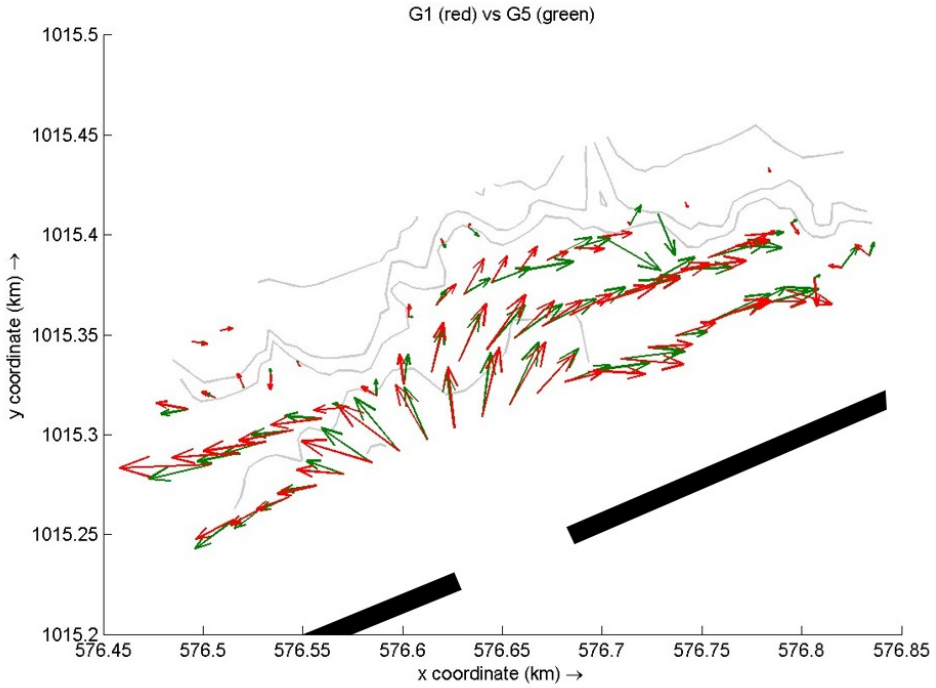

Figure 5.23: Flow velocity patterns nearshore for different gap widths (G1:narrow gap - G5:wide gap) during rising tide under storm conditions.

The comparison of the distance to the shore is shown in figure 5.24. Moving the breakwater further offshore (D5, orange) results in higher flow velocities near the mangrove fringe, especially behind a breakwater segment, where flow has had more space to accelerate after passing through the structure. In contrast, the closer placement (D1, purple) causes the flow acceleration through the gap to occur closer to the mangrove. Although peak velocities may not be higher, this jet reaches further into the sheltered area before it dissipates. This shifts the accelerated flow behind the gap closer to the mangrove fringe.

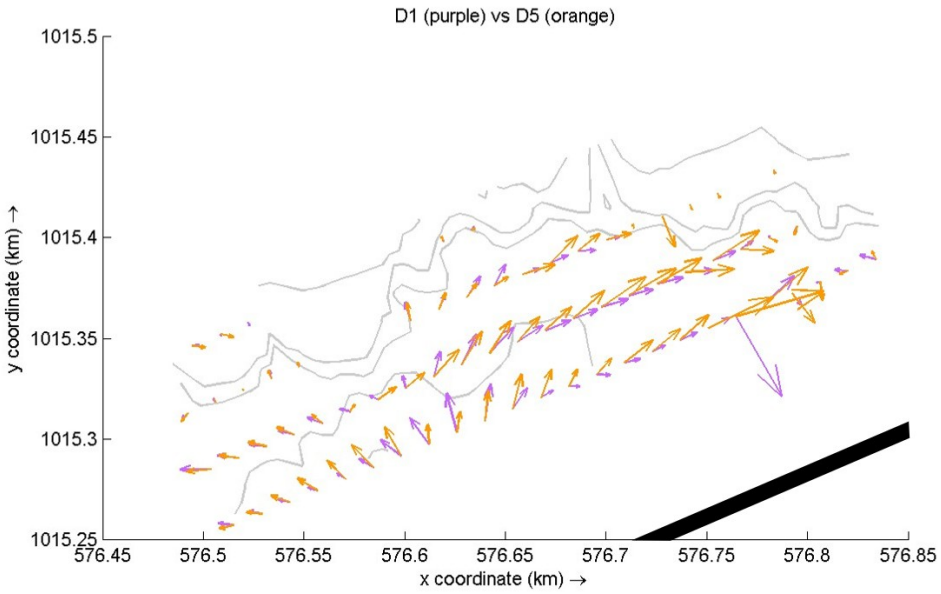

Figure 5.24: Flow velocity patterns nearshore for different distances to shore (D1:close to shore - D5: further offshore) during rising tide under storm conditions.

6

Discussion

This chapter aims to combine and analyse all findings of the study. By answering the sub-questions, reflecting on key limitations, and developing a conceptual model, the chapter assesses the effectiveness of the existing breakwater and explores the possibilities for future optimisation.

6.1. Reflection on Research Sub-Questions

This section will answer all research sub-questions (SQ), given in section 1.3.

> ***SQ1:*** *Which hydro- and morphodynamic conditions favour mangrove restoration, and how do the area's characteristics fail to provide these conditions?*

Mangrove restoration requires a stable, gently sloping (convex) tidal flat profile that provides sufficient sediment deposition and low bed shear stress to allow seedlings to establish roots during inundation-free periods. Optimal conditions include low wave energy and stable sediment supply to prevent erosion around mangrove roots, which anchors and protects the trees. In the Bạc Liêu area, however, the bathymetric profile shows a sharp drop in bed level at the mangrove fringe, which increases exposure to hydrodynamic forces. High bed shear stress near the mangroves causes sediment erosion around roots, destabilising mature trees and preventing seedling survival. For instance, in model scenarios representing the existing breakwater design, maximum bed shear stresses reached values above 0.8 N/m^2 during storm conditions, significantly exceeding the assumed critical threshold of 0.25 N/m^2 (section 5.3.2). This indicates that erosive forces remain strong enough to resuspend sediments and hinder stable sediment deposition near the mangrove fringe, even with the current structure in place. Although the permeable breakwater was built to reduce wave energy and encourage sedimentation, field observations show ongoing erosion at the mangrove fringe with erosion cliffs, indicating insufficient sediment deposition near the mangroves behind the structure. The higher bed level behind the breakwater compared to near the mangroves suggests sediment either does not reach the fringe or bed shear stresses remain too high for stable sedimentation. A similar situation was observed in Indonesia, where monitoring showed that limited sediment was deposited landward of permeable structures [45]. The bathymetric profile with different bed levels and the cliff is schematised in figure 6.1. These hydro- and morphodynamic conditions ultimately fail to create the windows of opportunity needed for successful mangrove establishment and growth.

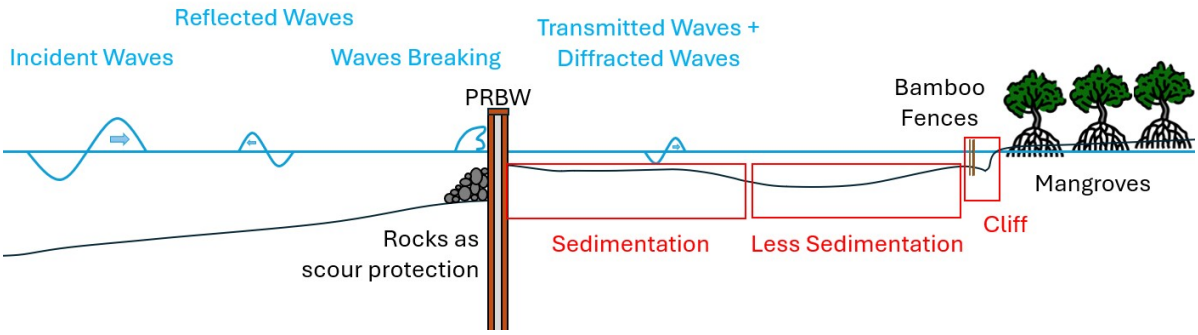

Figure 6.1: Schematic cross-section of the breakwater setup, showing wave transformation, sedimentation, and erosion at the mangrove fringe (cliff).

SQ2: *How do the hydrodynamic processes potentially drive sediment transport and morphologic changes in the study area?*

The combination of strong tidal currents and seasonal wave energy results in high bed shear stress, which can prevent sediments from settling (section 3.2.4, section 3.2.4). Subsidence deepens the coastal profile, increasing flow velocities and reinforcing erosion through a feedback loop. Upstream damming and sand mining reduce sediment supply, limiting sediment availability (section 3.1). The degradation of mangroves further impacts this process, as their root systems normally trap sediment and damp wave energy (section 1.1). PRBWs effectively dissipate short waves, but long waves may still penetrate and potentially contribute to erosion, especially near reflective structures and the mangrove fringe (section 3.2.4, section 3.2.3, section 5.1.1). Locally, waves diffract around and transmit through the breakwater gaps, causing flow acceleration that increases local bed shear stresses and sediment resuspension near the gaps. Attenuated wave energy and deflected currents promote sedimentation in sheltered shadow zones behind the structure.

SQ3: *Which design guidelines exist for breakwaters, and how does the current breakwater design compare to these guidelines?*

Design guidelines for permeable breakwaters suggest lengths of 60–240 m, gap widths of 10–100 m, and distances to shore between 80–230 m (section 2.2.4). The current breakwater design mostly fits within these ranges, though some segments exceed the recommended shore distance. However, the applicability of these broad guidelines to every site could be questionable. The sediment type in the study area, which is muddy, plays an important role in sediment dynamics and requires lower bed shear stress for deposition compared to sand. These guidelines are often based on sandy environments, where sediment transport differs. Therefore, breakwater designs should be investigated with the local site conditions, particularly for muddy coasts.

SQ4: *How does the current breakwater affect the maximum bed shear stress and flow pattern in the study area?*

Model results show that the existing breakwater reduces the maximum bed shear stress (τ_{max}) landward of the structure, with a clear decrease the area behind the breakwater. Significant wave height decreases by about 50% after passing through the breakwater at transect 2 during winter, demonstrating the effectiveness of the breakwater in attenuating wave energy. This reduction in wave height directly lowers bed shear stress through decreased orbital velocities (section 4.5). Under summer conditions, bed shear stresses remain below the critical threshold of 0.25 N/m^2 at both transects, while during winter this threshold is shortly exceeded at transect 1, suggesting potential to resuspension. The storm conditions result in maximum bed shear stresses far above the critical value in both transects, showing that the existing breakwater is not effective in reducing bed shear stress during extreme events (figure 5.12). Although such storms are typically short in duration, the intensity of the conditions is sufficient to cause significant erosion. Flow patterns shift significantly during storms, with flow accelerating through gaps and decelerating behind the structure, creating sheltered zones of reduced

velocity (figure 5.16). Sedimentation behind the breakwater has raised the bed level, further affecting flow dynamics. Without the breakwater, higher velocities would likely reach the mangrove fringe, increasing erosive forces.

SQ5: *How are the maximum bed shear stress and flow pattern influenced by the spatial dimensions of the breakwater?*

Gap width and offshore distance both influence the spatial distribution of maximum bed shear stress (τ_{max}) and flow patterns near the breakwater, with a distinct response between the two transects (section 5.3.2). Narrower gaps consistently reduce τ_{max} by limiting wave energy input, though they concentrate flow into narrow jets that increase local velocities behind the structure. Under storm conditions, this concentrated jet can reach further into the nearshore zone, while wider gaps result in more diffuse flow and lower peak velocities (figure 5.23). Offshore distance shows opposing trends: placing the breakwater closer to shore shelters transect 2 more effectively, reducing τ_{max} there, but simultaneously brings high-energy flow and waves from the gap closer to the near shore area of transect 1. In contrast, moving the structure further offshore increases dissipation space, reducing τ_{max} at transect 1 but exposing transect 2 to more hydraulic energy. These trade-offs result in an extrapolated optimal position 60–80 meters offshore, determined with the existing gap width kept constant and balancing bed shear stresses across both transects in winter. Under storm conditions, no such balance is found, and transect 1 consistently exhibits higher values. Since narrower gaps also increase the extent of the sheltered area, a larger part of the coast may behave like transect 2, potentially shifting the optimal offshore position. Simultaneously optimising gap width and offshore placement is therefore recommended to improve nearshore conditions. A strong correlation between τ_{max} and the significant wave height (H_s) is found, indicating the wave energy as a key driver of bed shear stress in this study. It should be noted that the model excludes important physical processes, like wave diffraction, long waves, and morphodynamic feedbacks, which could lead to different outcomes in wave energy distribution, flow patterns, and resulting bed shear stresses.

SQ6: *How do the modified hydrodynamics influence sediment transport and coastal erosion?*

Changes in gap width and distance to shore modify flow patterns and wave energy, which in turn affect sediment erosion, transport, and deposition (section 2.2). Narrower gaps limit wave energy in the sheltered area but concentrate flow, increasing velocities and bed shear stress around the gaps. This leads to stronger jets and localised sediment resuspension, which may result in scouring. In contrast, wider gaps distribute flow more evenly but allow more wave energy to enter the sheltered zone, increasing bed shear stress and potentially hindering sediment accumulation. Breakwaters placed closer to shore are more effective at reducing wave energy and bed shear stress near the mangroves, thereby supporting sedimentation. However, this placement limits the sheltered area and flow velocities have less space to dissipate, potentially increasing bed shear stresses near the shore. Placing the breakwater further offshore allows more hydraulic energy to reach the area behind the structure, which could increase the risk of erosion closer to shore, but it also facilitates natural sediment transport processes by enabling the flow to dissipate over a larger area before reaching the shore. The combined influence of gap width and distance to shore on sediment transport and coastal erosion requires a balance between these two parameters to create favourable conditions for sedimentation.

6.2. Limitations

The Delft3D model can be useful for comparing relative differences between design scenarios, but it is less reliable for predicting exact values as not all relevant processes are included. The limitations given below and described in section 4.1 need to be taken into account when analysing the findings.

Physical simplifications

The model leaves out several real-world features that could influence hydrodynamic and morphodynamic behaviour. For example, river inflows are not included, which can reduce or increase flow speeds

and bed shear stresses. It also does not account for scour protection rocks in front of the structure, bamboo fences near the mangroves, or environmental elements such as vegetation (including mangroves) that naturally dampen wave and current energy. Structural elements such as bridge columns were also excluded, though they may locally impact flow and turbulence. Additionally, the bathymetry used for the scenarios without the breakwater and for the variations in distance to shore was generated by smoothing the existing profile already shaped by the breakwater's presence. This creates a raised bed level in front of the structure in design D1, increasing the local flow velocity. The same elevation which is located behind the structure in D5, also affects flow dynamics. These effects are not caused by the design variations being tested and can make results harder to interpret. A key limitation of this study is the use of a morphostatic approach, where the bed level doesn't change throughout the simulation. In reality, updating the bed level over time could alter the relationship between the design parameters and sedimentation. This is important because the dynamics of flow patterns, bed shear stress, and sedimentation are not the same when assuming a fixed bed level. For example, sedimentation behind the breakwater could reduce local depths, lowering velocities and promoting further sedimentation. This is a positive feedback which is not included now. As a result for this example, the model would likely underestimates the long-term effectiveness of certain designs. Therefore, morphodynamic modelling is needed for more reliable predictions.

Numerical assumptions

Each simulation covers only four days, so longer seasonal trends are not included. The bathymetry is based on field data but interpolated and smoothed, which may misrepresent local bed features and thus affect flow patterns. A uniform Manning roughness from literature was used, rather than site-specific values, which introduces uncertainty in flow velocity and bed shear stress calculations. Model validation showed that simulated water levels and wave heights tend to underestimate observations, suggesting that τ_{max} is also likely underestimated. The breakwater is schematised as a porous plate with assumed transmission and resistance coefficients. This simplification cannot fully capture flow details near the structure, potentially affecting the simulated flow and stress patterns. Wave diffraction is not modelled, meaning wave energy does not bend into the sheltered area behind the breakwater. This particularly affects transect 2, leading to an underestimation of wave impact and thus bed shear stress in that zone, which limits the reliability of conclusions drawn for research sub-question 5. In addition, wave reflection at the breakwater was not activated, potentially underestimating local wave heights and altering near-structure hydrodynamics. Wave–current interaction was also disabled, meaning feedback mechanisms between waves and currents are not represented.

6.3. Conceptual Framework

The conceptual framework integrates all findings to provide a comprehensive understanding of how the breakwater design impacts hydrodynamics in relation to mangrove restoration. Over the past 22 years, the mangrove fringe in the study area has been retreating at an average rate of approximately 8 meters per year (figure 3.2). The main contributors to this retreat are likely human-induced coastal and estuarine squeeze from aquaculture and agricultural over-exploitation, natural coastal erosion, land subsidence, and a potential decrease in sediment supply from the Mekong River. This degradation of the mangroves can cause a positive feedback loop, further intensifying the erosive processes.

The model results indicate that the permeable breakwater significantly reduces bed shear stress in the sheltered areas by altering wave and flow dynamics. These large-scale modifications are schematically represented in figure 6.2. This suggests that with optimal design adjustments, such as smaller gap widths and adjusted distances to shore, short wave energy can be effectively dissipated. However, validation with field data shows that the model underestimates both water levels and significant wave heights. Additionally, model limitations, such as the exclusion of wave diffraction and long-wave effects, contribute to this underestimation of bed shear stress. So the assumed critical bed shear stress of 0.25 N/m^2 is likely exceeded more often than the model suggests.

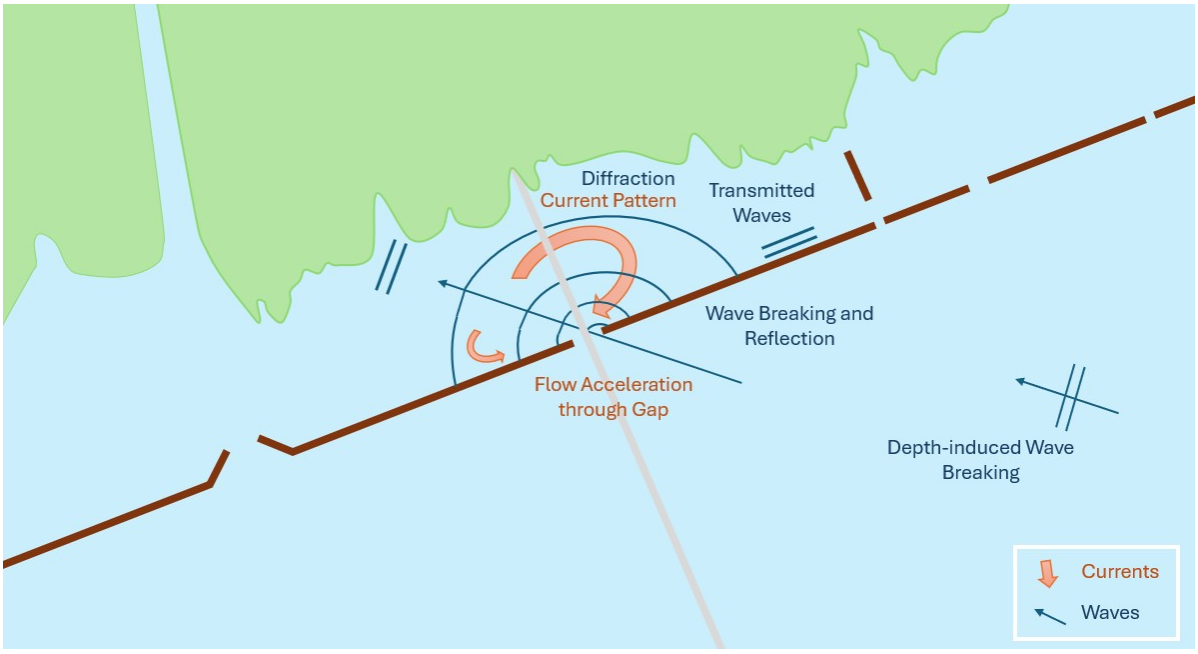

Figure 6.2: Schematic overview of waves and current patterns around the breakwater layout, including flow acceleration through gaps, wave diffraction, and sediment transport processes. The illustrated processes occur during rising tide with an average incident wave angle under winter conditions.

Long waves seem to be able to largely propagate through (section 5.1.1), which could suggest that the assumed permeability is too low for the long waves. To get an idea of this effect, simulations were conducted using the existing breakwater design with a permeability of 0.7. The results, detailed in appendix C.4.2, are used to estimate the transmission coefficient for long waves, assuming the storm conditions are representative. As shown in figure C.16, the significant wave height reduces by approximately 35%, corresponding to a transmission coefficient of approximately 0.65 for long waves. In contrast, the transmission coefficient for short waves is estimated at 0.5, based on the decrease in significant wave height across the breakwater under regular conditions for a permeability of 0.44. These values are indicated in figure 6.3, which schematically illustrates how short waves are more attenuated, while long waves continue to propagate and dissipate their energy nearshore, based on these assumptions.

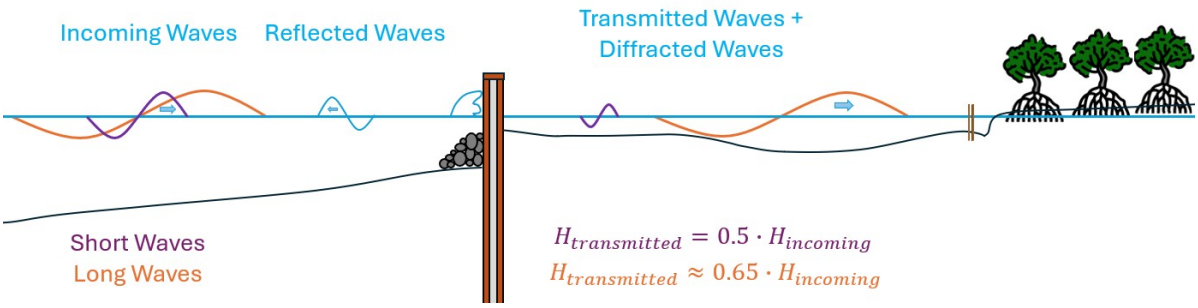

Figure 6.3: Schematic representation of wave transformation for the existing breakwater. Short waves are partially attenuated (transmission coefficient $\approx$ 0.5 for a permeability of 0.44), while long waves pass through more effectively (transmission coefficient $\approx$ 0.65 for a permeability of 0.7), reaching the mangrove fringe with significant wave energy.

The model results indicate that placing the breakwater further offshore results in a more uniform reduction in bed shear stress. However, this outcome is based on a fixed gap width. Narrowing the gaps could enlarge the sheltered area behind the breakwater, causing more similar behaviour to that observed along transect 2, so this could become more dominant. This may allow the breakwater to

be placed closer to shore then suggested in this study, though further research is needed to confirm this. Therefore, future studies should focus on optimising the spatial design by adjusting both the gap width and offshore distance. This includes investigating the combined effects of these parameters and including other important processes, such as long waves, wave diffraction, and variable permeability, to enable more accurate predictions and design recommendations. Additionally, a more detailed analysis of sediment type is essential to improve understanding of the area and to support the development of a reliable morphodynamic model, providing better insight into sedimentation processes.

7

Conclusion and Recommendations

This chapter answers the main research question by combining the findings of this study and drawing conclusions. Additionally, it provides recommendations for further research.

Main Research Question:

> *How do the spatial dimensions of the permeable breakwater affect the hydrodynamics controlling sediment dynamics relevant for mangrove restoration?*

7.1. Conclusion

This study investigated how the spatial design of the permeable breakwater influences hydrodynamic conditions relevant for sediment transport and mangrove restoration in Bạc Liêu, Vietnam. Field observations and data show insufficient sedimentation near the mangrove fringe, caused by unfavourable hydro- and morphodynamic conditions. To improve this, the focus is on creating conditions that favour sedimentation by adjusting two spatial design parameters of the permeable breakwater: the gap width and the distance to shore.

Narrowing the gaps limits the amount of wave energy entering the sheltered area, reducing bed shear stress near the mangroves. Although this concentrates the flow through the gaps and increases local velocities, model results show that wave energy remains the main factor influencing bed shear stress. Placing the breakwater closer to shore enhances shelter behind the structure, lowering bed shear stress in those areas. However, this also shifts the concentrated high-energy flow and waves at the gap more landward, which can reduce sedimentation near the mangroves in the area directly behind the gap. Moving the breakwater further offshore increases the space for dissipation behind the gaps and lowers bed shear stress in that region, but also allows more energy to reach the more sheltered area directly behind the breakwater.

The optimal design balances these effects and aims to minimise bed shear stress across the entire nearshore zone. This study finds that placing the breakwater approximately 70 metres further offshore and narrowing the gaps results in a more effective layout. Since narrower gaps already increase the extent of the sheltered area, the optimal offshore position may be slightly closer to shore than this estimate. Simultaneous adjustment of both parameters is therefore recommended to assess their combined impact.

The results show that the spatial design of the breakwater strongly influences local hydrodynamics and thereby sediment dynamics. Optimising the design offers potential to enhance the breakwater's effectiveness, but further research is needed to improve model accuracy and determine the most suitable breakwater design for the study area. These improvements are essential to support sedimentation and create stable conditions for mangrove survival and, ultimately, restoration.

7.2. Recommendations

This study has advanced the understanding of the spatial design of the breakwater in Bạc Liêu, but further research is needed to optimise its effectiveness. To find an optimal spatial design, future studies should explore a wider range of gap widths and distances to shore, including combinations where both parameters are adjusted simultaneously. To improve model accuracy, future simulations should include wave diffraction, long-wave processes, and longshore sediment transport. Additional field measurements, such as sediment grain size, settling velocity, and critical shear stress, would support morphodynamic modelling and improve understanding of the system. A morphodynamic model is recommended to capture sediment feedback loops and long-term system behaviour. Calibration using local field data is needed to better represent breakwater permeability and energy transmission. The relationship between breakwater placement and the breaker index could be investigated to assess any potential correlation. Longer monitoring periods are also recommended, as this study was limited to three days and maximum values, which may not capture representative variability. Alternative breakwater types should be considered, which could be more suitable for the area's environment. Long-term monitoring of various site characteristics is also advised to improve understanding of the area's behaviour and its response to interventions over time. Finally, further research is needed to understand all the factors contributing to mangrove failure. While this study focused on hydraulic and morphological aspects, other factors (such as ecological and anthropogenic influences) should also be considered to fully understand why mangroves are currently failing to survive and why restoration efforts are not succeeding, in order to develop more effective solutions.

These recommendations can inspire future activities within the Mangrove Living Lab. Field campaigns could focus on collecting more detailed data on sediment properties, flow conditions, and vegetation, to improve understanding of the area and build a better, site-specific model. Long-term monitoring of hydrodynamics, sedimentation, and mangrove response is recommended to validate morphodynamic modelling and assess how the coast actually responds to interventions over time. In addition, further investigation is needed into why mangrove restoration is failing, including ecological and human-related factors. Together, these efforts can help develop effective breakwater designs suited to local conditions.

References

[1] *About Delft3D*. https://oss.deltares.nl/web/delft3d/about. Accessed: 2024-09-26.

[2] Agence Française de Développement (AFD), European Union (EU), and Southern Institute of Water Resources Research (SIWRR). *Erosion processes in the Lower Mekong Delta Coastal Zones and measures for protecting Go-Cong and Phu-Tan*. Tech. rep. Contract No: AFD-SIWRR 2016. Ho Chi Minh City, Vietnam: Southern Institute of Water Resources Research, Dec. 2017. URL: http://www.siwrr.org.vn.

[3] Daniel M. Alongi. "Mangrove forests: Resilience, protection from tsunamis, and responses to global climate change". In: *Estuarine, Coastal and Shelf Science* 76.1 (2008), pp. 1–13. DOI: 10.1016/j.ecss.2008.03.027.

[4] Thorsten Balke et al. "Windows of opportunity: thresholds to mangrove seedling establishment on tidal flats". In: *Marine Ecology Progress Series* 440 (2011), pp. 1–9. DOI: 10.3354/meps09364.

[5] J.A. Battjes and M.J.F. Stive. "Calibration and verification of a dissipation model for random breaking waves". In: *Journal of Geophysical Research: Oceans* 90.C5 (1985), pp. 9159–9167. DOI: 10.1029/JC090iC05p09159.

[6] E.M. Van Bemmelen et al. *Uncovering Mangrove Successfulness in the Mekong Delta*. Vietnam Multidisciplinary Project (MDP). Nov. 2024. URL: Your%20URL%20here%20if%20applicable.

[7] Celine E.J. van Bijsterveldt, Rachael K. Griffin, Daniel A. Friess, et al. "To plant or not to plant: When can planting facilitate mangrove restoration?" In: *Frontiers in Forests and Global Change* 5 (2022), p. 813745. DOI: 10.3389/ffgc.2022.813745.

[8] Judith Bosboom and Marcel J.F. Stive. *Coastal Dynamics*. Version 1.2. Open access textbook licensed under CC BY-NC-SA 4.0. Delft, The Netherlands: TU Delft Open, 2023. ISBN: 978-94-6366-370-0. DOI: 10.5074/T.2021.001. URL: https://textbooks.open.tudelft.nl.

[9] T. Bouma, M. Friedrichs, and P. Klaassen. "Wave Reduction and Sediment Stabilization by Coastal Structures". In: *Estuarine, Coastal and Shelf Science* 150 (2014), pp. 218–230. DOI: 10.1016/j.ecss.2014.03.011.

[10] Laura Bricio, Vicente Negro, and J. Javier Diez. "Geometric Detached Breakwater Indicators on the Spanish Northeast Coastline". In: *Journal of Coastal Research* 24.5 (2008), pp. 1289–1303. DOI: 10.2112/07-0838.1. URL: https://www.researchgate.net/publication/242451581.

[11] C. Chassagne and T. S. van den Bremer. *Fluid Mechanics, CTB2110 Lecture Notes*. https://brightspace.tudelft.nl. Delft University of Technology, Quarter 1. 2023.

[12] CIFOR. *Mangroves in the Mekong Delta: Growing Opportunities or Going Under?* Accessed: 2024-09-16. 2022. URL: https://forestsnews.cifor.org/78722/mangroves-in-the-mekong-delta-growing-opportunities-or-going-under?fnl=en.

[13] Copernicus Climate Change Service (C3S). *ERA5: Fifth generation of ECMWF atmospheric reanalyses of the global climate*. https://cds.climate.copernicus.eu/datasets/reanalysis-era5-single-levels?tab=download. Accessed: 2024-01-07. 2017.

[14] J. Davis and H. Hanson. "Coastal Structures and Their Role in Shoreline Protection". In: *Coastal Engineering Journal* 45.3 (2018), pp. 223–245. DOI: 10.1016/j.coastaleng.2018.02.012.

[15] Deltares. *Delft3D QUICKIN User Manual*. Version 7.00, Revision 79761. Hydro-Morphodynamics & Water Quality. Deltares. Delft, The Netherlands, 2025. URL: https://www.deltares.nl/en/software-and-data.

[16] Deltares. *Delft3D-FLOW: Simulation of multi-dimensional hydrodynamic flows and transport phenomena, including sediments - User Manual*. Version 4.05. Accessed: 2024-09-26. Delft, The Netherlands, 2024. URL: file:///path/to/your/file/Delft3D-FLOW_User_Manual.pdf.

[17] Deltares. *Delft3D-WAVE: Simulation of short-crested waves with SWAN - User Manual*. Accessed: 2024-09-26. Delft, The Netherlands, 2024. URL: file:///path/to/your/file/Delft3D-WAVE_User_Manual.pdf.

[18] Deltares. *Land Subsidence*. Accessed: 2024-09-16. 2023. URL: https://www.deltares.nl/en/expertise/areas-of-expertise/land-subsidence.

[19] Deltares. *Mangrove Coasts under Threat*. Accessed: [Insert Date of Access]. 2023. URL: https://www.deltares.nl/en/expertise/projects/mangrove-coasts-under-threat.

[20] Deltares. *RGFGRID User Manual*. Version 7.00, Revision 79761. Delft, The Netherlands, 2025. URL: https://www.deltares.nl/en/software-and-data.

[21] Deltares. *Uncovering Mekong's Sand Debt*. https://www.deltares.nl/en/expertise/projects/uncovering-mekong-sand-debt. Accessed: 2024-09-10. 2023.

[22] T.J.F. (Tim) van Domburg. "Identifying Windows of Opportunity for Mangrove Establishment on a Mud Coast: A case study for the BioManCo project in Demak, Indonesia". MA thesis. Delft University of Technology, Sept. 2018. URL: http://repository.tudelft.nl/.

[23] Google Earth. *Google Earth Pro*. https://earth.google.com/. Accessed: 2024-10-01. 2024.

[24] Douglas A. Edmonds. "Restoration Sedimentology". In: *Nature Geoscience* 5 (2012), pp. 758–759. DOI: 10.1038/ngeo1620.

[25] Paul L.A. Erftemeijer et al. *Increasing coastal resilience through mangrove afforestation in the Mekong Delta: International examples and lessons learnt*. Tech. rep. Technical report commissioned by the Ministry of Economic Affairs and Climate Policy, Netherlands. Wetlands International and Royal Haskoning-DHV, Dec. 2021, p. 144.

[26] European Centre for Medium-Range Weather Forecasts (ECMWF). *ERA5 Reanalysis Data*. Accessed: 2024-02-28. 2024. URL: https://www.ecmwf.int/en/forecasts/dataset/ecmwf-reanalysis-v5.

[27] European Centre for Medium-Range Weather Forecasts (ECMWF). *GRIB Parameter Database - Wind*. Accessed: 14-Feb-2025. 2025. URL: https://codes.ecmwf.int/grib/param-db/?search=wind.

[28] Ken Fern. *Avicennia alba*. Tropical Plants Database. Accessed 2025-06-01. June 2025. URL: https://tropical.theferns.info/viewtropical.php?id=Avicennia+alba.

[29] Arniza Fitri et al. "Dynamics of Sediment Transport and Erosion-Deposition Patterns in the Locality of a Detached Low-Crested Breakwater on a Cohesive Coast". In: *Water* 11.8 (2019), p. 1721. DOI: 10.3390/w11081721.

[30] Wim Giesen et al. *Mangrove Guidebook for Southeast Asia*. Bangkok, Thailand: FAO and Wetlands International, 2006.

[31] Gary Griggs and Borja G. Reguero. "Coastal Adaptation to Climate Change and Sea-Level Rise". In: *Water* 13.2151 (2021). DOI: 10.3390/w13162151. URL: https://doi.org/10.3390/w13162151.

[32] Timothy O. Hodson. "Root-mean-square error (RMSE) or mean absolute error (MAE): when to use them or not". In: *Geoscientific Model Development* 15 (2022), pp. 5481–5487. DOI: 10.5194/gmd-15-5481-2022. URL: https://gmd.copernicus.org/articles/15/5481/2022/.

[33] Leo H. Holthuijsen. *Waves in Oceanic and Coastal Waters*. Cambridge, UK: Cambridge University Press, 2007. ISBN: 978-0-521-86028-4. URL: https://www.cambridge.org/9780521860284.

[34] Son Truong Hong. "Hydrodynamics of vegetated compound channels". PhD dissertation. Delft University of Technology, 2018. URL: https://doi.org/10.4233/uuid:4f28751a-2b9e-4a5a-87a6-5997f5c227b1.

[35] Zhan Hu et al. "Windows of opportunity for salt marsh vegetation establishment on bare tidal flats: The importance of temporal and spatial variability in hydrodynamic forcing". In: *Journal of Geophysical Research: Biogeosciences* 120.7 (2015), pp. 1450–1469. DOI: 10.1002/2014JG002870. URL: https://doi.org/10.1002/2014JG002870.

[36] *IANA Time Zone Database*. UTC+7 Time Zone Information. 2023. URL: https://www.iana.org/time-zones.

[37] IPCC. *Special Report on the Ocean and Cryosphere in a Changing Climate*. https://www.ipcc.ch/srocc/chapter/chapter-4-sea-level-rise-and-implications-for-low-lying-islands-coasts-and-communities/. Chapter 4: Sea Level Rise and Implications for Low-Lying Islands, Coasts and Communities. 2019.

[38] Tat Chien Khuong. "Shoreline Response to Detached Breakwaters in Prototype". PhD thesis. Delft University of Technology, 2016. ISBN: 978-94-6233-301-7. DOI: 10.4233/uuid:cdae6a2f-78dc-45fe-af01-43ed39c02ccc. URL: https://doi.org/10.4233/uuid:cdae6a2f-78dc-45fe-af01-43ed39c02ccc.

[39] Ken W. Krauss et al. "Woody Debris in the Mangrove Forests of South Florida". In: *Ecology* 84.4 (2003), pp. 971–981. DOI: 10.1890/0012-9658(2003)084[0971:WDIMFO]2.0.CO;2.

[40] Hoang-Anh Le et al. "The Multi-Channel System of the Vietnamese Mekong Delta: Impacts on the Flow Dynamics under Relative Sea-Level Rise Scenarios". In: *Water* 15.20 (2023), p. 3597. DOI: 10.3390/w15203597. URL: https://doi.org/10.3390/w15203597.

[41] Anne F. Van Loon et al. "Hydrological Classification, a Practical Tool for Mangrove Restoration". In: *PLOS ONE* 11.3 (2016), e0150302. DOI: 10.1371/journal.pone.0150302. URL: https://doi.org/10.1371/journal.pone.0150302.

[42] M. Losada, J. Lara, and R. Guanche. "Hydrodynamic Response and Morphological Changes Induced by Detached Breakwaters". In: *Coastal Engineering* 55 (2008), pp. 791–800. DOI: 10.1016/j.coastaleng.2008.02.014.

[43] Lowrance. *Lowrance Sonar Technology*. 2020. URL: https://www.lowrance.com/.

[44] Alejandra Gijón Mancheño. "Restoring Mangroves with Structures: Improving the Mangrove Habitat Using Local Materials". PhD thesis. Delft University of Technology, 2022. DOI: 10.4233/uuid:ed292367-ed2b-4bd3-a236-9f10d9c01da8. URL: https://doi.org/10.4233/uuid:ed292367-ed2b-4bd3-a236-9f10d9c01da8.

[45] Alejandra Gijón Mancheño et al. "Monitoring Pilot Study of Temporary Permeable Structures for Mangrove Restoration in Demak, Indonesia". In: *Water* 17.4 (2025), p. 558. DOI: 10.3390/w17040558. URL: https://www.mdpi.com/2073-4441/17/4/558.

[46] Patrick Marchesiello et al. "Erosion of the coastal Mekong delta: Assessing natural against man-induced processes". In: *Continental Shelf Research* 181 (2019), pp. 72–89. DOI: 10.1016/j.csr.2019.05.004. URL: https://doi.org/10.1016/j.csr.2019.05.004.

[47] Frontiers in Marine Science. "Mangrove restoration and zonation in the Vietnamese Mekong Delta". In: *Frontiers in Marine Science* 9 (2022), p. 1043943. DOI: 10.3389/fmars.2022.1043943. URL: https://www.frontiersin.org/articles/10.3389/fmars.2022.1043943/full.

[48] Kris May et al. *San Francisco Bay Tidal Datums and Extreme Tides Study*. Final Report. Accessed on 2025-01-28. San Francisco Bay Conservation, Development Commission, FEMA, and other contributors, Feb. 2016. URL: file:///C:/Users/Rosita%20Vos/Downloads/SFBay_TidalDatums_Extreme_Tides_Study.FINAL05.2.16.pdf.

[49] Yoshihiro Mazda et al. "Mangroves as a Coastal Protection from Waves in the Tong King Delta, Vietnam". In: *Estuarine, Coastal and Shelf Science* 54.1 (1997), pp. 65–70. DOI: 10.1006/ecss.1996.0179.

[50] A. L. McIvor et al. *Mangroves for Coastal Defence*. Tech. rep. The Nature Conservancy and Wetlands International, 2012. URL: https://www.nature.org/media/oceansandcoasts/mangroves-for-coastal-defence.pdf.

[51] H. Mitchener and H. Torfs. "Erosion of Mud–Sand Mixtures". In: *Coastal Engineering* 29.1-2 (1996), pp. 1–25. DOI: 10.1016/0378-3839(96)00002-6.

[52] R.N.A. Mussert. "The Design of Permeable Structures Aimed at Rehabilitating Mangroves: A Case Study in Demak, Indonesia". MA thesis. Delft University of Technology, Apr. 2024.

[53] Tran Sy Nam et al. “Optimizing Hydraulic Retention Time and Area of Biological Settling Ponds for Super-Intensive Shrimp Wastewater Treatment Systems”. In: *Water* 14 (2022), p. 932. DOI: 10.3390/w14060932. URL: https://doi.org/10.3390/w14060932.

[54] National Geographic. *Monsoon*. Accessed: 2024-10-25. 2024. URL: https://education.nationalgeographic.org/resource/monsoon/.

[55] National Oceanic and Atmospheric Administration (NOAA). *What is the intertidal zone?* Accessed: 16 January 2025. n.d. URL: https://oceanservice.noaa.gov/facts/intertidal-zone.html.

[56] Netherlands Organization for Scientific Research (NWO). *Rise and Fall: Awareness of Land Subsidence in the Mekong Delta*. https://www.nwo.nl/en/cases/rise-and-fall-awareness-of-land-subsidence-in-the-mekong-delta. Accessed: 2024-09-10. 2024.

[57] Hiep Van Nguyen et al. “Observation and Simulation of Wind Speed and Wind Power Density over Bac Lieu Region”. In: *Advances in Meteorology* 2021 (2021), pp. 1–17. DOI: 10.1155/2021/8823940. URL: https://doi.org/10.1155/2021/8823940.

[58] Nguyet-Minh Nguyen et al. “Experimental and numerical modeling of pile-rock breakwater gap arrangement for optimal coastal erosion protection in deltaic coasts”. In: *Ocean Engineering* 280 (2023), p. 114625. DOI: 10.1016/j.oceaneng.2023.114625. URL: https://doi.org/10.1016/j.oceaneng.2023.114625.

[59] Obscape. *Level Gauge - Continuous Water Level Monitoring*. Accessed: 25-Feb-2025. 2024. URL: https://obscape.com/site/products/level_gauge/.

[60] Obscape. *Obscape Products*. Accessed: 16-Oct-2024. 2024. URL: https://obscape.com/site/products/.

[61] Obscape. *Pressure Wave Gauge - Real-time Wave Monitoring*. Accessed: 25-Feb-2025. 2024. URL: https://obscape.com/site/products/pressure-wave-gauge/.

[62] Obscape. *Weather Station - Wireless Environmental Monitoring*. Accessed: 25-Feb-2025. 2024. URL: https://obscape.com/site/products/weather_station/.

[63] Oceanographic Magazine. *Research shows conservation of mangrove forests pays for itself in flood protection*. Accessed: 2024-11-01. 2024. URL: https://oceanographicmagazine.com/news/mangrove-forests-flood-protection/.

[64] Chris Paola and et al. “Natural Processes in Delta Restoration: Application to the Mississippi Delta”. In: *Annual Review of Marine Science* 3 (2011), pp. 67–91. DOI: 10.1146/annurev-marine-120709-142856.

[65] Hung Manh Phan. “Coastal and Seasonal Hydrodynamics and Morphodynamics of the Mekong Delta”. PhD thesis. Delft University of Technology, 2020. DOI: 10.4233/uuid:2bcb33bf-5b73-4873-9168-08b1e7a2836f. URL: https://doi.org/10.4233/uuid:2bcb33bf-5b73-4873-9168-08b1e7a2836f.

[66] Hung Manh Phan et al. “Tidal wave propagation along the Mekong deltaic coast”. In: *Estuarine, Coastal and Shelf Science* 220 (2019), pp. 73–98. DOI: 10.1016/j.ecss.2019.01.026. URL: https://doi.org/10.1016/j.ecss.2019.01.026.

[67] Linh Khanh Phan. “Wave attenuation in coastal mangroves: Mangrove squeeze in the Mekong Delta”. PhD dissertation. PhD thesis. Delft University of Technology, 2019. DOI: 10.4233/uuid:9397d964-1674-4838-a13a-504742dba55e. URL: http://repository.tudelft.nl/.

[68] Manh Hung Phan and Marcel J.F. Stive. “Managing mangroves and coastal land cover in the Mekong Delta”. In: *Ocean and Coastal Management* 219 (2022), p. 106013. DOI: 10.1016/j.ocecoaman.2021.106013. URL: https://www.sciencedirect.com/science/article/abs/pii/S096456912100311X.

[69] RVO team including Professor Emeritus Dr Marcel Stive et al. *Restoration and Sustainable Management of Coastal Forests in the Mekong Delta to enhance Environmental Change Adaptation Capacity*. Draft report as of December 19, 2023. Netherlands Enterprise Agency (RVO), 2023. URL: URL%20of%20the%20document%20if%20available%20online.

[70] Thamnoon Rasmeemasmuang and Jun Sasaki. *Wave Reduction in Mangrove Forests: General Information and Case Study in Thailand*. Tech. rep. Accessed: 2024-09-26. Handbook of Coastal Disaster Mitigation for Engineers and Planners, 2015. URL: file:///C:/path/to/your/file/Wave%20Reduction%20in%20Mangrove%20Forests_%20General%20Information%20and%20Case%20Study%20in%20Thailand.pdf.

[71] Z. Rong, Y. Li, and Y. Liu. "The Influence of Breakwater Length on Wave Energy Dissipation". In: *Marine Geology* 400 (2020), pp. 105–120. DOI: 10.1016/j.margeo.2020.105120.

[72] National Ocean Service and NOAA. *What are mangroves?* Tech. rep. Accessed: 2024-09-26. National Oceanic and Atmospheric Administration (NOAA), n.d. URL: https://oceanservice.noaa.gov/facts/mangroves.html#:~:text=Mangroves%20are%20a%20group%20of,allow%20fine%20sediments%20to%20accumulate..

[73] R. Silvester and J. Hsu. *Coastal Stabilization: Innovative Approaches*. Berlin, Germany: Springer, 1993. ISBN: 978-3-540-57342-5.

[74] R.L. Soulsby and S. Clarke. *Bed Shear-stresses Under Combined Waves and Currents on Smooth and Rough Beds*. Report TR 137, HR Wallingford, produced within Defra project FD1905 (EstProc), August 2005. 2005.

[75] R.L. Soulsby et al. "Wave-current interaction within and outside the bottom boundary layer". In: *Journal of Hydraulic Engineering* 119.5 (1993). Received 1 October 1992; accepted after revision 1 June 1993, pp. 716–731. DOI: 10.1061/(ASCE)0733-9429(1993)119:5(716).

[76] Tung Tran Thanh et al. "Modelling Storm Surge Hazard to Mekong Delta". In: *Proceedings of the 10th International Conference on Asian and Pacific Coasts (APAC 2019)*. Ed. by N. Trung Viet et al. Springer Nature Singapore Pte Ltd., 2019, pp. 1–10. DOI: 10.1007/978-981-15-0291-0_1. URL: https://www.researchgate.net/publication/336071997.

[77] The Fish Site. *The Sinking Aquaculture Dragon Struggles in the Mekong: Food Security*. https://thefishsite.com/articles/the-sinking-aquaculture-dragon-struggles-in-the-mekong-food-security. Accessed: 2024-09-10. 2023.

[78] The Nature Conservancy and Wetlands International. *Mangroves for Coastal Defence: Guidelines for Coastal Managers & Policy Makers*. Tech. rep. Accessed: [Insert Date of Access]. 2014. URL: https://www.nature.org/media/oceansandcoasts/mangroves-for-coastal-defence.pdf.

[79] Nirubha Raghavi Thillaigovindarasu. "Mangrove-Sediment Connectivity in the Presence of Structures Used to Aid Restoration: A Demak Case Study". Master's Thesis. Delft, The Netherlands: Delft University of Technology, Dec. 2023. URL: http://repository.tudelft.nl/.

[80] Pham Hong Tinh et al. *Mangroves restoration in Vietnamese Mekong Delta during 2015-2020: Achievements and challenges*. Technical Report. Accessed: 2024-09-16. Faculty of Environment, Hanoi University of Natural Resources and Environment, Hanoi, Vietnam, 2022. URL: file:///C:/Users/Rosita%20Vos/Downloads/fmars-09-1043943.pdf.

[81] Trung tâm Nghiên cứu Khai thác Tài nguyên Biển và Đới bờ - Viện Kỹ Thuật Biển. *Hệ thống thông tin dự báo, cảnh báo sớm thủy hải văn, môi trường*. https://marinemekong.com/. Accessed: 2025-03-04.

[82] TU Delft. *Mangrove Living Lab*. Accessed: 2025-01-31. n.d. URL: https://www.tudelft.nl/global/research/education-entrepreneurship/navigating-the-future-building-resilient-deltas-in-vietnam/mangrove-living-lab.

[83] Le Anh Tuan. *Erosion in the coastal areas of the Vietnamese Mekong Delta: Current challenges and solutions*. Technical Report. Accessed: 2024-09-10. College of Environment and Natural Resources, Cam Tho University, Viet Nam, 2024. URL: %5Curl%7Bfile:///C:/Users/Rosita%20Vos/Downloads/Erosion_in_the_coastal_areas_of_the_Vietnamese_Mek.pdf%7D.

[84] United Nations Environment Programme (UNEP). *An Inside Look at the Beauty and Benefits of Mangroves*. Accessed: [Insert Date of Access]. 2023. URL: https://www.unep.org/news-and-stories/story/inside-look-beauty-and-benefits-mangroves.

[85] Unknown. *CH 14 Mangrove-Mud Coasts*. Presentation. Focuses on sediment dynamics, mangrove ecosystem services, and coastal protection on muddy coasts. n.d. URL: Uploaded%20file,%20not%20publicly%20available.

[86] Utrecht University. *Land Subsidence in the Vietnamese Mekong Delta*. https://www.uu.nl/en/research/water-climate-and-future-deltas/land-subsidence-in-the-vietnamese-mekong-delta. Accessed: 2024-09-10. 2024.

[87] Cong Mai Van et al. "Bamboo Fences as a Nature-Based Measure for Coastal Wetland Protection in Vietnam". In: *Frontiers in Marine Science* 8 (2021), p. 756597. DOI: 10.3389/fmars.2021.756597. URL: https://www.frontiersin.org/articles/10.3389/fmars.2021.756597/full.

[88] L. Van Rijn. "Coastal Erosion and Sediment Transport". In: *Journal of Coastal Research* 50 (2011), pp. 1–17. DOI: 10.2112/JCOASTRES-D-11-00072.1.

[89] Jan Van Sickle. *GPS for Land Surveyors*. Fourth Edition. CRC Press, 2017. ISBN: 9781498762073.

[90] Gerbrant van Vledder, Marcel Zijlema, and Leo Holthuijsen. "Revisiting the JONSWAP bottom friction formulation". In: *Coastal Engineering Proceedings*. Accessed: 9 March 2025. 2011. DOI: 10.9753/icce.v32.waves.41. URL: https://www.researchgate.net/publication/49115774_Revisiting_the_JONSWAP_bottom_friction_formulation.

[91] Global Mangrove Watch. *Global Mangrove Watch*. https://www.globalmangrovewatch.org. Accessed: 2024-10-17. 2024.

[92] Wikipedia. *Mekong Delta*. https://en.wikipedia.org/wiki/Mekong_Delta. Accessed: 2024-09-10. 2024.

[93] C. J. Willmott and K. Matsuura. *Some measures of model performance*. Vol. 2. Wiley, 1982, pp. 387–392.

[94] Cort J. Willmott and Kenji Matsuura. "Advantages of the Mean Absolute Error (MAE) over the Root Mean Square Error (RMSE) in Assessing Average Model Performance". In: *Climate Research* 30.1 (2005), pp. 79–82. DOI: 10.3354/cr030079. URL: https://www.int-res.com/abstracts/cr/v30/n1/p79-82/.

[95] Tom Wilms, Bregje van Wesenbeeck, and Femke H. Tonneijck. *Permeable Structures: Building with Nature to restore eroding tropical muddy coasts*. Tech. rep. Accessed: 2025-02-04. Ecoshape Technical Report, Dordrecht, The Netherlands, 2017. URL: https://www.researchgate.net/publication/353074084.

[96] Johan C. Winterwerp, William G. Borst, and Mindert B. de Vries. "Pilot Study on the Erosion and Rehabilitation of a Mangrove Mud Coast". In: *Journal of Coastal Research* 21.2 (2005), pp. 223–230. ISSN: 0749-0208. DOI: 10.2112/03-832A.1.

[97] Johan C. Winterwerp et al. "Defining Eco-Morphodynamic Requirements for Rehabilitating Eroding Mangrove-Mud Coasts". In: *Wetlands* 33 (2013), pp. 515–526. DOI: 10.1007/s13157-013-0409-x.

[98] Johan C. Winterwerp et al. "Managing erosion of mangrove-mud coasts with permeable dams—lessons learned". In: *Ecological Engineering* 158 (2020), p. 106078. DOI: 10.1016/j.ecoleng.2020.106078.

[99] Eric Wolanski et al. "Fine-sediment Dynamics in the Mekong River Estuary, Vietnam". In: *Estuarine, Coastal and Shelf Science* 43 (1996), pp. 565–582.

[100] Yun-Ta Wu and Shih-Chun Hsiao. "Propagation of solitary waves over a submerged permeable breakwater". In: *Coastal Engineering* 81 (2013), pp. 1–18. DOI: 10.1016/j.coastaleng.2013.06.005. URL: http://dx.doi.org/10.1016/j.coastaleng.2013.06.005.

[101] Tu Le Xuan et al. "Hydraulic performance and wave transmission through pile-rock breakwaters". In: *Ocean Engineering* 218 (2020), p. 108229. DOI: 10.1016/j.oceaneng.2020.108229. URL: https://doi.org/10.1016/j.oceaneng.2020.108229.

[102] Dazhi Yang, Wenting Wang, and Tao Hong. "A historical weather forecast dataset from the European Centre for Medium-Range Weather Forecasts (ECMWF) for energy forecasting". In: *Solar Energy* 232 (2022), pp. 263–274. DOI: 10.1016/j.solener.2021.12.011.

[103] Mingjian Yin et al. “Flow pattern and hydrodynamic parameters of pile breakwater under solitary wave using OpenFOAM”. In: *Ocean Engineering* 235 (2021), p. 109381. DOI: 10.1016/j.oceaneng.2021.109381.

[104] B. Zanuttigh, J. Van der Meer, and M. Kramer. “Wave Transmission Behind Low-Crested Breakwaters: Implications for Coastal Protection”. In: *Ocean Engineering* 78 (2014), pp. 106–118. DOI: 10.1016/j.oceaneng.2013.09.007.

[105] M. Zijlema. *Lecture notes MFTBP: Computational modelling of flow and transport*. Delft, The Netherlands: Delft University of Technology, 2011.

[106] Claudia Zoccarato, Philip S. J. Minderhoud, and Pietro Teatini. “The Role of Sedimentation and Natural Compaction in a Prograding Delta: Insights from the Mega Mekong Delta, Vietnam”. In: *Scientific Reports* 8 (2018), p. 11437. DOI: 10.1038/s41598-018-29734-7. URL: https://doi.org/10.1038/s41598-018-29734-7.

A

Fieldwork Bạc Liêu

A.1. Fieldwork Data

To build a reliable model of the study area and to perform a data analysis, it is important to collect accurate field data. This section describes the data gathered, the equipment used, and the methodologies for each type of measurement. The data collection will focus on the following key elements: bathymetry, water pressure, bed shear strength, offshore hydrodynamics, and PRBW structure properties.

The data that is successfully gathered by the fieldwork are:

- Bathymetry
- Cross sections
- Wave pressure behind breakwater
- Weather data
- Water level
- Bed shear strength

Bathymetry and Cross-Sections

Bathymetry measurements are essential to map the underwater topography of the study area. The current bathymetry behind the breakwater is obtained using a sonar scan from a boat. The cross-sections are gathered by walking along cross-shore transects with a RTK (Real Time Kinematic) GPS. These transects are perpendicular to the structure and start onshore in the mangroves to obtain data through the vegetation. The measurements are referenced to mean sea level using information from a nearby tidal station for consistency.

Water Pressure

The water pressure is measured using two pressure sensors, which are called Pressure Wave Gauges. The output supports the understanding of effect of the structure on the current patterns and hydrodynamics. The pressure sensors will record the time series data of water levels, allowing the separation of tidal and wave contributions. Wave properties will then be derived from the wave-induced changes in water levels. Atmospheric pressure corrections will be applied using local weather station data or a portable CTD (Conductivity, Temperature, and Depth sensor), which will be placed nearby. Firstly, the sensors will be placed in transect 4. Position T4A will serve as the reference point, with one sensor remaining there while the other is relocated after one day. This ensures that each dataset of the second sensor covers a full tidal cycle as it moves sequentially from T4B to T4C, and finally to T4D. A comparison of these datasets with the dataset from the sensor at T4A provides a dissipation parameter behind the gap. Secondly, the sensors will be deployed along transect 2, with one positioned seaward (T2A) of the structure and the other landward (T2B). These measurements will assess differences in flow conditions between the sheltered area and the open sea, providing insight into how the permeable breakwater (PRBW) affects currents. Additionally, sensors will be placed along transect 1 in the same

positions as in transect 2. Since transect 1 is farther from the gap, it may yield different results, offering insights into the gap's influence on dissipation parameters. This final deployment is optional and will only be conducted if the time allows it, considering potential delays or issues during the field trip.

Offshore Water Level and Wind

Offshore water level and wind data are used to validate the numerical model. Water levels are measured by a tide gauge 3.4 km offshore, capturing tidal fluctuations. Wind speed and direction are recorded by the weather station. These data provide realistic boundary conditions for the model, ensuring accurate simulation of hydrodynamics in the study area.

A.2. Devices

To gather the data, five devices are used during fieldwork. Three of these, namely the water level gauge, wave pressure gauge, and weather station, were developed by Obscape. Living Lab collaborates with Obscape, which provides compact, solar-powered monitoring equipment with real-time data transmission via the Obscape Data Portal [60].

A.2.1. Hydrodynamics

The hydrodynamic data is measured with the Obscape devices, listed below. The wave pressure and weather gauges sampled every 60 minutes, and the water level gauge recorded data every 30 minutes. The set-up can be observed in figure 5.2.

Water Level Gauge

The Obscape Level Gauge measures hydrostatic pressure, which correlates directly with water depth based on the equation:

$$P = \rho g h \tag{A.1}$$

where P is pressure, ρ is water density, g is gravitational acceleration, and h is water depth. Atmospheric pressure compensation improves accuracy. The processed data is transmitted wirelessly, providing continuous water level monitoring. [59]

Wave Pressure Gauge

The Obscape Pressure Wave Gauge measures wave characteristics by converting hydrostatic and dynamic pressure variations into water level fluctuations. A pressure transducer detects changes in water column height as waves pass over the sensor, converting them into electrical signals. These signals are processed to determine wave height, period, and direction, with real-time data transmission to the Obscape Data Portal [61].

Weather Gauge

The Obscape Weather Station measures wind, temperature, pressure, humidity, rainfall, and solar radiation. Wind speed and direction are determined using a four-arm anemometer that detects changes in sound speed. Temperature is measured with a thermistor or infrared sensor, and pressure is recorded by a sensor that converts membrane movement into an electrical signal. Humidity is measured with a sensor that estimates moisture through vapour pressure. Rainfall is tracked by counting drops with gold-plated pins, and solar radiation is measured using a silicon-cell pyranometer. All data is processed by a microcontroller and sent wirelessly to the Obscape Data Portal for real-time monitoring [62].

(a) Water level gauge **(b)** Wave pressure gauge **(c)** Weather station

Figure A.1: Obscape monitoring instruments used for environmental data collection [60]. The water level gauge tracks tidal variations, the wave pressure gauge measures hydrodynamic forces, and the weather station records meteorological parameters such as wind speed, temperature, and atmospheric pressure.

A.2.2. Cross-Sections

For coastal cross-section surveys, RTK (Real-Time Kinematic) GPS provides precise elevation and position measurements along transects. The output is accurate on centimeter level by resolving carrier phase measurements, reducing errors from atmospheric delays and satellite drift. The system consists of a base station, which calculates positional errors, and a rover, which applies real-time corrections via radio or internet [89].

A.2.3. Bathymetry

The Lowrance Fish Radar is a sonar-based system used for bathymetric surveys in coastal and estuarine areas. It sends out high-frequency CHIRP (Compressed High-Intensity Radiated Pulse) sonar signals, which bounce off the seabed. The system calculates water depth by measuring the time it takes for the signal to return. During surveys, the device is mounted on a boat and records depth along navigated route. It also uses GPS to link depth measurements to specific locations, creating bathymetry maps [43].

A.3. Diary Fieldwork Bạc Liêu

This section contains a diary documenting the activities during the fieldwork.

Day 1 (01-12-2024)

16:00 Arrival in Bạc Liêu city. No activities planned.

Day 2 (02-12-2024)

9:00 We first went to Nhà Mát. We went on the pier to observe the breakwater and have a first glance at the bathymetry and mangroves during low tide.

10:00 After Nhà Mát we went to the Hoà Bình 1 wind farm resort to meet with the field work team, namely Khanh, Anh and Tung. We had a short meeting about the plan for the day and the rest of the week. The weather station was being installed on a pole to have a fast deployment at the measurement location.

11:00 We walked over the pier to the breakwater to observe the area, focusing on the breakwater, mangroves and bathymetry. You could clearly see a lot of sedimentation just behind the breakwater.

11:30 After we came back, a small car drove us and the field work team over the pier to the deployment location, 6 km offshore. The water level sensor was already installed the day before. The weather station was installed next to it, as showed in figure A.2. Next, we drove a bit further to take a look at

where the wave buoy will be placed. At this location we also observed a strong cross shore current, induced by the rising tide.

Figure A.2: Deployment of the weather station

13:00 After observing the area and taking a lot of pictures and videos for later observations, we drove back by car and we had lunch with the team.

14:00 Working in the cafe.

15:30 We went back during high tide. The water was penetrating into the mangroves. But not until the dike. You could clearly see the effect of the breakwater. Long waves still reach the shore and break just before or inside the mangroves. Hung said he thinks the long waves have a big effect on the erosion. He thinks the breakwaters should always be placed close to the mangroves, otherwise only settling just behind it too far from the mangroves.

16:00 Wave buoy was deployed close to the location of the weather station and water level device. However, the wave buoy seemed to be offline. Needs to be redeployed tomorrow

Day 3 (03-12-2024)

9:00 Working day in the hotel.

While driving through the area, clear signs of subsidence can be observed, especially around the bridges. The transitions between the bridges and the roads show significant elevation differences, with the roads being much lower than required for a smooth connection. So it seems that the ground level has significantly dropped since the bridges were constructed.

Day 4 (04-12-2024)

9:00 Meeting up with the whole Living Lab team at Hoà Bình 1.

10:00 Going to the measurement location at the end of the pier. It was observed that the waves are a bit larger in between the windmill park, this is due to the bathymetry Hung said. Going back to the breakwater, Tung observed the sediment behind the breakwater is more muddy than in front of the breakwater. Just behind the breakwater the sediment is still a bit sandy but going further to the mangroves, the sediment becomes more muddy. There is a cliff in front of the mangroves. Bamboo fences are placed closely in front of the cliff. It can be observed there is still ongoing erosion in between

the bamboo fences and the mangroves. An assumption can be that the reflective waves are creating the erosion. Cliffs at the locations with and without bamboo fences seem similar, so the effect seems minimal. Rocks are placed in front and at the gaps against scour holes.

Figure A.3: The Living Lab team and the observed eroding mangroves

12:00 Lunch

13:00 Meeting about Living Lab. Discussion about the organisation and about future plans. We contributed by giving feedback from the student perspective. Due to regulations, we found out we are not allowed to perform the measurements directly. So we discussed how we can contribute to the fieldwork as much as possible in the upcoming days.

18:00 Dinner with the whole team.

Day 5 (05-12-2024)

9:00 Meeting up with the whole Living Lab team at Hoà Bình 1. We discussed measuring the suspended sediment concentration during falling and rising tide. We can help with performing these measurements because it can be done safely from the bridge. We also brought the shear vane test to the site to test it and discuss suitable locations. Additionally, we evaluated new measurement devices, namely water level loggers, which can be installed within the mangroves to measure the water level. We explained to Khanh how he can do a qualitative assessment of the mangrove roots, and naked him to do it at the location with severe erosion (Hoà Bình 1) and a location with stable mangroves (West of Hoà Bình 1) we asked him to take a lot of pictures near the cliffs.

12:30 Lunch

13:30 Giving instructions to Khanh about the shear vane test with the corresponding locations. Saying goodbye to the team, except for the fieldwork team. Agreements are made with the whole Living Lab team about follow-up actions and communication.

14:30 We drove along the coast to the west of the wind farm. At this part of the coast the shoreline seems to be more stable, based on satellite images. The mangroves were not accessible. We observed that the land use in this location is completely the same as at the location where severe erosion is happening. Along the whole coast people build their houses on the seaward side of the dike. This means that they completely rely on the earthen dike built in between the natural mangroves and the fisheries. This implies that even during storms and spring tides, the water rarely reaches the area behind the earthen dike. This was later confirmed by Tung.

16:00 We went back to the pier at the Hoà Bình 1 wind farm. To collect samples for the suspended sediment concentration (SSC). First we went to the location at the end of the pier. Anh prepared a simple set-up with a plastic bottle with a brick and a rope attached to it. By lowering the bottle into

the water, a sample is collected. This sample will later be dried and will be used to calculate the SSC. The same technique is used at a location closer to the shore. We have doubts about the effectiveness and accuracy of this method, because the bottle does not sink immediately to the bottom, and has to be dunked in and out the water to fill it up little by little. Therefore only water from the top layer with relatively little sediment is collected.

Figure A.4: Collecting and comparing the SSC samples

Day 6 (06-12-2024)

9:00 Meeting up with the team at Hoà Bình 1. Khanh came back with the results of the work he did for us. In the end he only went to the Nhà Mát location (newly planted mangroves), and not to Hoà Bình 1 (severe erosion) and west to Hoà Bình 1 (stable mangroves), due to time limitations and hard conditions. This means that there is not enough information for a qualitative assessment of the roots. The shear vane test was performed at two locations in Nhà Mát. One near the mangroves and one half way between the mangroves and the breakwater. Brainstorming with Tung how we can install ceramic divers to log the water level in the field.

10:00 Tung and Khanh go down the ladder from the pier in Hoà Bình 1. They walk a new bathymetry transect with the RTK. starting close to the earthen dike all the way to the cliff. On the way, Tung installs the water level logger on a trunk and Khanh does a shear vane test and takes photos of the roots. From these photos and also observations from the bridge, it seems that no new root systems have formed over time.

11:00 Lunch with the team

13:00 Working in the cafe

15:00 Going back to the measuring location to collect more water samples for the SSC calculation.

18:00 Dinner with the director of the windmill park

B

Modelling

B.1. Model Input

B.1.1. Bathymetry

Nested Grid

The depth values of the manually added samples in the nested grid are as follows:

- **Mangroves landward**: d = - 1.95 m
- **Mangroves sea side**: d = - 1.35 m
- **Cliffs**: d = - 0.65 m
- **Behind breakwater**: d = -0.9 m
- **In front of breakwater**: d = -0.4 m
- **River**: d = 0.3

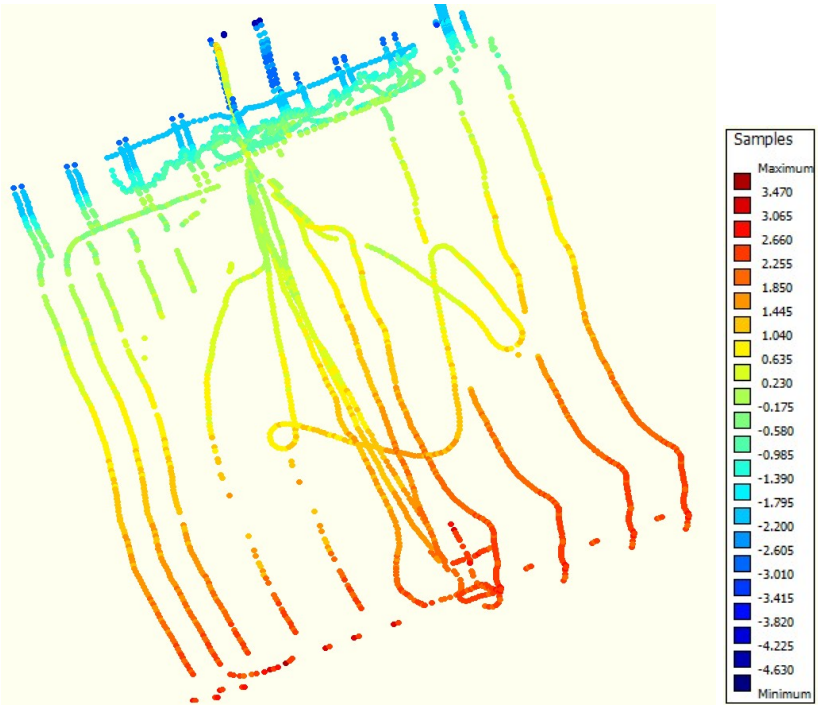

Figure B.1: Depth samples of the bathymetry collected during fieldwork, including manually added values, used for the coarse and nested grid bathymetry.

Coarse Grid

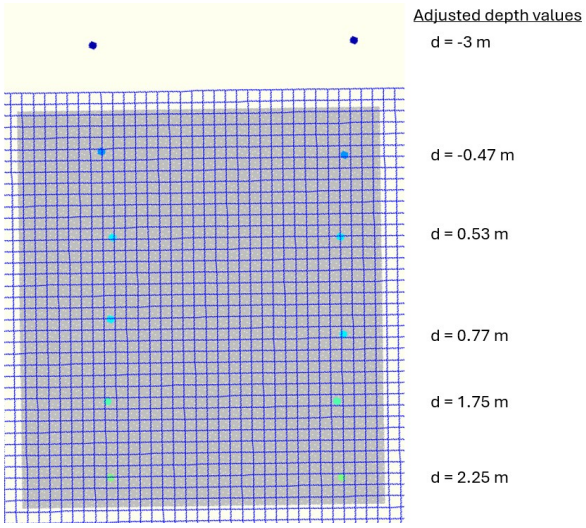

Figure B.2: The location and depth values of the manually added samples in the coarse grid are shown in the coarse grid compared to the nested grid. These values are based on the fieldwork measurements to ensure a smooth transition between the different grids.

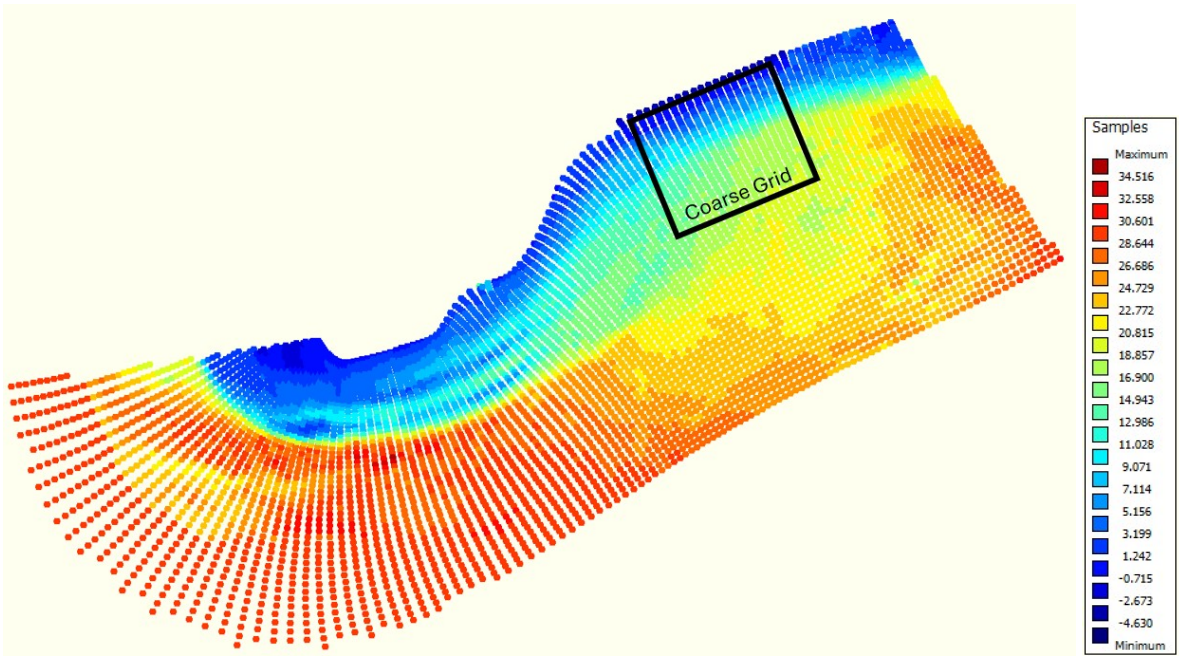

Figure B.3: Depth samples of the bathymetry around the Mekong Delta, used for the coarse grid bathymetry.

B.1.2. Tidal Constituents

Tidal constituent	Name	Amplitude [m]	Phase [deg]
Semidiurnal			
Principal lunar	M_2	1.08	118
Principal solar	S_2	0.39	177
Lunar-elliptical	N_2	0.07	65
Lunar-solar declinational	K_2	0.05	180
Diurnal			
Lunar-solar declinational	K_1	0.67	3
Principal lunar	O_1	0.45	310
Principal solar	P_1	0.16	340
Other			
Semi-annual	S_a	0.16	280
Storm surge (High energy conditions) [76]	A_0	1.1	0

Table B.1: Main tidal constituents of the study area used as input for the Delft3D model [66][46]

B.1.3. Offshore Data

A distinction is made between summer (May to October), winter (November to April), and storm conditions to account for seasonal variability. Offshore wave and wind data were obtained from the ERA5 reanalysis dataset [13]. The high temporal resolution and global coverage makes it suitable for representing the offshore boundary conditions. The offshore boundary location for the large-scale grid in the WAVES module is set at longitude 106.0°E and latitude 9.0°N, approximately 32 kilometers offshore with a depth of approximately 20 meters. The dataset has a temporal resolution of 60 minutes and covers the period from 2014 to 2024. The average offshore conditions over this eleven-year period are similar to the values reported by Phan [65], indicating the reliability of the dataset.

Figure B.4: Measurement locations for offshore hydrodynamic conditions and their distances from the shore [23]. One location represents the mean offshore conditions for summer and winter (approximately 32 km offshore at 9°N, 106°E), while the other marks the location for storm conditions (approximately 40 km offshore).

Mean Wave Conditions

The wave condition datasets and their corresponding mean values are shown in figure B.5. These mean values are used as boundary conditions for the summer and winter scenario simulations.

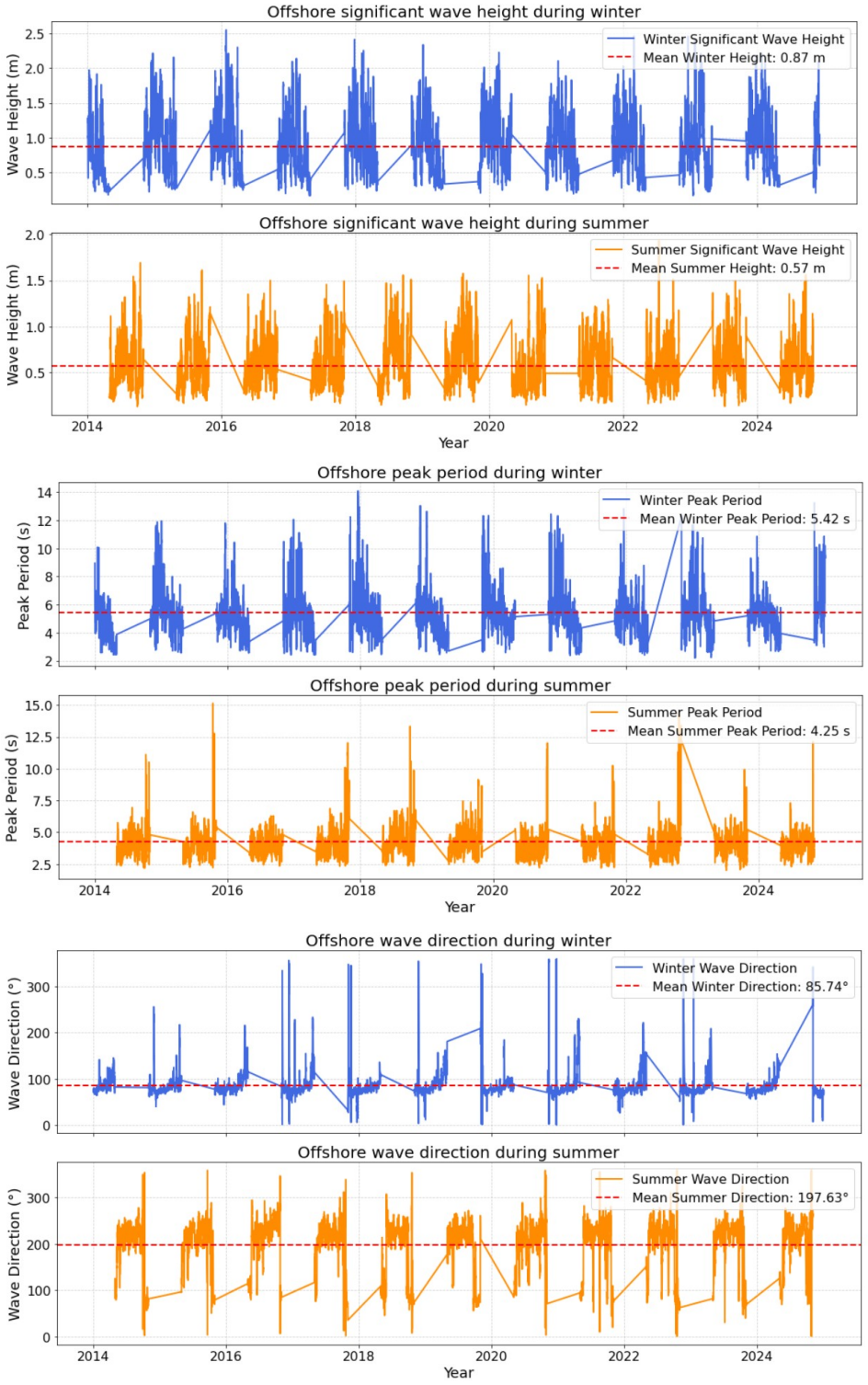

Figure B.5: Wave conditions and corresponding mean values for the summer and winter monsoon seasons (2014–2024) [13].

Mean Wind Conditions

The V10 data represents the component of wind at a height of 10 meters above the Earth's surface, indicating how much of the wind is moving towards the north. Similarly, the U10 data represents the eastward component of wind at the same height, showing how much of the wind is flowing towards the east [27]. These average values of these components during the monsoon seasons are calculated separately and then combined to determine the overall wind speed and direction at 10 meters above ground level [102].

The formulas for calculating wind speed and wind direction from the U10 and V10 wind components, as derived using Yang, Wang, and Hong [102], are as follows:

$$V = \sqrt{u^2 + v^2} \tag{B.1}$$

$$\phi = \mathrm{mod}\left(180 + \frac{180}{\pi}\,\mathrm{atan2}(v, u), 360\right) \tag{B.2}$$

where:

- V is the wind speed [m/s], calculated as the magnitude of the wind vector from the (u) and (v) components.
- ϕ represents the meteorological wind direction, measured in degrees from which the wind is blowing (0° = North, 90° = East, etc.)
- u is the zonal (east-west) wind component (U10)
- v is the meridional (north-south) wind component (V10)

The mean wind values used as model input are:

- Summer (May–Oct): Wind speed: 3.82 m/s, Wind direction: 241.87°
- Winter (Nov–Apr): Wind speed: 5.67 m/s, Wind direction: 77.95°

The corresponding wind roses are shown below in figure B.6.

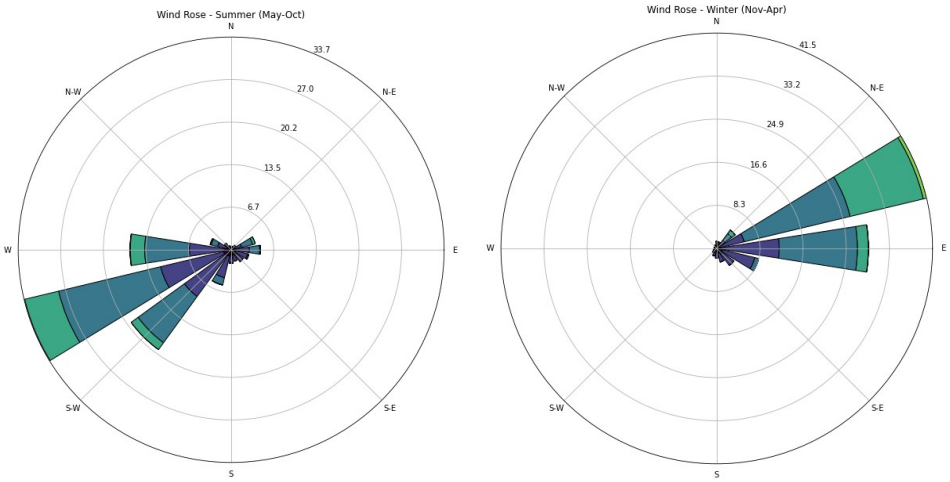

Figure B.6: Wind roses for the summer and winter monsoon seasons (2014–2024) [13].

Storm Conditions

The storm conditions at the coast of Bạc Liêu are based on [76]. These conditions correspond to a 10-year return period and are classified as Beaufort scale 9. The storm conditions are approximately 40 km offshore, with a water level of 235 + 22 cm. During the storm, the maximum significant wave

height reaches 5.29 m, with a maximum wave period of 8.96 seconds. The maximum wind speed is recorded at 22 m/s, and both the mean wave and wind direction are 90° (East).

B.1.4. Breaker Index

The breaker index γ is computed using the formula from Battjes and Stive [5]:

$$\gamma = 0.5 + 0.4 \tanh(33 s_0) \tag{B.3}$$

where the deep-water wave steepness s_0 is given by:

$$s_0 = \frac{H_s}{L_{\text{deep}}} \tag{B.4}$$

The deep-water wavelength is calculated using the linear wave dispersion relation:

$$L_{\text{deep}} = \frac{g T_p^2}{2\pi} \tag{B.5}$$

where $g = 9.81$ m/s² is the gravitational acceleration.

Table B.2: Breaker index γ per modelling condition

Condition	H_s [m]	T_p [s]	L_{deep} [m]	s_0 [-]	γ [-]
Summer	0.57	4.25	28.20	0.0202	0.73
Winter	0.87	5.42	45.87	0.0190	0.72
Storm	5.29	8.96	125.34	0.0422	0.85

B.2. Spatial Designs

The design parameters that will be modified are illustrated in figure B.7.

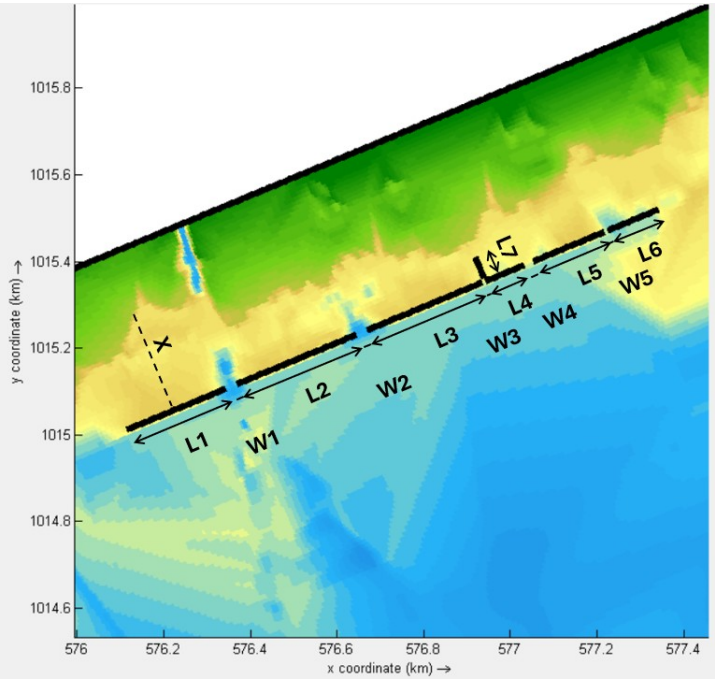

Figure B.7: Considered design parameters for the different design scenarios: L = Structure length, G = Gap width, D = Distance to the mangrove fringe.

Table B.3: Dimension details of the breakwater design variations

Design	G3/D3 (Existing Structure)	G1	G2	G4	G5	D1	D2	D4	D5
Structure Length (m)									
L1	225	240	235	220	210	225	225	225	225
L2	274	284	274	264	264	274	274	274	274
L3	282	292	292	283	277	282	282	282	282
L4	94	99	99	89	84	94	94	94	94
L5	177	182	177	172	172	177	177	177	177
L6	120	135	130	115	105	120	120	120	120
L7	50	60	55	45	40	50	50	50	50
Gap Width (m)									
W1	30	20	25	35	40	30	30	30	30
W2	31	21	26	36	41	31	31	31	31
W3	9	4	4	14	14	9	9	9	9
W4	23	13	18	28	33	23	23	23	23
W5	9	4	4	9	14	9	9	9	9
Distance to Mangrove Fringe (m)									
X	96–289	96–289	96–289	96–289	96–289	56–249	76–269	116–309	136–329

B.2.1. Delft3D

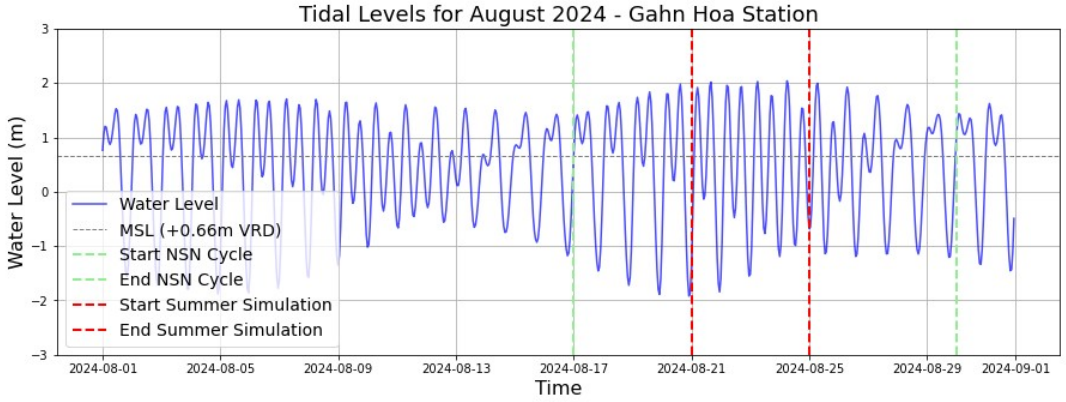

(a) Tidal levels at Ganh Hao station [81], used to identify the summer NSN (neap–spring–neap) cycle (August 17, 00:00 – August 30, 00:00). The spring tide occurred from August 21, 00:00 – August 25, 00:00.

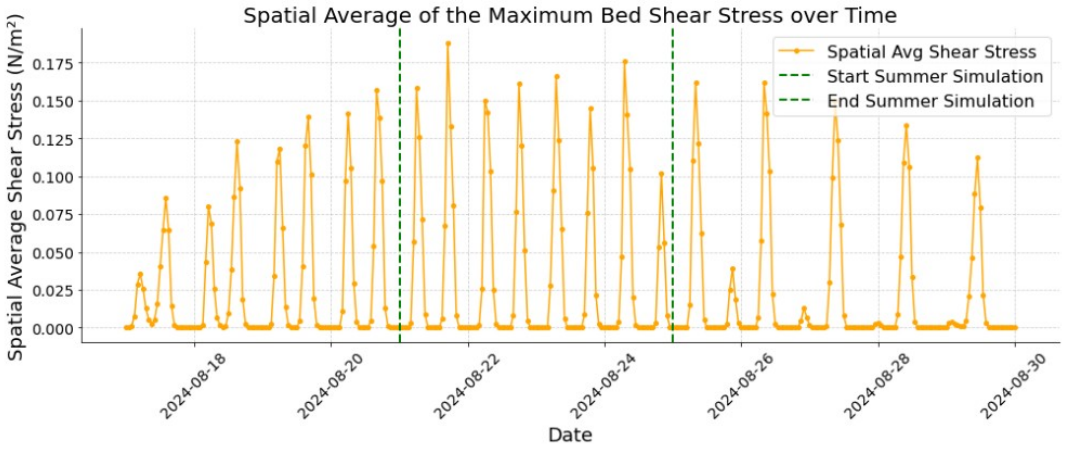

(b) The spatial average of maximum bed shear stress over the full area behind the breakwaters in the study area. The peak values align with the spring tide period.

Figure B.8: Summer simulation period based on tidal levels and the maximum bed shear stress. The simulation covers four days during the spring tide (August 21, 00:00 – August 25, 00:00), when hydrodynamic forcing and bed shear stresses are highest.

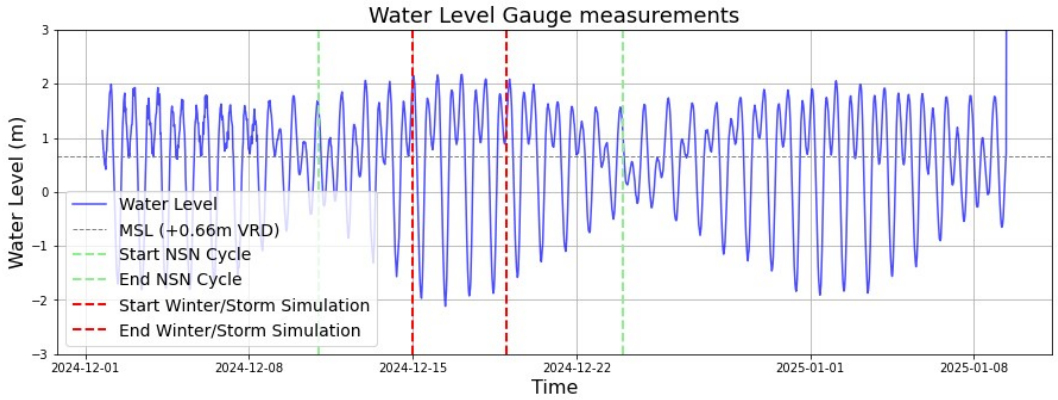

(a) Water level measurements from fieldwork showing the winter NSN cycle (December 11, 00:00 – December 24, 00:00). The spring tide occurred between December 15, 00:00 and December 19, 00:00.

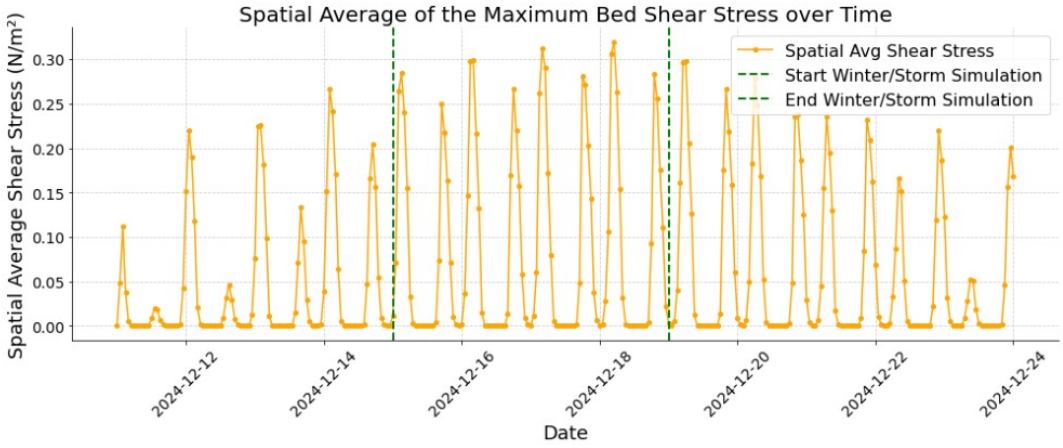

(b) Spatial average of maximum bed shear stress over the area behind the breakwaters in the study area. Shear stress was highest during the spring tide period.

Figure B.9: Winter simulation period based on field-measured tidal levels and the maximum bed shear stress. The simulation covers four days during the spring tide (December 15, 00:00 – December 19, 00:00).

B.3. Soil Samples

Figure B.10: Locations of the taken soil samples: Cross-section 4 in Nhà Mát and cross-section 5 at the Hòa Binh wind farm (study area) [6]

Location	Sample	Sand [%]	Silt [%]	Clay [%]	D_{50} [mm]
Cross-Section 4	NM1	17.8	60.3	21.9	0.0252
Nha Mat	NM2	14.3	62.2	23.5	0.0232
	NM3	23.8	54.3	22.0	0.0273
Cross-Section 5	M1	3.5	52.6	43.8	0.0070
Hoa Binh	M2	2.0	53.5	44.4	0.0070
	M3	21.9	69.7	8.3	0.0345
	M4	98.1	1.4	0.5	0.1750

Figure B.11: Table of the soil properties at the researched locations [6]

B.4. Output Analysis

Table B.4: Locations and Bed Levels for Transect 1 (M=385) and Transect 2 (M=416)

Location	N	Bed Level (m)	Distance from Mangroves Location (m)
Transect 1 (M=385)			
Mangroves	332	1.7 (MHW)	0
Cliff	320	0.9	40
Near Shore	323	0.5	90
Gap (Breakwater)	313	-0.3	200
Offshore	304	0.0	250
Transect 2 (M=416)			
Mangroves	330	1.7 (MHW)	0
Cliff	324	0.9	70
Near Shore	322	0.5	90
Behind Breakwater	314	-0.3	185
Offshore	304	0.0	250

C

Results

C.1. Cross-Sections

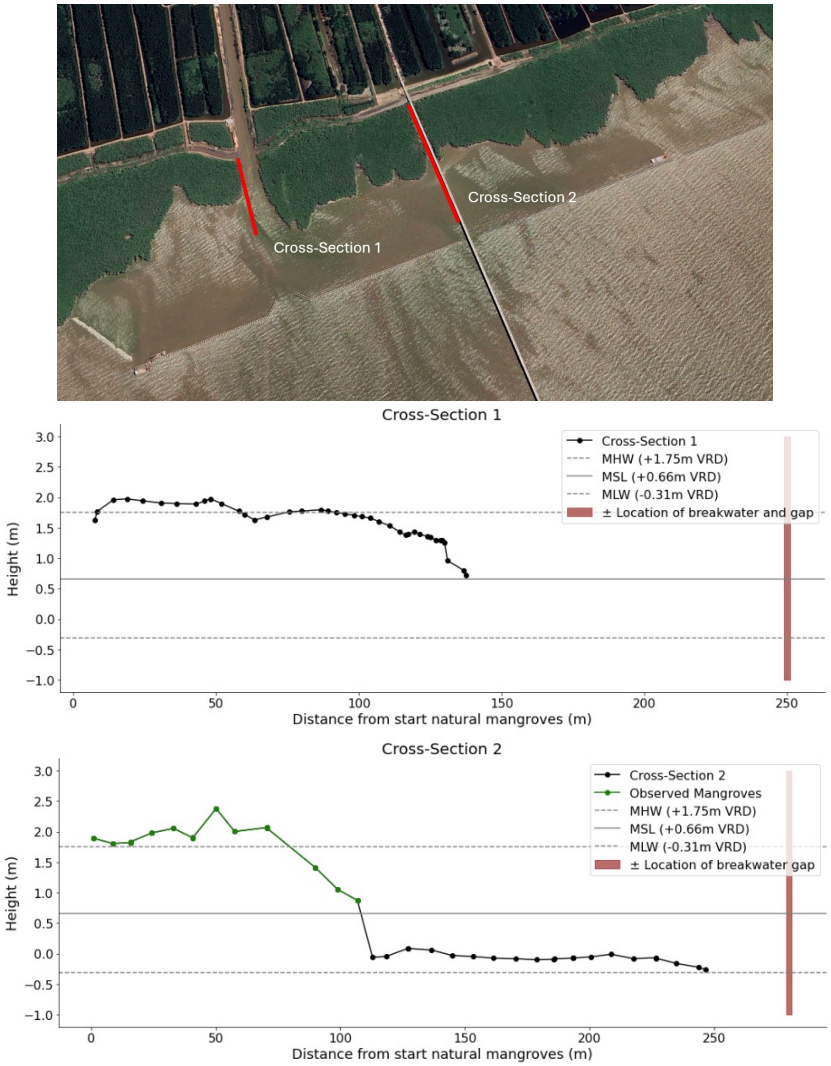

Figure C.1: Cross-sections collected during fieldwork, illustrating the measured profiles in the study area.

C.2. Offshore Conditions for the Validation and Calibration

The offshore conditions are recorded at the same time and interval as the analysed wave pressure gauge shown in figure 5.5, with a time interval of 60 minutes from 4 December 2024 to 6 December 2024. These conditions are presented in figure C.2 and are also obtained from Copernicus Climate Change Service (C3S) [13] at the location shown in figure B.4.

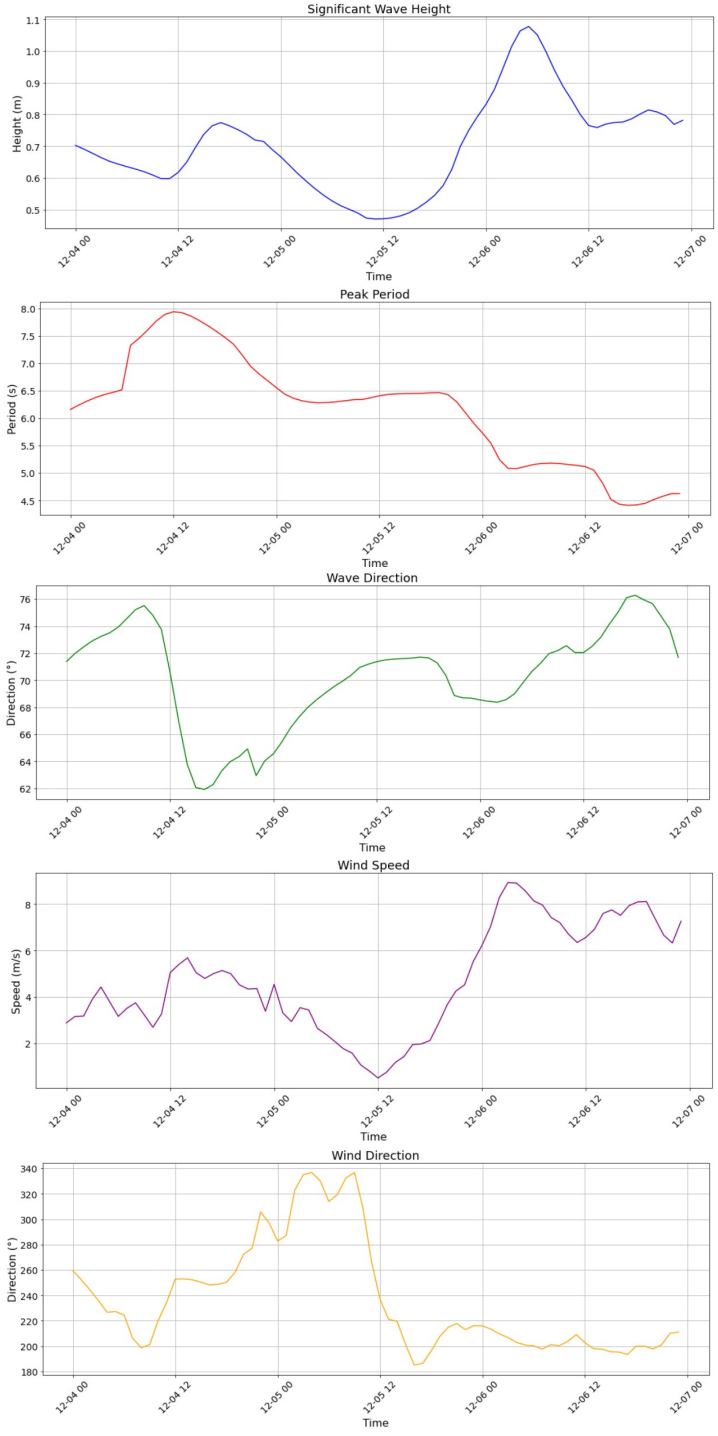

Figure C.2: The offshore conditions used for Delft3D model validation [13].

C.3. RMSE

The Root Mean Square Error (RMSE) is a commonly used metric to measure the accuracy of predictions compared to observed data. It is particularly useful because it provides the errors in the same unit as the observed values, making it directly interpretable in physical terms [94]. This is especially relevant for this model, where deviations in water levels and wave heights are assessed. Although RMSE tends to emphasise larger errors due to the square root transformation, this characteristic is beneficial in identifying significant deviations that could impact the effectiveness of breakwater designs. Given that the focus is on evaluating large-scale hydrodynamic effects, the RMSE provides a meaningful assessment of the model performance [93]. The formula, as described by Hodson [32], is as follows:

$$RMSE = \sqrt{\frac{1}{n}\sum_{i=1}^{n}(y_{\text{pred},i} - y_{\text{obs},i})^2} \tag{C.1}$$

where:

- $y_{\text{pred},i}$ represents the predicted values (from the Delft3D model).
- $y_{\text{obs},i}$ represents the observed values (from field measurements).
- n is the total number of observations.

The RMSE values for water level and significant wave height are 0.2062 m and 0.1077 m, respectively. When validating with tidal constituents and constant wave and wind conditions, the RMSE for water level increases to 0.6736 m, while the RMSE for significant wave height is 0.1375 m.

C.4. Model

C.4.1. Significant Wave Height

Different Conditions

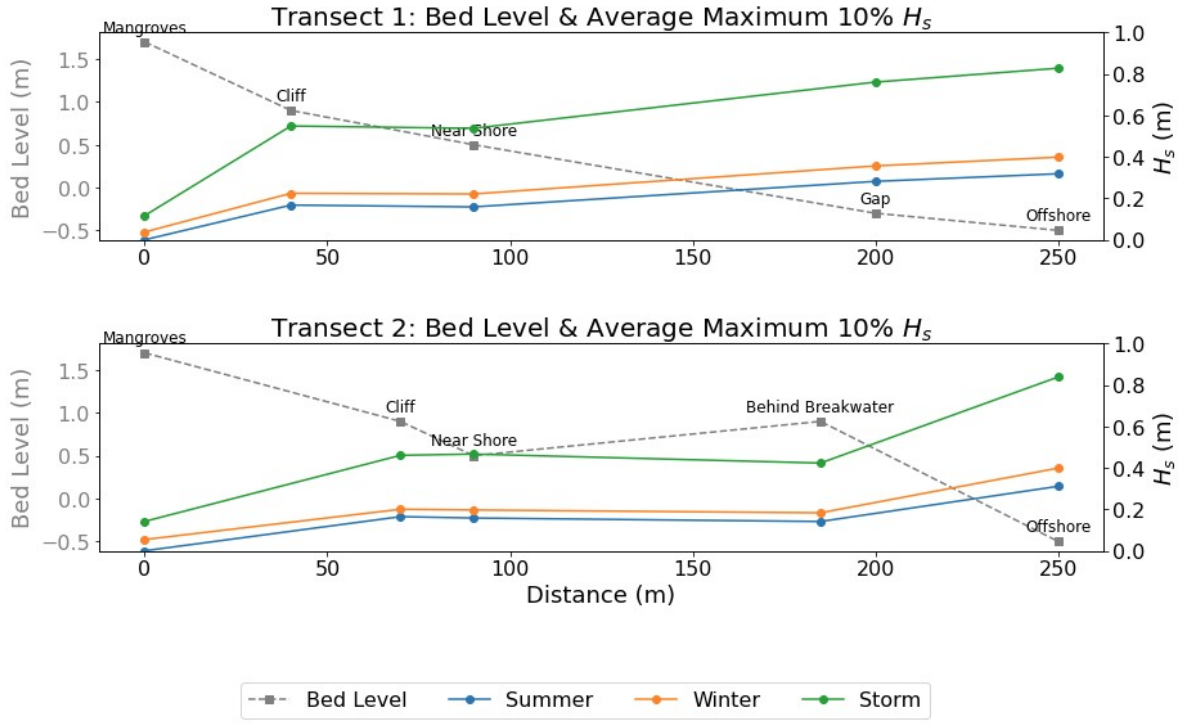

Figure C.3: Modelled maximum significant wave height along the transects under different conditions.

Transects

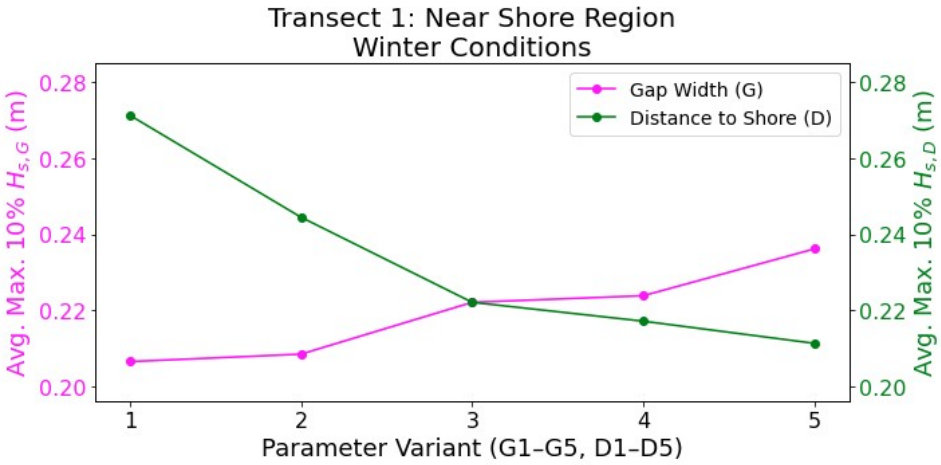

Figure C.4: Comparison of the maximum significant wave height along transect 1 for each design variation under winter conditions.

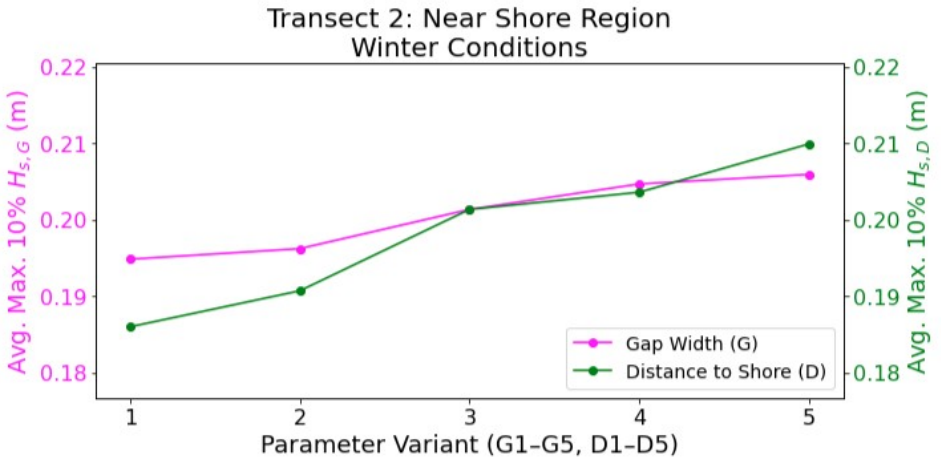

Figure C.5: Comparison of the maximum significant wave height along transect 2 for each design variation under winter conditions.

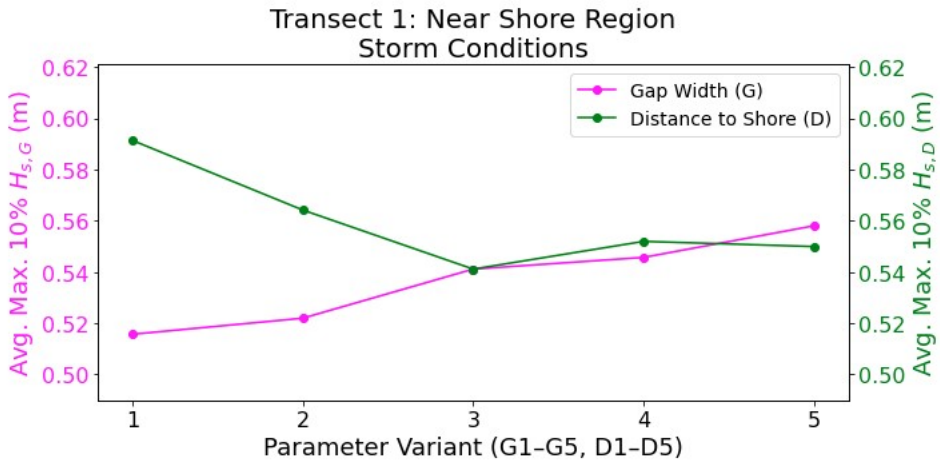

Figure C.6: Comparison of the maximum significant wave height along transect 1 for each design variation under storm conditions.

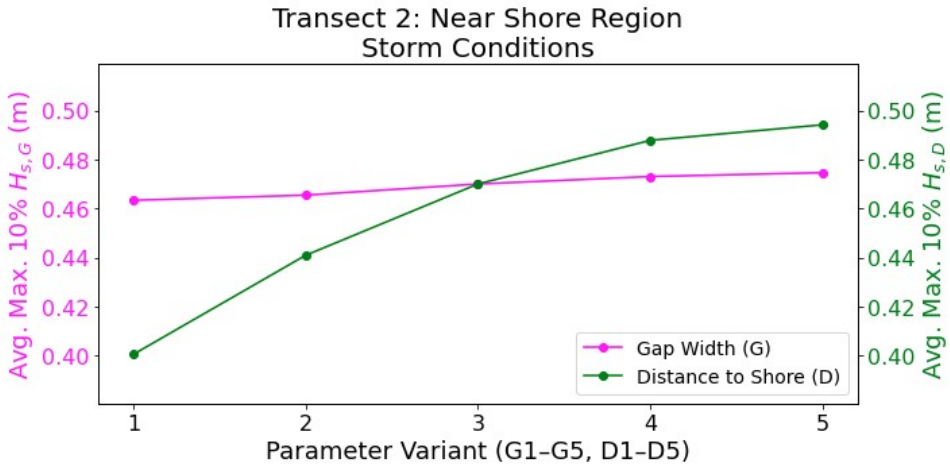

Figure C.7: Comparison of the maximum significant wave height along transect 2 for each design variation under storm conditions.

Spatial Distribution

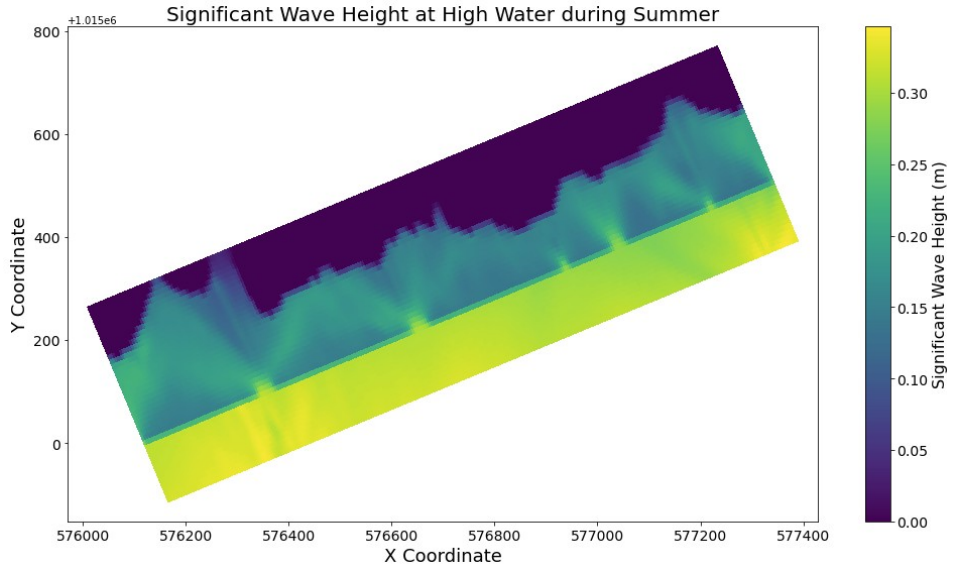

Figure C.8: Spatial distribution of the significant wave height at high tide for the existing breakwater design under summer conditions.

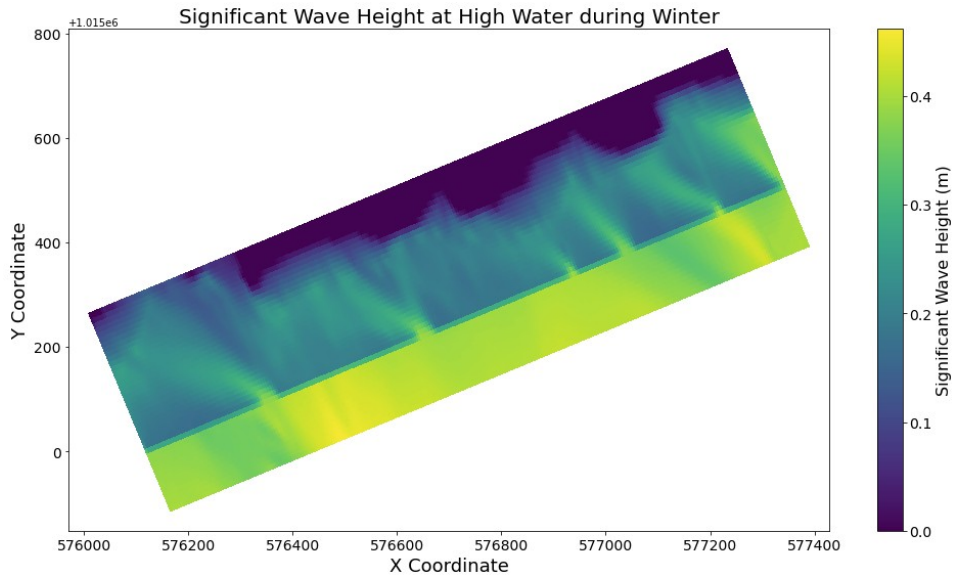

Figure C.9: Spatial distribution of the significant wave height at high tide for the existing breakwater design under winter conditions.

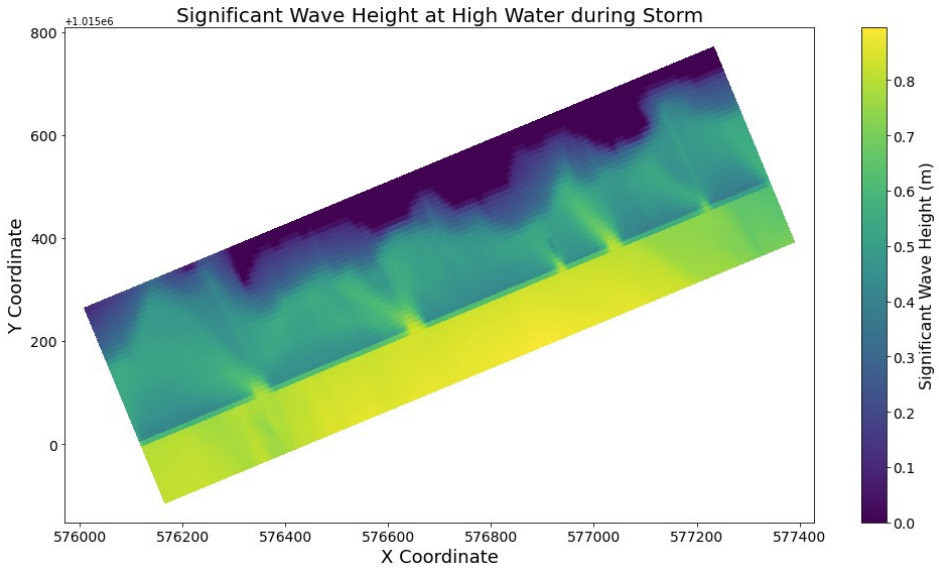

Figure C.10: Spatial distribution of the significant wave height at high tide for the existing breakwater design under storm conditions.

C.4.2. Permeability

Different Conditions

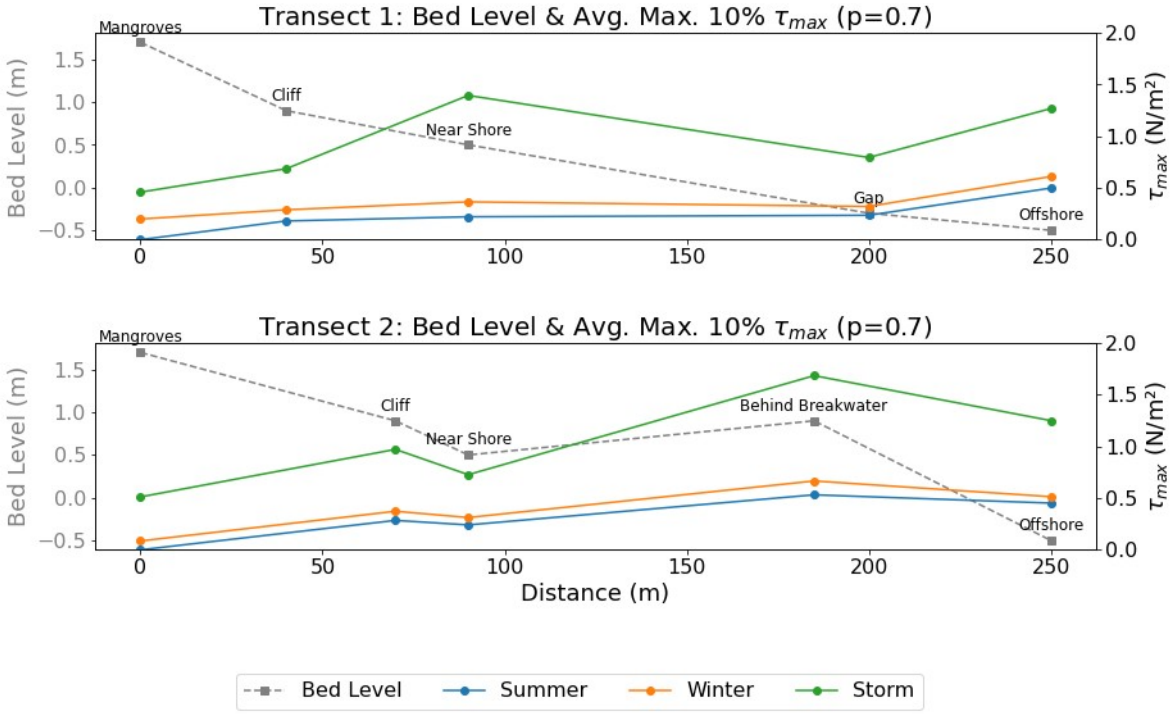

Figure C.11: Modelled average of the top 10% highest τ_{max} along the transects for different conditions with the existing breakwater, assuming a permeability of 0.7.

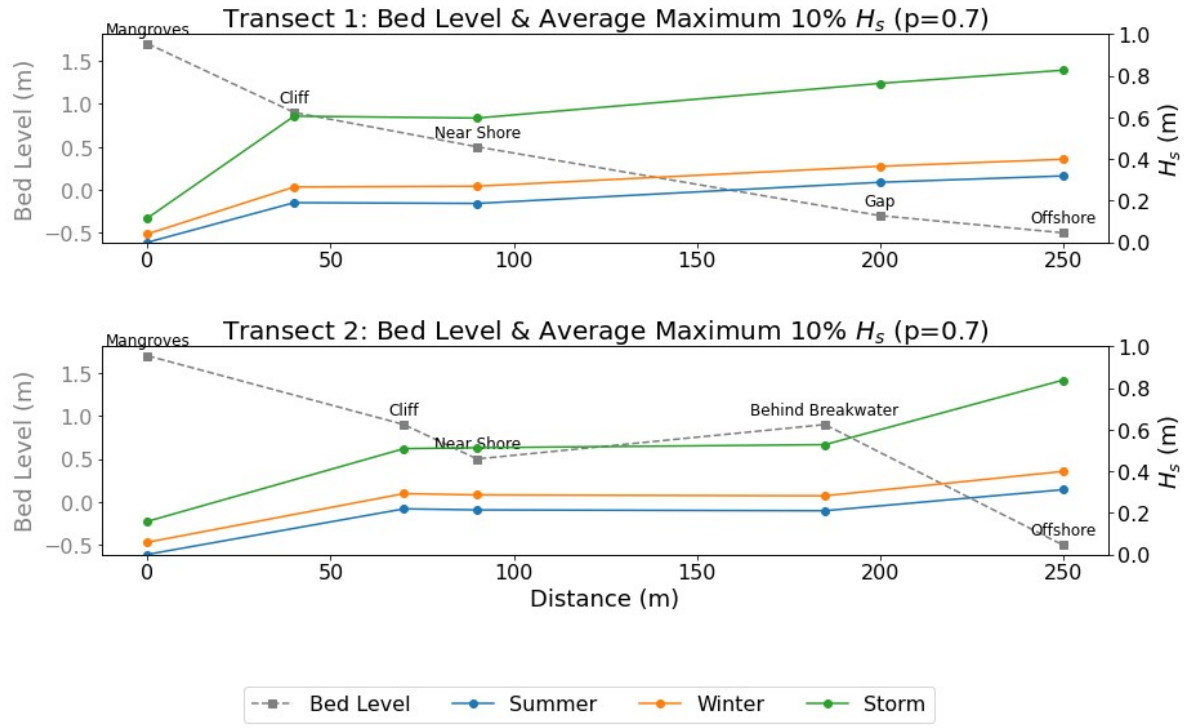

Figure C.12: Modelled average of the top 10% highest significant wave height along the transects for different conditions with the existing breakwater, assuming a permeability of 0.7.

Winter Conditions

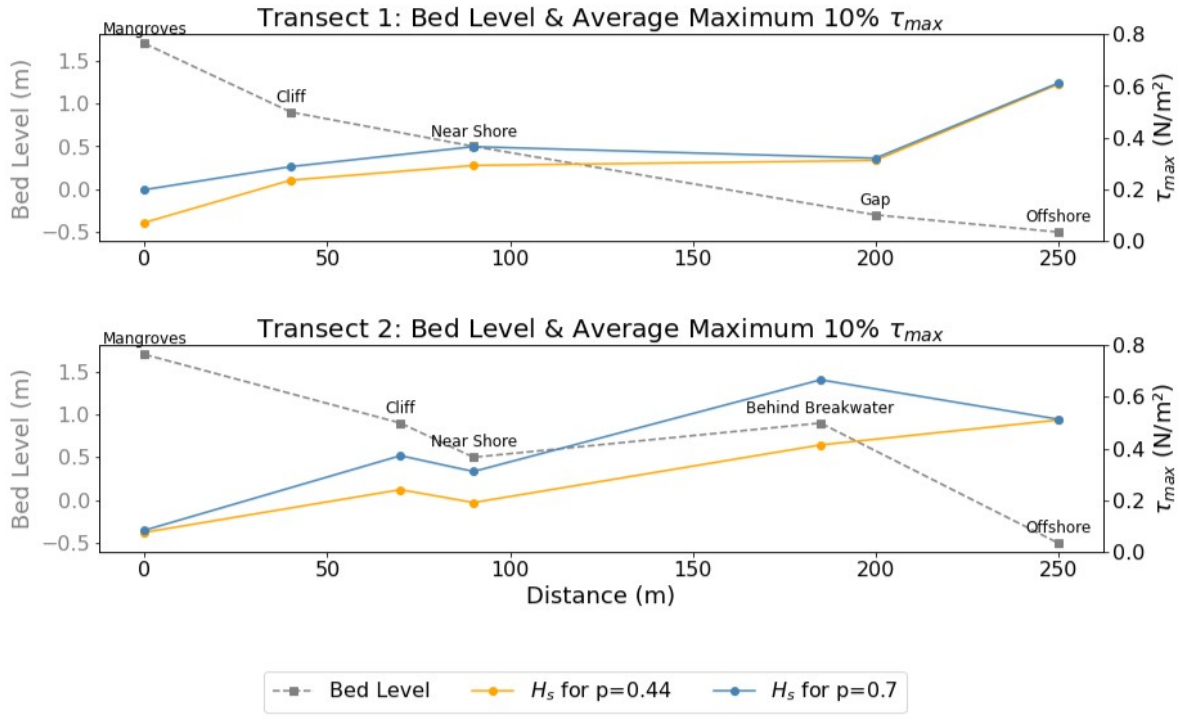

Figure C.13: Modelled average of the top 10% highest τ_{max} along the transects comparing p = 0.44 and p = 0.7 under winter conditions.

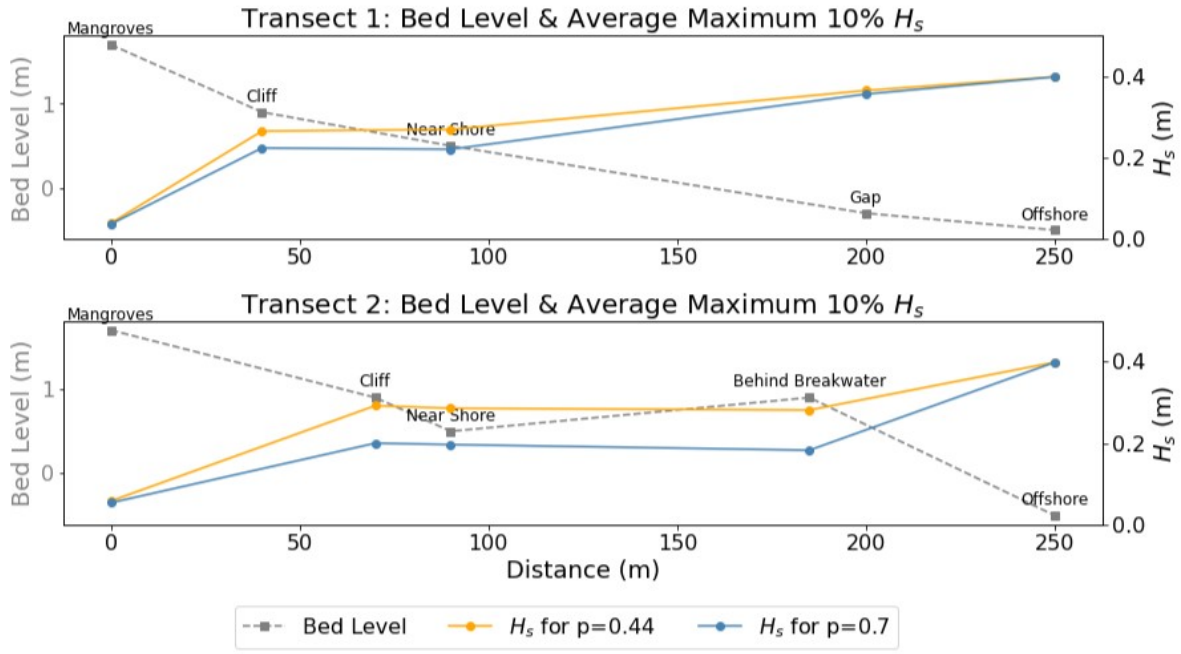

Figure C.14: Modelled average of the top 10% highest significant wave height along the transects comparing p = 0.44 and p = 0.7 under winter conditions.

Storm Conditions

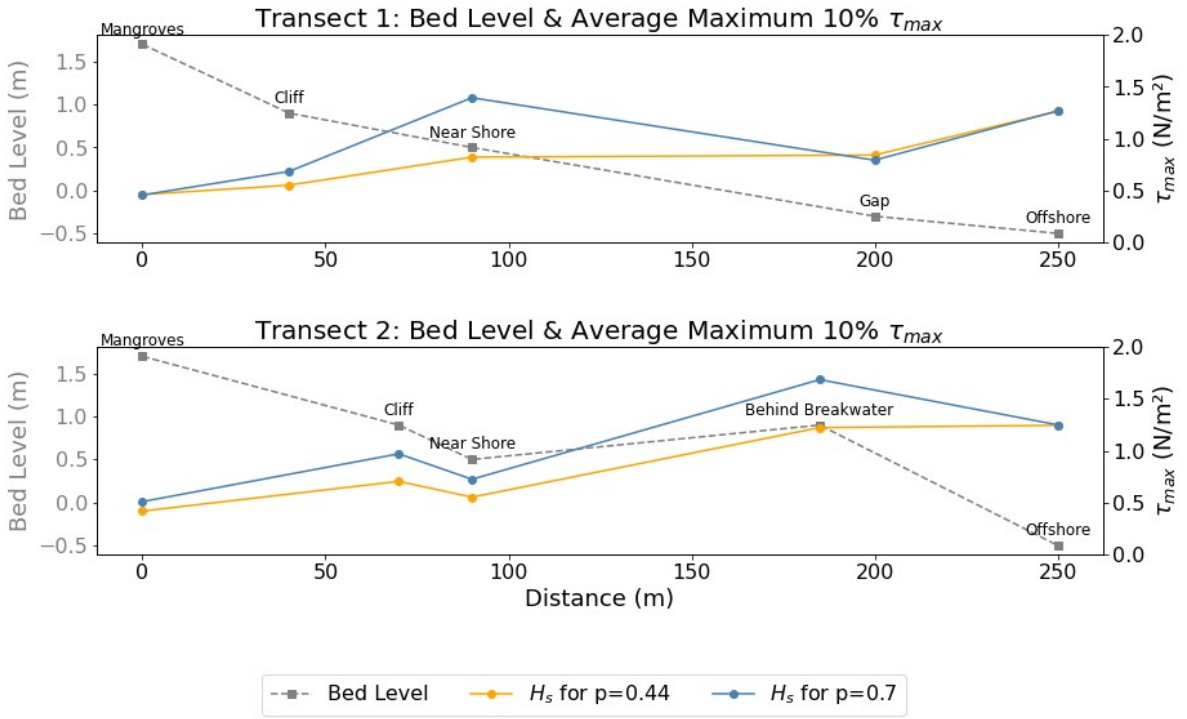

Figure C.15: Modelled average of the top 10% highest τ_{max} along the transects comparing p = 0.44 and p = 0.7 under storm conditions.

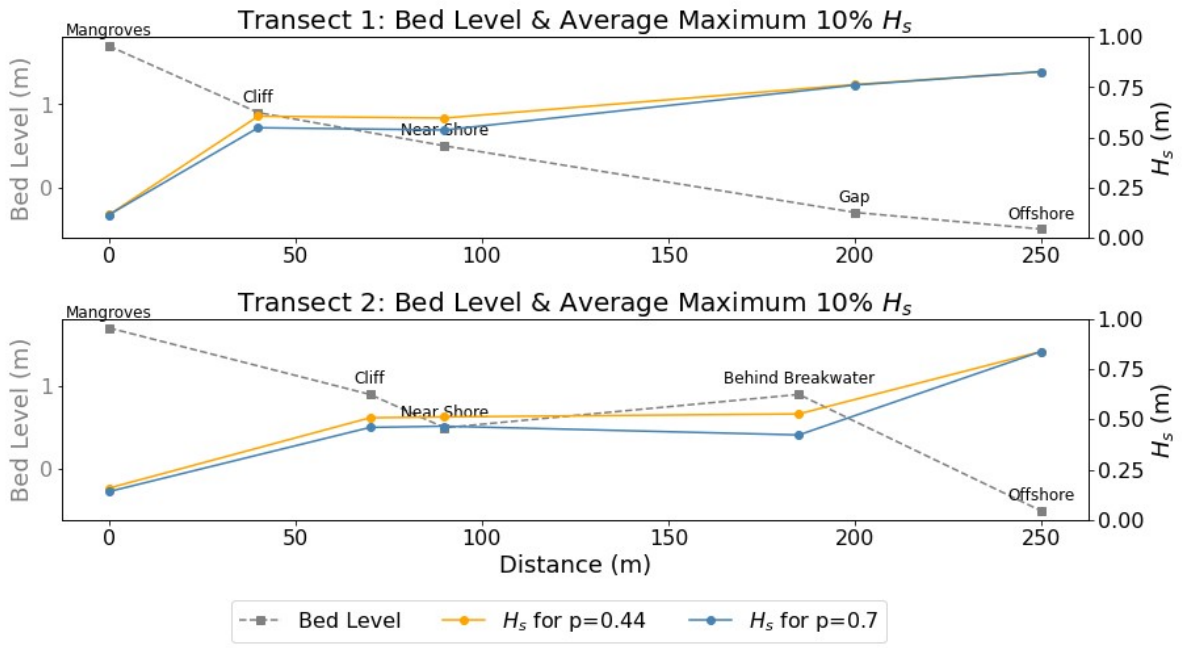

Figure C.16: Modelled maximum significant wave height along the transects comparing p = 0.44 and p = 0.7 under storm conditions.

Spatial Distribution

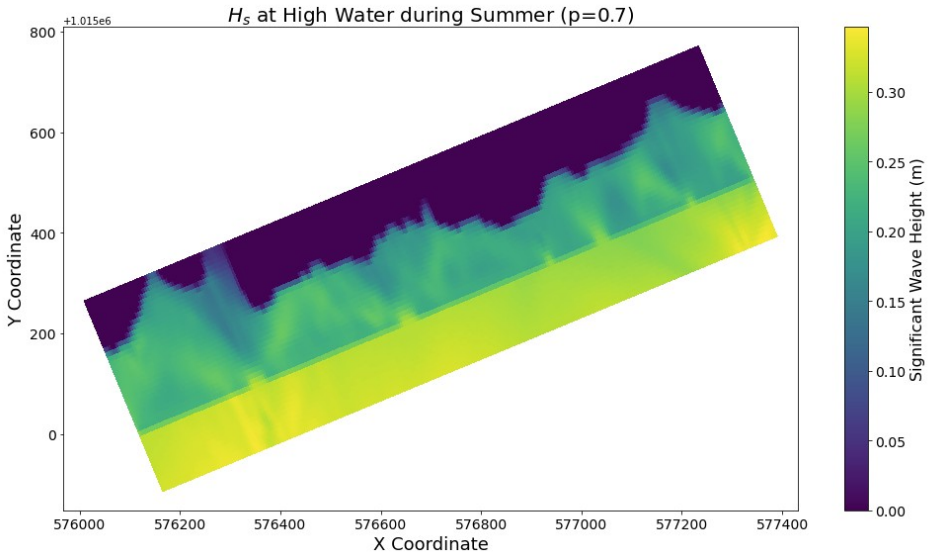

Figure C.17: Spatial distribution of the significant wave height at high tide for the existing breakwater design under summer conditions, assuming a breakwater permeability of 0.7.

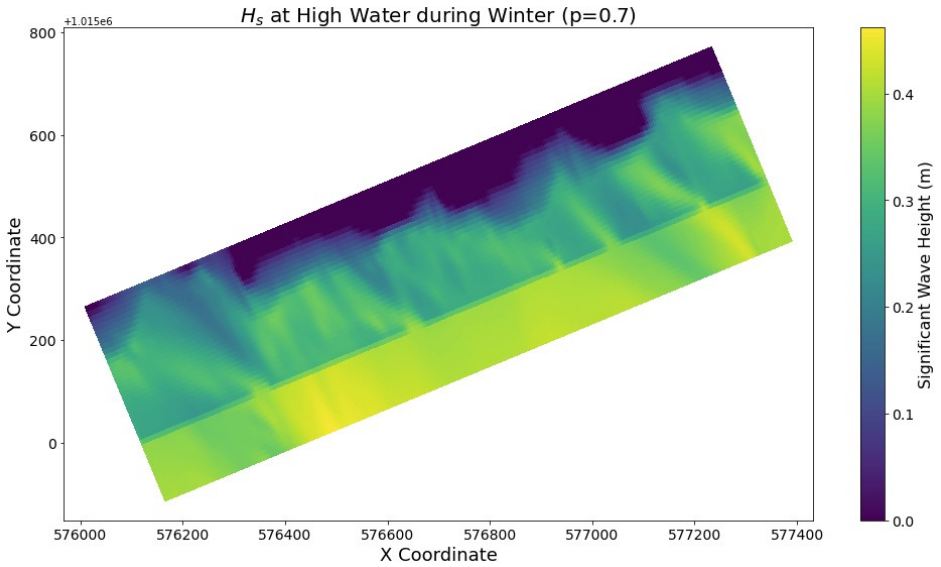

Figure C.18: Spatial distribution of the significant wave height at high tide for the existing breakwater design under winter conditions, assuming a breakwater permeability of 0.7.

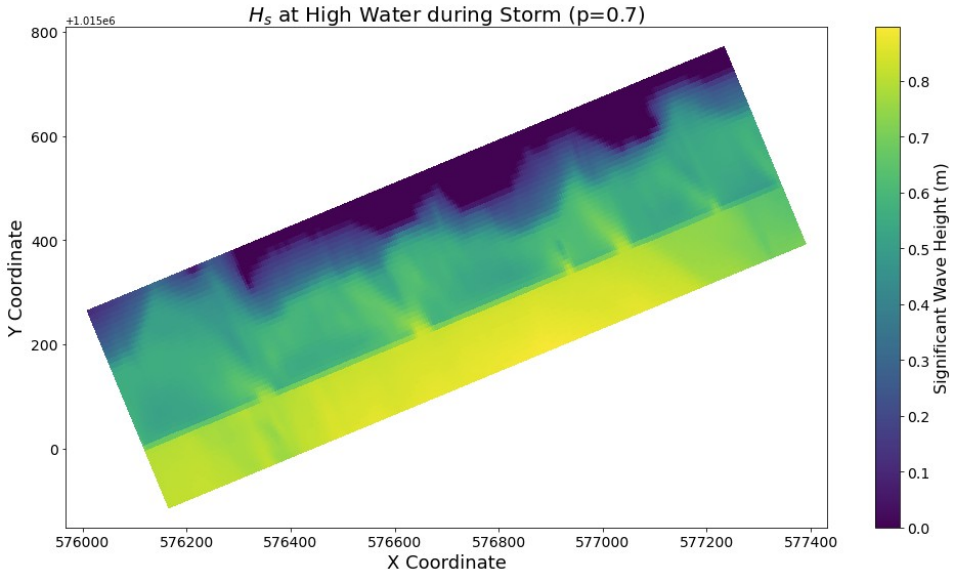

Figure C.19: Spatial distribution of the significant wave height at high tide for the existing breakwater design under storm conditions, assuming a breakwater permeability of 0.7.